

THE UNIVERSITY OF SOUTHERN QUEENSLAND

FACULTY OF ENGINEERING AND SURVEYING



THE EFFECTIVENESS OF AN AEROFOIL SHAPED PIER IN REDUCING DOWN STREAM VORTICES AND TURBULENCE

A Dissertation By

Dirk MacDonald Drysdale

In fulfillment of the requirements of

Courses ENG4111 and ENG4112 Research Project

Towards the degree of

Bachelor of Engineering (Civil)

Submitted: October, 2008



ABSTRACT

This research has examined the phenomenon of vortex shedding that occurs behind a circular pier and an aerofoil shaped pier. A literature review has been conducted in order to assess current knowledge of flow around piers and the effects piers have on downstream turbulence and vortex shedding.

The velocity profile down stream of the model piers was measured so that the finer changes in the flow due to the presence of the pier could be observed. This was done with an Acoustic Doppler Velocimeter. These experiments were carried out in the Water Engineering and Thermodynamics Laboratory of the University of Southern Queensland.

Two piers were modelled in the research. This consisted of a circular pier with 78mm diameter and an aerofoil pier with a 78mm diameter circular front. The dimensions of the piers were scaled from the Bremer River Bridge using the Froude scaling method. The bridge is located in South East Queensland, Australia.

Results were analysed in Microsoft Excel and FLUENT™. The research showed that the aerofoil pier produces a decrease in the drag exerted when compared to the circular pier. The aerofoil pier produces a considerable reduction down stream vortices and turbulence.



ENG4111 & ENG4112 *Research Project*

LIMITATIONS OF USE

The Council of the University of Southern Queensland, its Faculty of Engineering and Surveying, and the staff of the University of Southern Queensland, do not accept any responsibility for the truth, accuracy or completeness of the material contained within or associated with this dissertation.

Persons using all or any part of this material do so at their own risk, and not at the risk of the Council of the University of Southern Queensland, its Faculty of Engineering and Surveying or the staff of the University of Southern Queensland.

This dissertation reports an educational exercise. The sole purpose of the course pair entitled "Research Project" is to contribute to the overall education within the student's chosen degree program. This document, the associated hardware, software, drawings, and other material set out in the associated appendices should not be used for any other purpose: if they are so used, it is entirely at the risk of the user.



CERTIFICATION

I certify that the ideas, designs and experimental work, results, analyses and conclusions set out in this dissertation are entirely my own effort, except where otherwise indicated and acknowledged.

I further certify that the work is original and has not been previously submitted for assessment in any other course or institution, except where specifically stated.

Dirk Drysdale

Student Number: 0050026586

A handwritten signature in black ink, appearing to be 'Dirk', written over a horizontal line.

Signature

30th October, 2008
Date



ACKNOWLEDGEMENTS

This research has been carried out under the principal supervision of Assoc Prof Mark Porter.

Appreciation is also due to Terry Byrne for his work on the mechanical frame for the Acoustic Doppler Velocimeter; to Daniel Eising for his assistance in the Hydraulics Laboratory and Ruth Mossad for assisting with FLUENT™ modeling.

Thanks are due to Rusty, Shirley, Jessica, and Calman for their continued support and interest in the completion of this dissertation.



Table of Contents

Abstract	2
Limitations of Use.....	3
Certification	4
Acknowledgements.....	5
List of Figures	10
List of Tables	12
Nomenclature.....	13
Chapter 1 - Introduction.....	15
1.1 Outline.....	15
1.2 Introduction	15
1.3 Research Problem.....	16
1.4 Objectives.....	17
1.5 Summary	18
Chapter 2 - A Description of Vortex Shedding	19
2.1 Introduction	19
2.2 Types of Fluid Flow	19
2.3 Flow around piers.....	22
2.3.1 Vortex Shedding	22
2.3.2 Scour	25
2.4 How Piers Affect Flow.....	26
2.5 Strouhal Number	28
2.6 Summary	29
Chapter 3 - Vortex Shedding on Bridge Piers	30
3.1 Outline.....	30
3.2 Pier Design	30



3.3	Vortex Shedding and Transverse Wave Formation	31
3.4	Reduction of Vortices, and Scour.	32
3.5	Scour Estimation	33
3.5.1	Current Practice of Scour Estimation	33
3.5.2	Contraction Scour Depth.....	33
3.5.3	Local Pier Scour Depth.....	35
3.6	Hydrodynamic Forces on Piers	37
3.7	Summary	38
Chapter 4 - Methodology and Equipment.....		39
4.1	Outline.....	39
4.2	Equipment and Facilities.....	39
4.2.1	Hydraulic Flume	39
4.2.2	Acoustic Doppler Velocimeter	40
4.2.3	Collect V Software.....	41
4.2.4	Mechanical Frame.....	43
4.3	Development of the Models	45
4.3.1	Dimensional Analysis	45
4.3.2	Froude Scaling Method.....	46
4.3.3	The Aerofoil Pier	49
4.3.4	Pier Construction	50
4.4	Experimental Method.....	51
4.5	Summary	52
Chapter 5 - FLUENT™ and GAMBIT™		53
5.1	Outline.....	53
5.2	GAMBIT™	53
5.2.1	Developing the Mesh.....	54



5.3	FLUENT™	54
5.3.1	The Principles of FLUENT	54
5.3.2	The Equations of Motion	55
5.4	FLUENT Analysis.....	55
5.5	FLUENT Results.....	56
Chapter 6 - Analysis and Discussion of Results		57
6.1	Outline.....	57
6.2	Experiments.....	57
6.3	Quality Assurance of the System	57
6.4	The Circular Pier	59
6.5	The Aerofoil Pier.....	61
6.6	Comparative Conclusions	63
6.7	Summary	66
Chapter 7 - Future Research		68
References.....		70
Bibliography		71
Appendices.....		74
Appendix A - Project Specification		75
Appendix B - FLUENT Results.....		76
Flow Around the Aerofoil Pier Over A 20 Second Period.....		88
Flow Around the Circular Pier Over A 10 Second Period		91
Appendix C - FLUENT Case Summary		93
Circle Case Summary		93
Aerofoil Case Summary		98
Appendix D - GAMBIT Design		103
Appendix E - Measured Velocities Using the ADV		105



Appendix F - Recorded Velocities for the 65mm Pier	115
Herron's Results	115
Measured Velocities	117
Appendix G - Bremer River Bridge Design Information	119
Bremer River Bridge Cross Section - Courtesy of DMR QLD	119
Bremer River Flow Data - Courtesy of DNRW QLD	121
Bremer River Design Sheets - Courtesy of DMR QLD	123
Appendix H - Schoharie Creek Bridge Failure.....	126



LIST OF FIGURES

Figure 1.2-1 - Vortex shedding in nature - Clouds flowing past a mountain peak.....	16
Figure 1.4-1 - Coefficients of drag versus Reynolds number for axisymmetric bodies. (Schrader, 2005).....	18
Figure 2.2-1 - Laminar Flow.....	19
Figure 2.2-2 - Turbulent Flow	19
Figure 2.2-3 - Fluid flow past a circular cylinder. (Schlichting, 2000).....	20
Figure 2.3-1 - The flow pattern and scour hole at a cylindrical pier. The downflow, horseshoe vortex and wake vortex are the principal cause of local bed erosion. (Hamill, 1999).....	23
Figure 2.3-2 - Formation of vortex shedding.....	25
Figure 2.4-1 - Effect of Many Piers Across a River System	26
Figure 2.4-2 - Specific Energy Curve (Featherstone 2001).....	27
Figure 2.4-3 - Flow Past a Pier (Bernoulli 2004).....	28
Figure 2.5-1 - Flow Regimes for a Circular Cylinder (Schlichting 2000).....	29
Figure 3.2-1 - Types of bridge piers (Troitsky 1994)	30
Figure 3.4-1 - Effect of splitter plate in the wake of a circular cylinder, after A. Roshko (1967). $Re = 14,500$ the laminar - turbulent transition takes place immediately after laminar separation. Taken from Schlichting, <i>Boundary Layer Theory</i> , 2000.....	32
Figure 3.5-1 - Pier skew correction factor for use with equation 3.9. If $\phi < 5^\circ$ K_{2p} can be ignored. (Hamill, 1999).....	36
Figure 4.2-1 - Cross Section of the Flume.....	39
Figure 4.2-2 - A signal is emitted from the centre of the probe, and a return signal is received by each of the three probes.....	41
Figure 4.2-3 - This is the plotted output of a probe check from CollectV. This data has been exported and plotted with Microsoft Excel™. The plot shows signal strength vs the time/distance.	42
Figure 4.2-4 - Relative position of ADV to the flume.....	43
Figure 4.3-1 - Cross section of the channel with pier.....	48
Figure 4.3-2 - Typical aerofoil design, with relevant features.....	49
Figure 4.3-3 - Symmetrical aerofoil.....	50
Figure 4.3-4 - Circular fronted aerofoil, based on a symmetrical aerofoil.	50



Figure 4.3-5 - Aerofoil Pier	Figure 4.3-6 - Circular Pier	50
Figure 4.4-1- Frame used to hold piers in place, without obstructing flow.....		51
Figure 4.4-2 - Method used to record velocities at the pier.		52
Figure 5.4-1 - Mesh developed in GAMBIT and used in FLUENT.....		56
Figure 6.3-1 - Velocity contours downstream of the 65mm pier. Q = 305L/min. Lines represent velocity contours. (Herron, 2007)		58
Figure 6.3-2 - Measured Velocities 100mm (in the centre) behind 65mm pier. Blue = Cross Stream Velocity, Red = Downstream Velocity.		58
Figure 6.4-1 - Plot showing progress of FLUENT drag coefficient calculations with respect to time.		59
Figure 6.5-1 - Plot showing progress of FLUENT drag coefficient calculations with respect to time.		61
6.5-2 - Drag coefficient comparison. Red = Circular pier, Blue = Aerofoil pier.....		62
Figure 6.6-1 - Velocity vectors produce by FLUENT. The circular pier is 78mm diameter. Marked points show where velocities were recorded.		63
Figure 6.6-2 - Velocity vectors produce by FLUENT. The circular pier is 78mm diameter. The dense patches on either side of the pier are due to the mesh used for the analysis. This mesh has not affected the flow around the pier and can be ignored. Marked points show where velocities were recorded.....		64
Figure 6.6-3 - Down stream velocity contours produce by FLUENT.		65
Figure 6.6-4 - Contours of downstream velocity produced by FLUENT.....		66



LIST OF TABLES

Table 3.5-1 - Exponents for determining live-bed contraction scour for use with equation 3.8. Calculate U_1^* / w using the footnotes, then determine the appropriate values of $k1$ and $k2$ to be used in equation 3.8. (Hamill, 1999).....	35
Table 3.5-2 - Adjustment factor for pier nose shape applicable when $\phi < 5^\circ$	36
Table 3.5-3 - Increase in equilibrium pier scour depths for various bed conditions. (Hamill, 1999)	37
Table 4.2-1	42
Table 6.6-1 - Comparison of measured velocity magnitudes and FLUENT velocity magnitudes for the circular pier.	63
Table 6.6-2 - Comparison of measured velocity magnitudes and FLUENT velocity magnitudes for the aerofoil pier.	64



NOMENCLATURE

A	Cross Sectional Area of Flow	m^2
b	Either Width of Pier or Width of Channel	m
C_d	Drag Coefficient	
C_l	Lift Coefficient	
D	Diameter of Pier	m
D_{50}	Median diameter at which 50% of material by weight is smaller than the size denoted	
E_s	Specific Energy	m
F	Froude Number	
F_D	Drag Force	
F_L	Lift Force	
f	Shedding Frequency	Hz
g	Gravity (Assume 9.81)	$m.s^{-2}$
K	Coefficient for Shape and Angle of Different Piers	
k_s	Coefficient for Flow	
L	Characteristic Length	m
p	Pressure	$kN.m^{-2}$
P	Wetted Perimeter	m
Q	Discharge	$m^3.s^{-1}$
R	Hydraulic Radius	m
Re	Reynolds Number	



Re_f	Roughness Reynolds Number	
St	Strouhal's Number	
t	Time	s
U	Velocity	$m.s^{-1}$
u	Velocity	$m.s^{-1}$
V	Velocity	$m.s^{-1}$
x	Distance	m
y	Distance	m
y	Depth of Flow	m
Y	Mean Depth of Flow	m
z	Elevation	m
λ_y	Froude Scaling Coefficient in Y-Direction	
λ_x	Froude Scaling Coefficient in X-Direction	
μ	Coefficient of Dynamic Viscosity	$kg.m^{-1}.s$
ρ	Density of Fluid	$kg.m^{-3}$
τ	Shear Stress	$N.m^{-2}$
ν	Kinematic Viscosity of Fluid	$m^2.s^{-1}$



CHAPTER 1 - INTRODUCTION

1.1 OUTLINE

This research further studies the phenomenon of vortex shedding from bridge piers. There is little knowledge of what happens when the pier is no longer circular or a standard shape. This study investigates the effectiveness and feasibility of an aerofoil shaped pier under hydraulic circumstances.

1.2 INTRODUCTION

Engineers have successfully constructed bridges over obstacles for thousands of years. Possibly the earliest permanent river bridge of any significance was built somewhere between 810 and 700_{BC} across the River Euphrates at Babylon (Overman, 1975). The bridge was around 120m long, with stone piers 10m wide and 22m in length. (Hamill, 1999).

By today's standards, these historical bridges are not only a considerable measure of mankind's abilities; but are also considerably over designed which is why they have stood throughout the ages. Engineers of modern bridges need to optimise their materials and design, so that the structural requirements are achieved for minimum financial cost. A major expense in bridge design and construction is securing the piers so they will not be susceptible to failure in flooding conditions.

Vortex shedding is a naturally occurring phenomenon that can be seen when any fluid passes a stationary physical structure intruding the flow. This means that it can occur on many different levels; from water flowing past a plant in a river, to clouds flowing past a mountain peak high in the atmosphere.

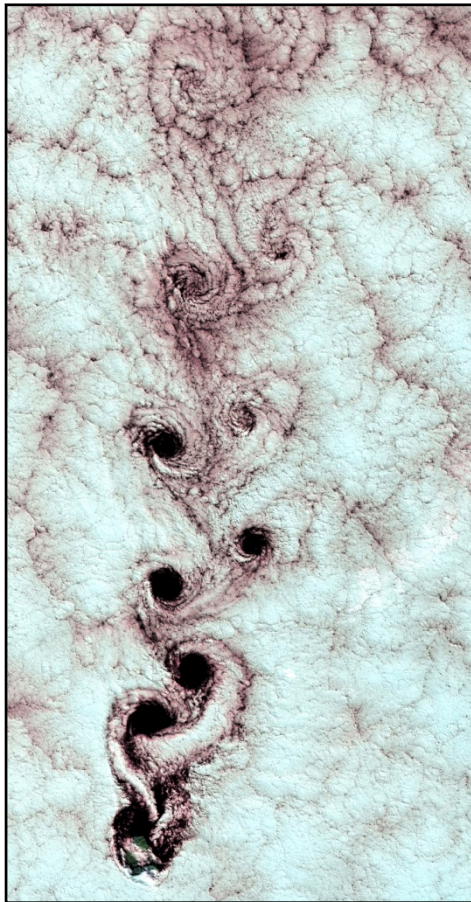


Figure 1.2-1 - Vortex shedding in nature - Clouds flowing past a mountain peak.

Vortex shedding is commonly known as down-stream turbulence. What many people see as turbulence on the downstream side of a bridge is quite often vortex shedding, this is the swirling motion that oscillates from side to side. In more technical terms, this is the separation of boundary layers occurring around a bluff body. As a result vortices are formed and shed from alternate sides of the body.

Because of vortex shedding, many bridges around the world have failed. This is because the onset of vortex shedding aids in local scour, and can aid in harmonic destruction of a structure. This is when the frequency of the vortices match the natural frequencies of the structure. Famous examples of this are the failures of the Tacoma Narrow Bridge and the Schoharie Creek Bridge (information about the Schoharie Creek failure can be found in appendix H).

Vortex shedding has been studied extensively over the years due to its engineering significance. The phenomenon not only contributes to hydraulic engineering applications, but to pollutant dispersion modelling, high rise placement and design, micrometeorology and many other applications. The theory involved has been applied to many measuring devices across a range of applications. The majority of vortex shedding problems induced in river systems is caused by the presence of man-made obstacles, commonly bridge piers.

1.3 RESEARCH PROBLEM

Bridges around the world have failed due to undermining of piers due to vortices and harmonic resonance of the structure itself. After many years of experience and failures, engineers have realised that vortex shedding and the specific nature of fluid flow contribute to the structural degradation of structures; particularly bridges.



The problem of vortex shedding continues to be a well researched, but largely unpredictable phenomenon. This research will give further insight into the phenomenon of vortex shedding as well as vortex shedding from an aerofoil shaped pier. This will require a good understanding of current literature on pier design and vortex shedding.

1.4 OBJECTIVES

The objective of this research is to determine whether or not an aerofoil shaped pier will significantly reduce the onset of vortex shedding, opposed to traditional circular shaped piers. Hence shedding light on a more effective option for pier design.

In this project dimensional analysis has been used to scale part of a real river system, the Bremer River, which is located in the South Eastern Corner of Queensland, Australia. The river system was then modelled in a flume and vortex shedding was analysed. An Acoustic Doppler Velocimeter (NORTEK AS 2000) was used to examine the formation of vortex shedding. The Bremer River was simulated in flood conditions, those favourable to bridge failure due to scour as a result of vortex shedding. The flow will then be modelled using CFD software, FLUENT.

Round piers exert a considerable drag force when subject to high flows, this is directly related to vortex shedding i.e. the higher the drag force, the more extreme the vortex shedding. By reducing the drag force the downstream vortices may also be reduced.

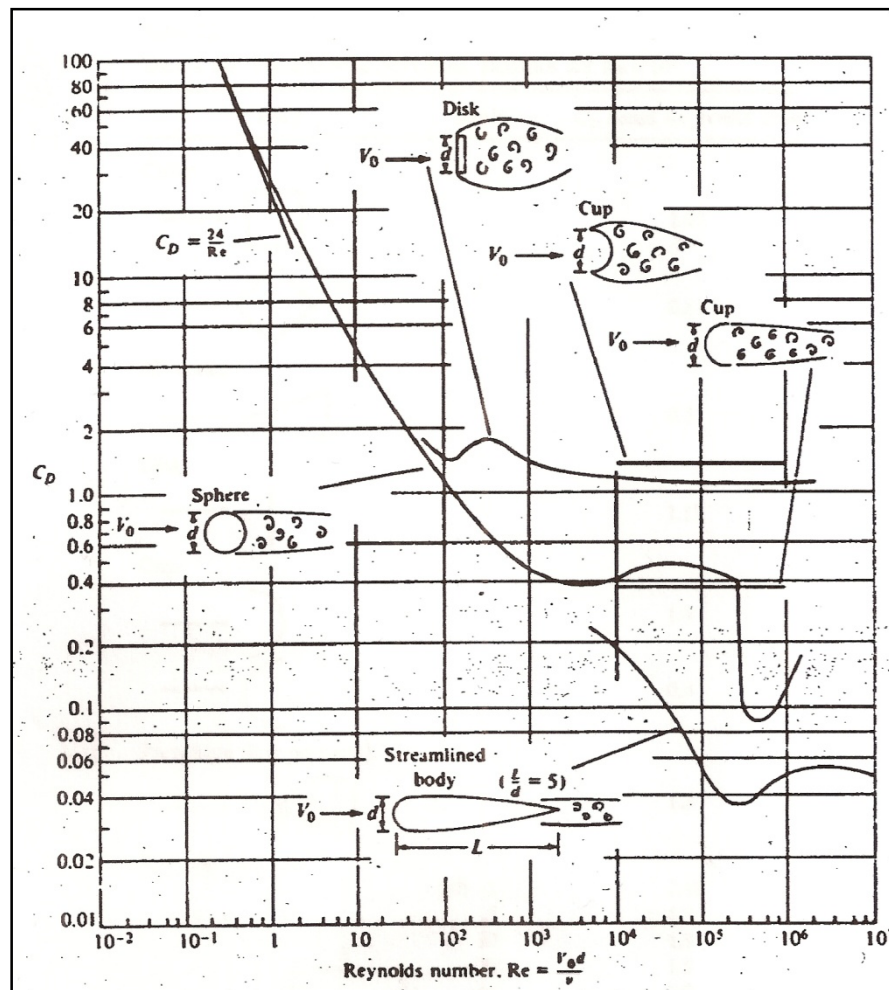


Figure 1.4-1 - Coefficients of drag versus Reynolds number for axisymmetric bodies. (Schrader, 2005)

1.5 SUMMARY

This dissertation aims to describe how and when the phenomenon of vortex shedding occurs in the form of a literature review. Background theory will be compared with data gathered through experimentation. The outcome is expected to provide an alternative hydraulic solution to available pier types. It will make way for further research in the topic.

In order to provide this alternate solution, an understanding of contributing factors to vortex shedding is required. Comparative results between a circular pier and an aerofoil pier will be based on these factors. This will be done using measured velocities and FLUENT. A comprehensive explanation of the factors contributing to vortex shedding is outlined in future chapters.

CHAPTER 2 - A DESCRIPTION OF VORTEX SHEDDING

2.1 INTRODUCTION

This chapter will include a detailed description of vortex shedding, outlining the properties of fluid flows that are necessary for vortex shedding to occur. It will describe the types of flow that commonly occur in water and the flows that engineers commonly deal with in the real world scenario. The dimensionless equations for these flows will be described in detail. The ways in which vortex shedding occurs will also be discussed.

2.2 TYPES OF FLUID FLOW

There are generally two kinds of flow that can be assimilated with fluid flow, particularly water. These are *laminar flow* and *turbulent flow*. When the flow is laminar, the fluid particles move along a smooth layer, one layer gliding over another adjacent layer (Nalluri & Featherstone, 2001). An example of laminar flow is shown in figure 2.2-1.

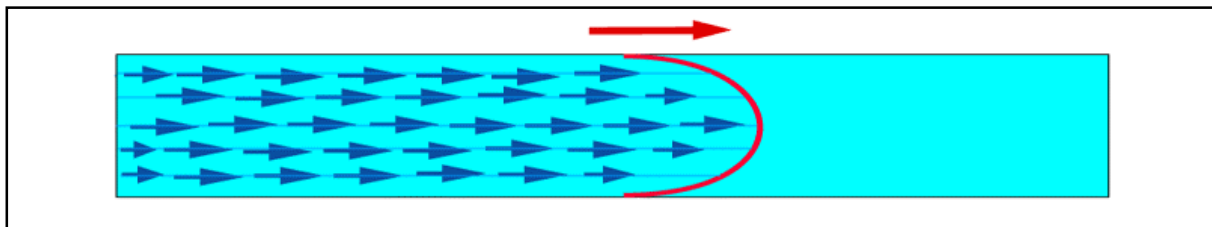


Figure 2.2-1 - Laminar Flow

However under turbulent conditions, which is the most common flow encountered in hydraulic engineering applications, the fluid particles move about in an erratic manner causing complex and variable flow patterns with varying instantaneous velocities at any given point in the flow. An example of turbulent flow is shown in figure 2.2-2.

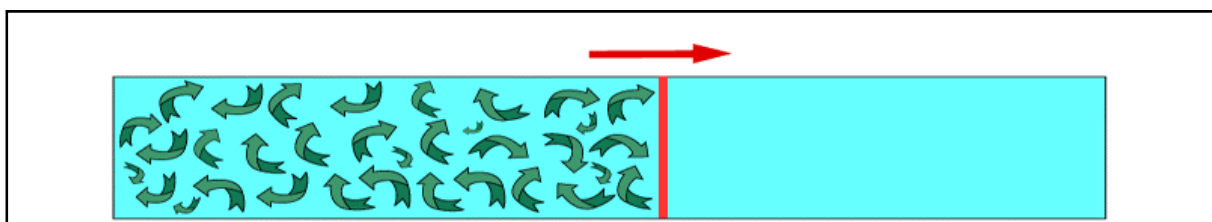


Figure 2.2-2 - Turbulent Flow



Laminar and turbulent flows are defined by the characteristics of the catchment in which the fluid is flowing. These characteristics together make up a dimensionless number called Reynolds number, Re . Flows with $Re < 2.0 \times 10^3$ are considered laminar; in flows where $2.0 \times 10^3 < Re < 4.0 \times 10^3$ the regime is considered transitional, it is neither perfectly laminar or turbulent. When $Re > 4.0 \times 10^3$ the flow is turbulent.

For the this research, it is important to know how fluid flows past an object under various flow conditions. Shown in figure 2.2-3 is the transition from laminar flow to turbulent flow past a circular pier.

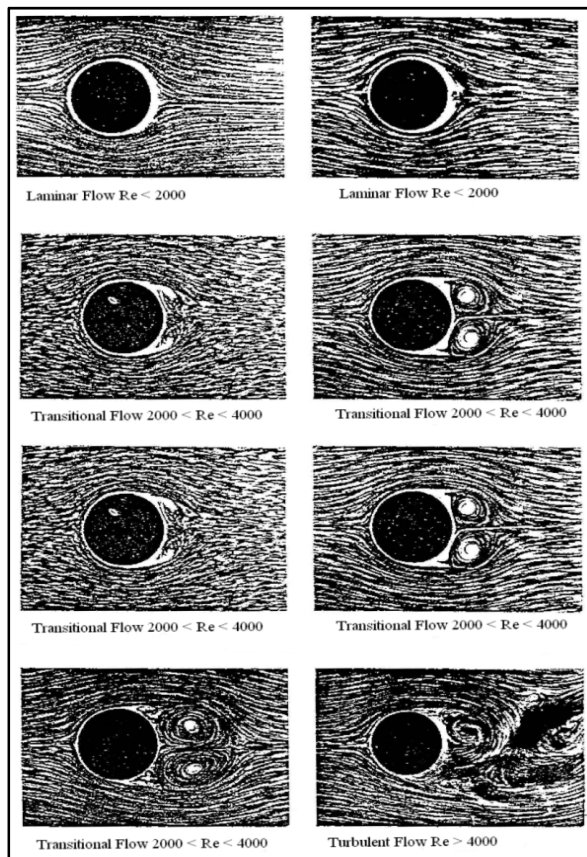


Figure 2.2-3 - Fluid flow past a circular cylinder. (Schlichting, 2000)

Under steady conditions (laminar flow) the pier will not have a great effect on the state of flow. Any disturbances will be damped out as the viscous forces outweigh the disturbing forces. Under this flow condition the stream lines will return to their original parallel condition after a disturbance, in this case a pier. (Pope, 2000)



When flow is in the transitional form, as shown in figure 2.3 the flow is neither turbulent nor is it laminar, however in the turbulent region the flow is broken and distorted.

Osbourne Reynolds (1842-1912) developed experiments used to examine the condition of flow. These experiments showed the turbulence was as function of fluid velocity, viscosity, and a dimension. This lead to the development of Reynolds Number (Borthwick, 2004).

Reynolds number is a dimensionless number used to describe the onset of turbulent flow. It is a ratio of inertia forces and viscous forces. Reynolds number is also linked to the phenomenon of vortex shedding where it may be expressed as a function of velocity, characteristic length, and dynamic viscosity. The characteristic length may be defined in a number of ways resulting in a number of different forms of Reynolds numbers. (Herron, 2007)

Reynolds number can be expressed in a number of ways in a variety of flow situations. The most common of these are for a pipe and an open channel.

$$Re_{pipe} = \frac{UD\rho}{\mu} = \frac{UD}{\nu} \quad \text{Equation 2.1}$$

Equation 2.1 defines Reynolds number in a pipe. Where D is the diameter of the pipe, μ is the coefficient of dynamic viscosity of the fluid, ρ is the density, and U is the velocity of the fluid; ν is the viscosity of the fluid.

$$Re_{channel} = \frac{UR\rho}{\mu} \quad \text{Equation 2.2}$$

Equation 2.2 defines Reynolds number in a channel. Where R is the hydraulic radius of the channel, μ is the coefficient of dynamic viscosity of the fluid, ρ is the density, and U is the velocity of the fluid.

The hydraulic radius is simply the ratio of the cross sectional area to the wetted perimeter; whereby the wetted perimeter is the length of the wetted surface measured normal to the direction of flow. (Borthwick, 2004) However for considerably wide channels, R may be assumed to be equal to the depth of flow.



There is also a roughness Reynolds number where;

$$\text{Re}_f = \frac{U k_s \rho}{\mu}$$

Equation 2.3

For this research project equation 2.2 will be used.

2.3 FLOW AROUND PIERS

Over the last 150 years, civilisation has seen impressive feats of engineering in bridge design and construction. However there have been many failures and lives lost due to lack of consideration, poor construction techniques, and none more evident than lack of knowledge in the hydraulic phenomenon's that occur around bridges.

The most common reason for bridges to fail (other than fatigue) is that in a significant flood event, the fast flowing water causes significant scour at and around the piers, leaving the bridge vulnerable to collapse.

Bridges by today's standards are generally well constructed under strict supervision and last the specified design life. However when unexpected events occur, particularly flood events; if the flood event is over the design, then chances are the bridge will fail. As a result of this, bridges are considerably expensive because of the need to ensure safety for the public.

2.3.1 VORTEX SHEDDING

Scour is a bi-product of vortex shedding. Vortex shedding is the effect that is seen when a fluid flows past a bluff body. As the flow velocity increases, so do the intensity of the vortices. It is because of this vortex shedding that scour occurs. This is shown in figure 2.3-1.

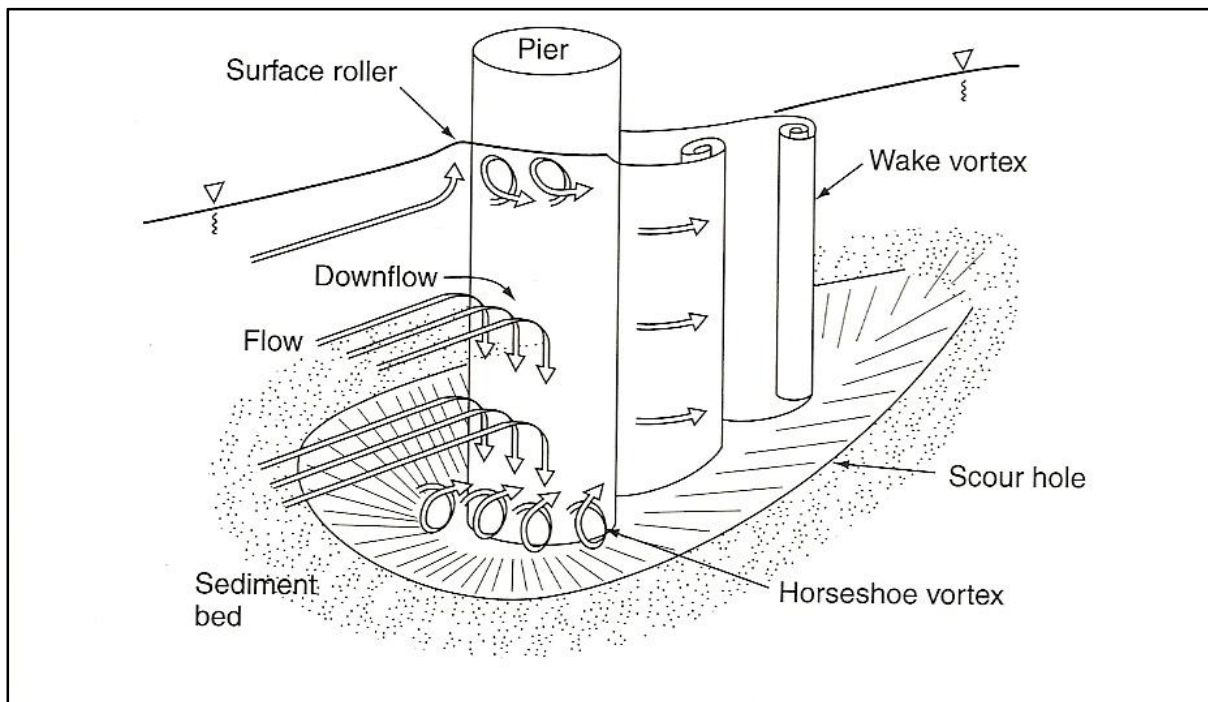


Figure 2.3-1 - The flow pattern and scour hole at a cylindrical pier. The downflow, horseshoe vortex and wake vortex are the principal cause of local bed erosion. (Hamill, 1999)

Vortex shedding is caused because of different velocities that arise in the flow around a pier. It was explained in section 2.2 that under laminar flow a fluid will return to its original parallel state of flow, and under turbulent flow conditions there will be an unstable region behind the pier. This is where vortex shedding occurs.

Vortices are formed as a result of boundary layer separation and can be explained using the fundamental concepts of fluid dynamics; these are the laws of conservation of mass, energy and momentum.

According to Borthwick (2004) the continuity equation can be defined as;

$$Q_{in} = Q_{out} \quad \text{Equation 2.4}$$

Meaning that (assuming no losses or gains to the system) the total amount of energy entering the system will be equal to the amount of energy leaving the system. Bernoulli's equation as expressed below assumes that no energy is lost through friction. (Borthwick 2004)

$$\frac{p_1}{\rho g} + \frac{u_1^2}{2g} + z_1 = \frac{p_2}{\rho g} + \frac{u_2^2}{2g} + z_2 = H = \text{constant} \quad \text{Equation 2.5}$$



Where; p_1 and p_2 are pressures at points 1 and 2 respectively; u_1 and u_2 are the corresponding velocities; z_1 and z_2 are the potential or elevation head; g is gravity; and ρ is the density of the fluid.

The momentum equation is based on the principle of momentum where;

$$P_{in} (\rho \cdot \delta Q_1 \cdot \delta t \cdot u_1) = P_{out} (\rho \cdot \delta Q_2 \cdot \delta t \cdot u_2) \quad \text{Equation 2.6}$$

Where δQ_1 and δQ_2 are the change in momentum at points 1 and 2 respectively; δt is the time interval.

All fluids are viscous and 'Newtonian fluids' obey the linear relationship;

$$\tau = \mu \frac{du}{dy} \quad \text{Equation 2.7}$$

Which is Newton's law of viscosity, where τ is the shear stress; $\frac{du}{dy}$ is the velocity gradient; μ is the coefficient of dynamic viscosity.

Kinematic viscosity (used in the calculation of Reynolds number) is the ratio of dynamic viscosity to mass density. Water is a Newtonian fluid having a kinematic viscosity of $1.0 \times 10^{-6} m^2 \cdot s^{-1}$ at 20 degrees Celsius. (Nalluri 2001)

When a Newtonian fluid passes by a bridge pier the fluid directly in front of the pier is compressed and subject to a higher pressure. Because of this the fluid will flow at a slower rate than the water surrounding it, causing it to curve. Once the fluid has passed the pier it is still in an area of lower pressure and travelling slower than the surrounding fluid. The surrounding fluid will try to reach equilibrium with the slow moving water and will begin to swirl. Figure 2.3-2 best describes the development of the phenomenon. The final step (e) shows the shedding relative to a circular pier. Due to the nature and the symmetry of the situation, the phenomenon oscillates as shown in figure 1.2-1.

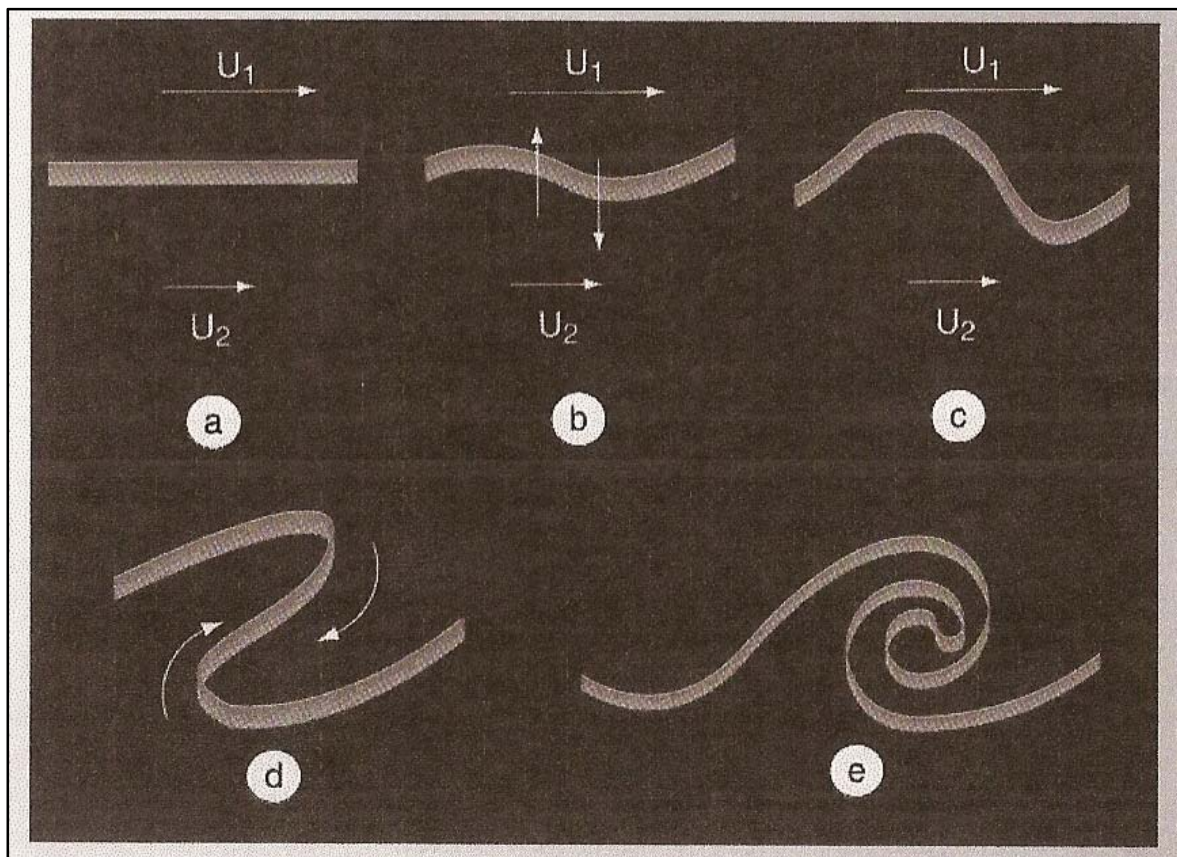


Figure 2.3-2 - Formation of vortex shedding.

2.3.2 SCOUR

In any turbulent flow conditions, depending on the strength of the river bed, scour will begin to form. Zhao (2008) discovered that for the complex flow field around the pier, turbulence plays an important role in the scouring process. As the scouring depth increases, the turbulent intensity increases.

Also at the upstream of the pier, a low-pressure region exists near the centre of the primary horseshoe vortex where the fluctuating pressure is also large. At the downstream region of the pier, the pressure becomes negative and the fluctuating pressure is higher than that at the upstream region of the pier. As the scouring depth increases, the maximum fluctuating pressure and the vertical pressure gradient gradually increase, which cause the bed sediments near the foundation to be sucked up. (Zhao 2008)

Scour reaches a state of equilibrium which is relative to the object it is flowing past and the velocity of the flow. This research focuses on the downstream vortex shedding which occurs



on bridge piers, and horseshoe vortices are not considered. As a result experiments will be carried out in a lined channel, where scour will not be possible, hence the formed vortices may be unstable. (Kirkil n.d.)

2.4 HOW PIERS AFFECT FLOW

Piers do not always affect the overall outcome of the flow regime within the system, this is particularly common in the United Kingdom where the abutments are generally the cause of flooding or failure. However in places where bridges are built over long spanning sections, where many piers are required, it becomes obvious that the piers will be a major consideration in the design. (Hamill, 1999)

Consider the scenario in figure 2.4-1.

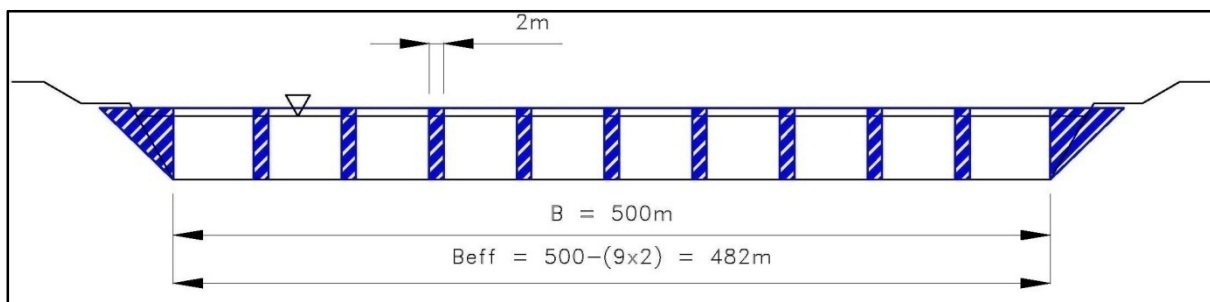


Figure 2.4-1 - Effect of Many Piers Across a River System

The river system is 500m wide, and to bridge the river system will require 2 abutments and 9 piers each 2m wide. The significance of the piers will outweigh the significance of the abutments because of the number of piers. The 9 piers will effectively reduce the width of the river by 18m. Which will make a significant difference when planning for flooding and determining the height of the bridge deck. (Hamill, 1999)

Any flow around a vertical cylinder such as a bridge pier will be turbulent. The Reynolds number may be used to describe the turbulence caused by the bridge pier. (Herron, 2007)

Previous sections have mentioned that formed vortices will cause variations in the velocity profile. These sudden changes will cause variations in the energy of the flow. The transition of the flow may be solved using the specific energy equation. The specific energy is measured relative to the bed. (Featherstone 2001)



$$E_s = y + \frac{\alpha V^2}{2g}$$

Equation 2.8

The specific energy equation (equation 2.8) allows for the determination of the depth of flow for a given state of energy. For any given depth there are two flow types, sub-critical and super-critical. However there is a point of minimum specific energy in any system which occurs at the critical depth y_c . By plotting the depth of flow against the specific energy, the following curve is obtained.

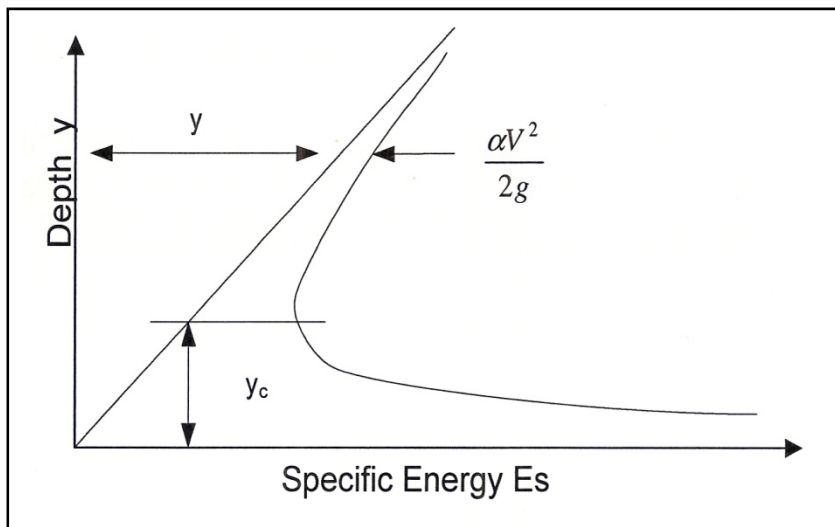


Figure 2.4-2 - Specific Energy Curve (Featherstone 2001)

To put it simply, when flow regime is super-critical, the flow is quite deep, and even though it may well be turbulent flow it does not appear to be fast moving. When the flow is sub-critical the flow will appear quite shallow and will be moving with considerable speed. The critical depth is an equilibrium point for both types of flow.

Figure 2.4-3, shows flow past a bridge pier (Borthwick 2001). This flow condition described will only occur under a specific flow condition. The diagram merely covers the possibilities of flow past a bridge pier.

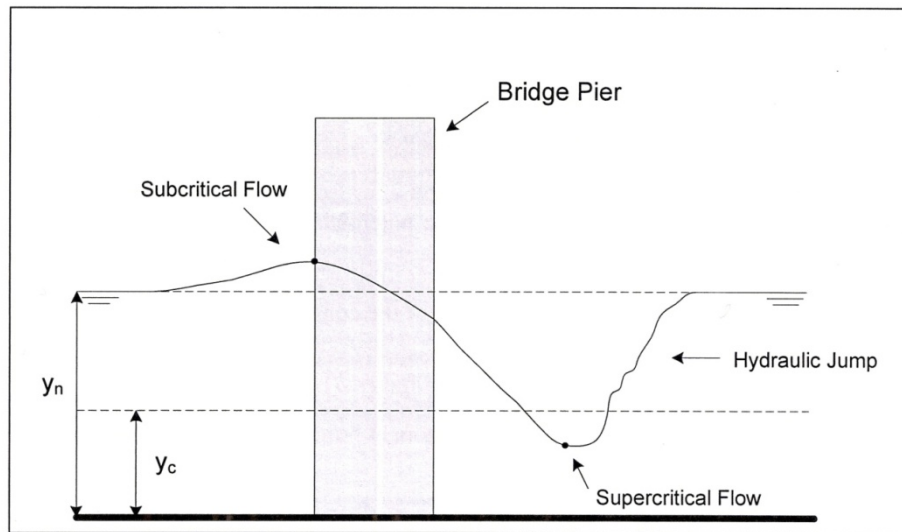


Figure 2.4-3 - Flow Past a Pier (Bernoulli 2004)

2.5 STROUHAL NUMBER

As explained in earlier sections, when a fluid flows past a circular pier, vortex shedding occurs. This vortex shedding is dependent upon the velocity of the flow, the diameter of the pier, and the roughness of the pier. These vortices oscillate in a continuous manner, a means of measuring how often the vortex shedding occurs is by applying Strouhals formula. Vincenc Strouhal (1850 - 1922) is the founder of the Strouhal number.

The Strouhal number is defined as;

$$St = \frac{fL}{U} \quad \text{Equation 2.9}$$

Where St represents the Strouhal number; f is the oscillation frequency; L is the characteristic length; and U is the velocity of the flow.

The Strouhal number represents a measure of the ratio of forces due to local acceleration, to changes in velocity from one point to another. (unknown, 2005)

Borthwick (2004) reported that experiments have shown that for circular piers;

$$St = 0.198 \left(1 - \frac{19.7}{Re} \right), \quad \text{for } 250 < Re < 2 \times 10^5 \quad \text{Equation 2.10}$$



The table below shows the different Strouhal numbers for different flow states around circular piers.

Table 1.1. Flow regimes at a circular cylinder (incompressible flow)
Reynolds number $Re = V d / \nu$
Strouhal number $Sr = f d / V$

Reynolds number regime	Flow regime	Flow form	Flow characteristic	Strouhal number Sr	Drag coefficient c_D	Separation angle θ_S
$Re \rightarrow 0$	Creeping flow		Steady, no wake	–	see Fig. 1.12	–
$3 - 4 < Re < 30 - 40$	Vortex pairs in wake		Steady, symmetric separation	–	$1.59 < c_D < 4.52$ ($Re = 30$) ($Re = 40$)	$130^\circ < \theta_S < 180^\circ$ ($Re = 35$) ($Re = 5$)
$\frac{30}{40} < Re < \frac{80}{90}$	Onset of Karman vortex street		Laminar, unstable wake	–	$1.17 < c_D < 1.59$ ($Re = 100$) ($Re = 30$)	$115^\circ < \theta_S < 130^\circ$ ($Re = 90$) ($Re = 35$)
$\frac{80}{90} < Re < \frac{150}{300}$	Pure Karman vortex street		Karman vortex street	$0.14 < Sr < 0.21$		
$\frac{150}{300} < Re < \frac{10^5}{1.3 \cdot 10^5}$	Subcritical regime		Laminar, with vortex street instabilities	$Sr = 0.21$	$c_D \approx 1.2$	$\theta_S \approx 80^\circ$
$\frac{10^5}{1.3 \cdot 10^5} < Re < 3.5 \cdot 10^6$	Critical regime		Laminar separation Turbulent reattachment Turbulent separation Turbulent wake	No preferred frequency	$0.2 < c_D < 1.2$	$80^\circ < \theta_S < 140^\circ$
$3.5 \cdot 10^6 < Re$	Supercritical regime (transcritical)		Turbulent separation	$0.25 < Sr < 0.30$	$c_D \approx 0.6$	$\theta_S \approx 115^\circ$

Figure 2.5-1 - Flow Regimes for a Circular Cylinder (Schlichting 2000)

2.6 SUMMARY

The fundamental laws of fluid dynamics describe the phenomenon of vortex shedding. Conservation of mass, momentum and energy are used to explain the changes in the state of fluid flow past a pier.

The separation of fluid from the boundary layer causes vortex shedding to occur. This separation is due to the changes in velocities and pressures around the pier.

Scour is directly related to vortex shedding. The magnitude of the scour is proportional to the strength of the bed, the velocity of the flow, and also the size of the pier.

CHAPTER 3 - VORTEX SHEDDING ON BRIDGE PIERS

3.1 OUTLINE

This chapter will outline the extent to which vortex shedding will affect piers, and the methods used to determine hydrodynamic forces on the piers. It will also describe, in short, piers that are commonly used today, other phenomenon's that coincide with vortex shedding, along with current control methods.

3.2 PIER DESIGN

There is a reasonable range of pier types used in hydraulic engineering applications today. A brief range of these is shown in figure 3.2-1.

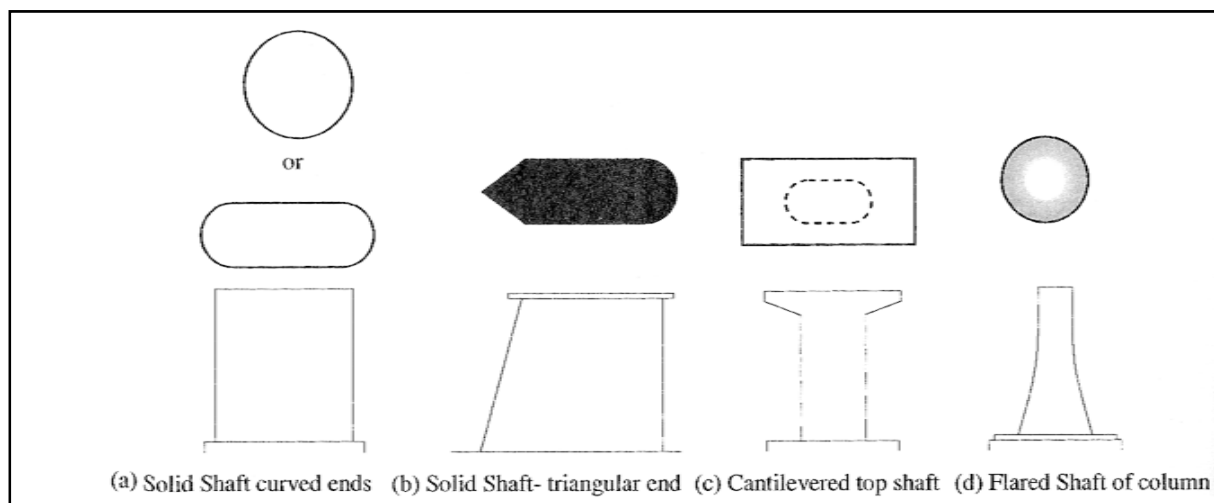


Figure 3.2-1 - Types of bridge piers (Troitsky 1994)

Vortex shedding will contribute to local scour at bridge piers. At the centres of shed vortices there will be an area of relatively low pressures. This low pressure area coupled with the movement of the vortex will cause localised scour. The severity of the scour will be influenced by the shape of the pier, the number of piers, and the alignment of the piers relative to the flow (Herron, 2007).



3.3 VORTEX SHEDDING AND TRANSVERSE WAVE FORMATION

Zima and Ackermann (2002) discovered that the ratio of frequencies of vortex shedding and transverse waves can be described mathematically. As in equation 3.1.

$$\frac{f_s}{f} = \frac{StV}{D} \sqrt{\frac{4\pi l}{ng \tanh \frac{n\pi h}{l}}} \quad \text{Equation 3.1}$$

$$f = \sqrt{\frac{gn}{4\pi l} \tanh \frac{n\pi h}{l}} \quad \text{Equation 3.2}$$

$$l = \frac{nL}{2} \quad \text{Equation 3.3}$$

Where; f_s is the shedding frequency, f is the frequency of surface waves, L is the wavelength, n is mode of wave oscillation, and h is depth of flow.

When the frequency ratio (found using equation 3.1) is equal to unity. The force function having a frequency f_s , is equal to one of the natural frequencies of the transverse waves. Vortex shedding then creates a condition of resonance where the energy content on the transverse wave is amplified.

It is known that structural vibration of an object will occur when the natural frequency of the structure matches the shedding frequency. Experiments carried out by Goswami (1993), where vortex frequencies were matched with the natural frequencies of circular piers, showed while matching frequencies repeatedly synchronisation was not able to be reproduced at will.

From this it could be concluded that structural failure of a bridge is going to be more likely from scour, rather than structural vibrations due to wake vortices.

3.4 REDUCTION OF VORTICES, AND SCOUR.

A. Roshko (1967) discovered that by introducing a splitter plate behind the pier the negative pressure could be reduced significantly, by up to nearly 60% in some cases.

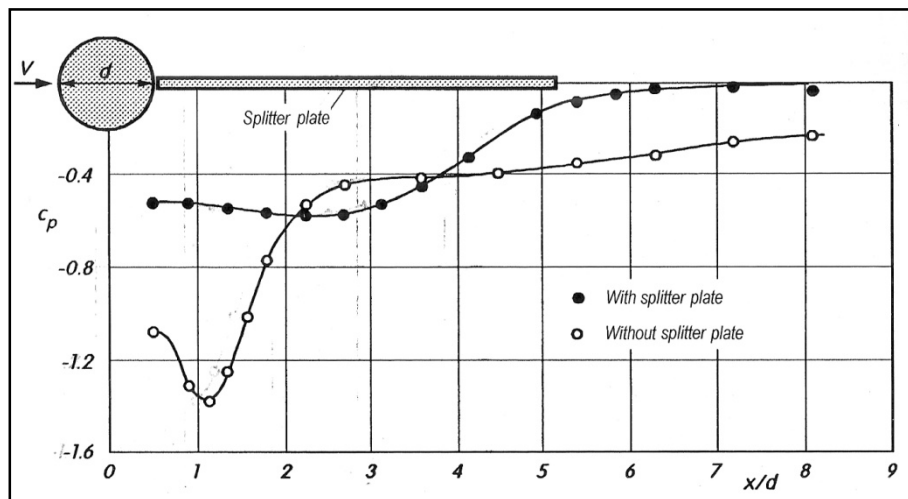


Figure 3.4-1 - Effect of splitter plate in the wake of a circular cylinder, after A. Roshko (1967). $Re = 14,500$ the laminar - turbulent transition takes place immediately after laminar separation. Taken from Schlichting, *Boundary Layer Theory*, 2000.

Other changes to pier design include the attachment of collars with different shapes to a cylinder. The results obtained in the literature indicate that collars positioned at a certain distance relative to the original bed can reduce the scour depth. (Dargahi, 1990)

A river flowing past a bridge pier will exert a hydrodynamic force on the pier, the component of which in the direction of flow is known as drag and the component normal to the flow as lift. In fully turbulent flow, the force is generated from a combination of the shear stress against the pier face and the pressure differential caused by flow separation at the pier tail. (Farraday, 1983)

This means that the hydraulic forces acting on a pier, horseshoe vortices and down stream vortices are a significant feature in the design process. Scour around the front of a bridge pier is caused by horseshoe vortices, and the scour downstream of the pier is caused by the vortices that form behind the pier, known as wake vortices.

By using the aerofoil shape it may be possible to reduce if not eliminate downstream vortex shedding. It is known that the smaller the diameter of the cylinder, the smaller will be the



horseshoe vortices (Dargahi, 1990). Hence by reducing the downstream vortices (the reduction in negative pressure surcharges in flooding conditions) the structural requirements for the pier may be reduced, allowing for a smaller pier diameter. The overall result being a significant reduction on scour. This last comment will not be analysed in this research, it is merely an observation of potential for the research.

3.5 SCOUR ESTIMATION

3.5.1 CURRENT PRACTICE OF SCOUR ESTIMATION

Current practice is to estimate the scour depth that can occur around a particular pier, and to ensure the safety of the structure the depth of the pier is positioned well beyond this depth. There are several ways to estimate scour depth, and these vary depending on the type of fluid flowing past the pier. The two determining factors are whether or not the flow is 'clear-water' or 'live-bed'. Live bed meaning that there is sediment in the flow, and the bed is 'moving' and clear water is simply flowing water with little or no sediment.

There are two types of scour that are directly related with bridge construction these are contraction scour and local scour. Each can occur with either clear water or live bed conditions and are determined with a different set of formulae.

3.5.2 CONTRACTION SCOUR DEPTH

Contraction scour occurs as a result of the narrowing of a channel by the presence of a bridge and highway embankments. The effect of the constriction is to reduce the flow area and increase the velocity. The higher velocity results in an increased erosive force so that more bed material is removed from the contracted reach than is transported into it from upstream, where there may be no transport at all (clear-water conditions) or a lower transportation rate (live-bed) conditions. However, as the bed elevation is lowered and a scour pit develops, the cross-sectional area increases and the velocity falls again so eventually some form of equilibrium is reached. This can be achieved either when the velocity in the contracted section falls below the critical value required to initiate motion (clear-water scour) or when the rate of transport of material into and out of the scour hole are equal (live-bed equilibrium scour). (Hamill, 1999)



The velocity at which bed material will begin to move with clear-water is determined by equation 3.4.

$$V_s = 6.0Y^{\frac{1}{6}}D_{50}^{\frac{1}{3}} \quad \text{Equation 3.4}$$

This can be further evaluated by applying the continuity equation to become;

$$Y_2 = \left(\frac{Q_2^2}{36b^2(D_M)^{\frac{2}{3}}} \right)^{\frac{3}{7}} \quad \text{Equation 3.5}$$

Where;

Y = Average Depth (m) in the Bridge Opening

Q_2 = Corresponding Discharge in the Bridge Opening (cumecs)

b = Effective Width of the Bed at the Bridge (i.e. Total width less sum of pier width)

$$D_M = 1.25D_{50}$$

D_{50} = Median diameter at which 50% of material by weight is smaller than the size denoted (m).

This can be further evaluated to apply in a situation where by the overall depth of flow does not change, and the area increases (as equilibrium is reached). By assuming continuity between the mainstream channel and the contracted section equation 3.5 can be written in terms of velocity as;

$$Y_2 = Y_1 \left(\frac{B}{b} \right)^{\frac{6}{7}} \left(\frac{V_1^2}{36(Y_1)^{\frac{1}{3}}(D_M)^{\frac{2}{3}}} \right)^{\frac{3}{7}} \quad \text{Equation 3.6}$$

Where;

B = Bottom width of the upstream main channel



To determine the scour depth is then simply a case of ;

$$d_{sc} = Y_2 - Y_1 \quad \text{Equation 3.7}$$

Where Y_1 is depth of unobstructed flow (usually just upstream of the structure).

Laursen (1962) developed the following equation to estimate live-bed scour depths.

$$Y_2 = Y_1 \left(\frac{Q_2}{Q_1} \right)^{\frac{6}{7}} \left(\frac{B}{b} \right)^{k_1} \left(\frac{n_2}{n_1} \right)^{k_2} \quad \text{Equation 3.8}$$

Where all components are the same as in clear-water scour, Q_2 is the discharge through the contracted channel (width b), Q_1 is the flow transporting sediment upstream of the structure, k values are determined from table 3.5-1 shown below and n values are Mannings roughness coefficients.

Value of U_1^*/w	k_1	k_2	Mode of bed material transport
< 0.50	0.59	0.07	Mostly contact bed material
0.50–2.0	0.64	0.21	Some suspended bed material discharge
> 2.00	0.69	0.37	Mostly suspended bed material discharge

$U_1^* = (g Y_1 S_{F1})^{1/2}$ is the shear velocity in the upstream section (m/s)
 g = acceleration due to gravity (9.81 m/s²)
 Y_1 = average depth in the upstream main channel (m)
 S_{F1} = slope of energy grade line in main approach channel (dimensionless). Usually assumed $S_F = S_0$.
 w = the median fall velocity (m/s) of the bed material based on D_{50} (see Fig. 8.18)
 After Richardson *et al.* (1993)

Table 3.5-1 - Exponents for determining live-bed contraction scour for use with equation 3.8. Calculate U_1^* / w using the footnotes, then determine the appropriate values of k_1 and k_2 to be used in equation 3.8. (Hamill, 1999)

3.5.3 LOCAL PIER SCOUR DEPTH

Local pier scour is influenced by pier shape and alignment in addition to the characteristics for the channel and approach flow. As a general guide the ratio of pier scour depth to width (d_{sp} / b_p) for round-nosed piers aligned with the flow does not exceed about 2.3 or 2.4 when Froude number is less than 0.8, but can range up to 3.0 for larger Froude Numbers.

For clear-water and live-bed conditions Richardson *et al.* (1993) recommended the Colorado State University (CSU) equation for the estimation of equilibrium pier scour depth (d_{sp}).



$$d_{sp} = 2.0 Y_2 K_{1p} K_{2p} K_{3p} \left(\frac{b_p}{Y_2} \right)^{0.65} F_2^{0.43}$$

Equation 3.9

Where Y_2 is the flow depth (m) at the bridge section directly upstream of the pier (m), K_{1p} is an adjustment factor for pier nose shape obtained from table 3.2 for $\phi < 5^\circ$, K_{2p} is an adjustment factor for the angle of attack ($\phi < 5^\circ$) obtained from figure 3.3, K_{3p} is an adjustment factor for bed configuration from table 3.3, b_p is the pier width (m), F is the Froude Number where

$$F = \frac{V_2}{\sqrt{g Y_2}}$$

Note: If $\phi > 5^\circ$ then K_{1p} can be taken as 1.0

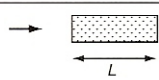
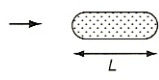

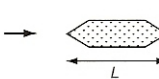
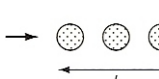
Shape of pier		K_{1p}
Square nose		1.1
Round nose		1.0
Circular cylinder		1.0
Sharp nose		0.9
Group of cylinders		1.0

Table 3.5-2 - Adjustment factor for pier nose shape applicable when $\phi < 5^\circ$

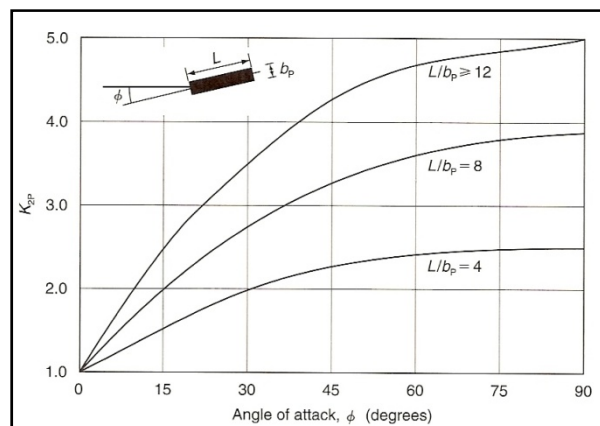


Figure 3.5-1 - Pier skew correction factor for use with equation 3.9. If $\phi < 5^\circ$ K_{2p} can be ignored. (Hamill, 1999)



<i>Bed condition</i>	<i>Dune height, H (m)</i>	<i>K_{3p}</i>
Clear-water scour	Not applicable	1.1
Plane bed and antidunes	Not applicable	1.1
Small dunes	0.6–3.0 m	1.1
Medium dunes	3.0–9 m	1.1–1.2
Large dunes	> 9 m	1.3

Table 3.5-3 - Increase in equilibrium pier scour depths for various bed conditions. (Hamill, 1999)

3.6 HYDRODYNAMIC FORCES ON PIERS

The hydrodynamic forces on piers are the drag forces (downstream of the pier) caused by wake vortices and the lift forces (upstream of the pier) caused by horseshoe vortices.

Drag Force

$$F_D = \frac{C_d \rho V^2 YL}{2000} \quad \text{Equation 3.10}$$

Lift Force

$$F_L = \frac{C_L \rho V^2 YL}{2000} \quad \text{Equation 3.11}$$

Where; C_L and C_d are the dimensionless coefficients of lift and drag respectively, ρ is the density of the water, V is the approach velocity, Y is the depth of flow upstream of the pier, L is the length of the pier in the direction of flow.

The hydrodynamic forces on piers are usually small, when compared with ship impact calculations. C_d and C_L depend on factors such as the shape and spacing of the piers, the angle of attack, and Reynolds number of the flow (Apelt and Isaacs, 1968; Farraday and Charlton, 1983).

Refer to figure 1.4-1 for approximate drag coefficient values.



3.7 SUMMARY

Ensuring safety to civilians is of paramount importance when designing civil structures. Engineering failures have been the cause of significant research focused on the hydraulic phenomenon's occurring behind bridge piers.

When designing bridge piers, not only are the structural and impact requirements important design criteria, but consideration to the effects of scour are just as important.

Drag and lift coefficients of piers have an immense impact on the hydrodynamic forces exerted on piers. This is indirectly related to the degree of scour and vortex shedding that will occur. Generally it is safe to assume that a pier with a large drag coefficient will have a larger scour pattern and shed a higher degree of vortices than that with a smaller drag coefficient.



CHAPTER 4 - METHODOLOGY AND EQUIPMENT

4.1 OUTLINE

This chapter will focus on the methods and defining factors that will provide the basis for testing.

The aim of the experiments is to confirm that results are similar to those of Herron's (2007) and then determine differences between the aerofoil pier and a circular pier. Testing will provide a better understanding of vortex shedding that occurs behind the two pier types.

4.2 EQUIPMENT AND FACILITIES

4.2.1 HYDRAULIC FLUME

Data collection for the research will be carried out at the University of Southern Queensland's *Water Engineering and Thermodynamics Laboratory*. Tests will be performed in a hydraulic flume with a bed width of 0.61m and depth of 0.125m.

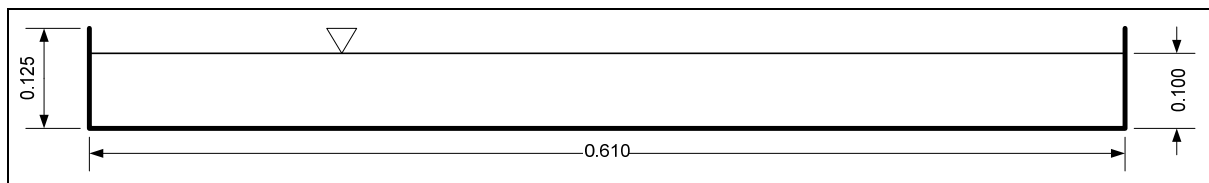


Figure 4.2-1 - Cross Section of the Flume

The flume is capable of producing sub-critical flows as well as super-critical flows. There is a weir at the down stream end of the channel that allows the transition between super-critical and sub-critical flows. There is also a set of rails on the flume, these are what the measuring device will operate on, this will be discussed later in the chapter.

A centrifugal pump circulates the flow within the flume and runs at a constant speed. The flow rate is controlled by a valve at the pump outlet. There is a flow-meter attached to the valve which displays the flow rate in litres per minute.



4.2.2 ACOUSTIC DOPPLER VELOCIMETER

An Acoustic Doppler Velocimeter (ADV) was used to measure flow velocities within the channel. This is made up of a probe that is able to measure velocities in three dimensions within the flow, and a connection cable so that a computer can record data.

The velocity measurements collected by the ADV are vector-averaged internally. The averages of the measurements are outputted and recorded at the chosen sampling rate. The default sampling rate for the probe is 1Hz. The sampling rate may be set between 0.1Hz and 25Hz. A sampling rate of 100Hz is also possible. For this research the default sampling rate was used.

The sample sizes available to be used are 3mm, 6mm, or 9mm (9mm is the default). Smaller sample sizes result in an increase in noise, thus a decrease in precision of measurements. The sample size is simply the number of measurements that are averaged in the velocity calculation (Herron, 2007).

There are various detachable probes that can be used with the ADV. This research is concerned with velocities travelling in the down stream direction and cross stream direction. As a result the probe used will be one that faces the direction of flow. This can be seen in figure 4.2-2.

The probe consists of an emitter and three receivers. A signal is emitted from the centre of the probe end, and the three receivers are able to interpret three dimensional velocities by variations in the return signal.

In order to obtain sufficient time averaged velocities, the ADV must record over a specific period of time (determined by the user, and varies according to the application it is being used for). For this research, velocities were recorded for a period of 50 seconds, as the phenomenon of vortex shedding would have occurred several times in this interval.

There are possible problems that can be associated with the Nortek ADV the main ones being noise and spiking in the data. Reflective materials have been known to create noise problems when measuring velocities near their surface. By dampening the surface the noise may be reduced (Nortek AS 2000).

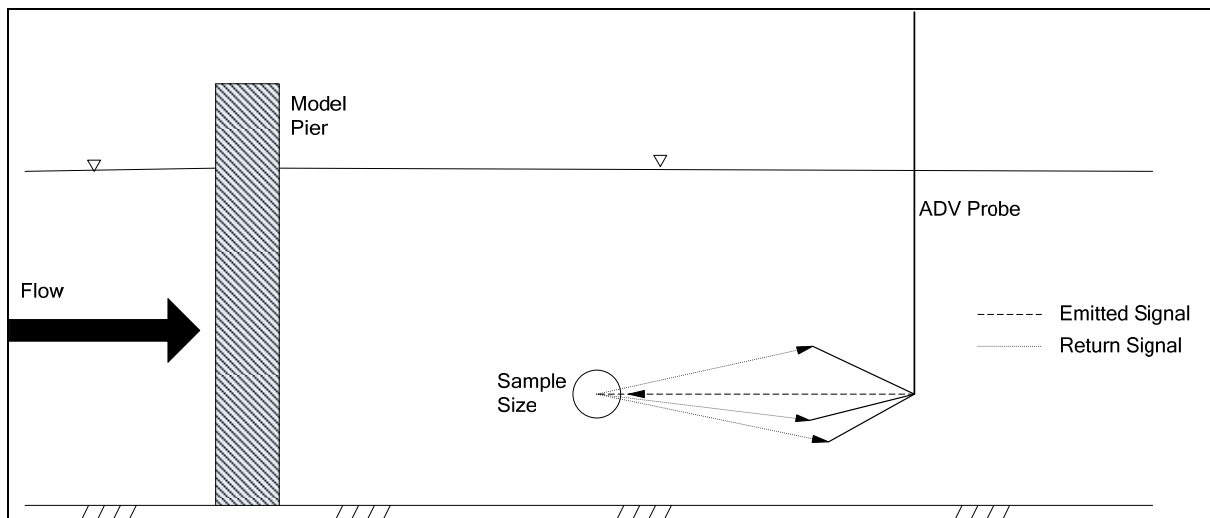


Figure 4.2-2 - A signal is emitted from the centre of the probe, and a return signal is received by each of the three probes.

4.2.3 COLLECT V SOFTWARE

The ADV is able to attach to a computer via a cable to a com port. There are several software packages that can collect data from the ADV. The software that USQ uses is CollectV™. CollectV software can be used to determine boundary profiles within the channel and collect velocities recorded by the ADV. Whilst velocities are being recorded they are displayed on the screen as a moving plot that shows velocities(cm/s) vs time(s). This data can be interpreted by the user instantly whilst recording, or the data can be saved as a 'csv' file for use on other computers.

The software enables the user to determine the condition of the probes, this can be done with a configuration section within the software. A display of the probe check is shown in figure 4.2-3 and with reference to the CollectV software manual, it can be confirmed that the probes are working correctly.

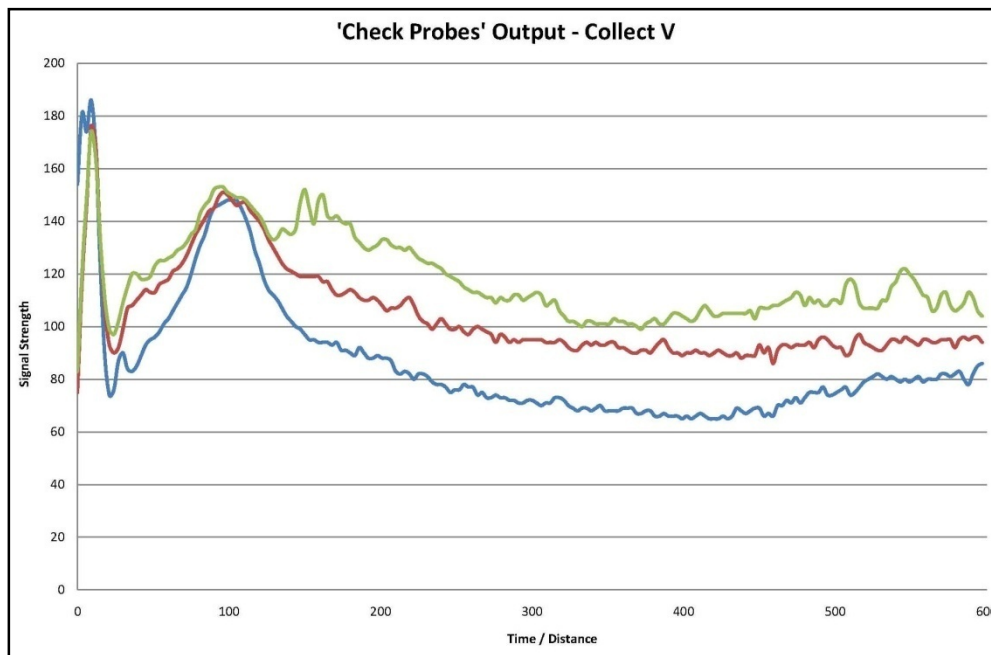


Figure 4.2-3 - The is the plotted output of a probe check from CollectV. This data has been exported and plotted with Microsoft Excel™. The plot shows signal strength vs the dime/distance.

While data is being collected the plot may be paused. This will pause the plotting of velocities against time only. The data collection will not be paused. It is possible to flag important events such as changes to the flow. In the exported data file a number will represent the time period after a flagged event. In the exported data file a number will represent the time period after a flagged event. If no data is flagged this value will remain 0. This value will increase for every event that is flagged. Table 4.2-1 shows the columns of an extracted velocity file. Column 1 counts the velocity recordings. Column 2 is the relative time at which the recording was taken. Column 3 shows the flagged data. The last three columns show the velocities in the x, y, and z directions (in this case, x = cross stream velocity, y = down stream velocity, and z = vertical velocities within the fluid flow) (Herron, 2007)

Sample	Time	Event Counter	Velocity		
			x	y	z
1	1.5	0	2.62	-18.71	-0.99
2	2.5	0	3.37	-17.78	0.15
3	3.5	1	4.02	-18.35	0.11
4	4.5	1	2.11	-18.69	-0.44

Table 4.2-1



For this research only two-dimensional velocities have been considered. This is because the bottom of the flume is non-erodible and as a result vertical velocities within the flume would be unrealistic.

4.2.4 MECHANICAL FRAME

The mechanical frame used has been constructed by USQ staff. It is an electrical frame that is designed to hold the ADV and position it accordingly. It is set up so that there is a point (0,0), which is well out of the water and to one side of the flume, each time the frame is turned on, it will default to this position. From here a coordinate system can be developed. This is done so by entering an x distance and a y distance. The frame will then move from the position (0,0) to the specified location.

Through experimental procedure, it was found that the centre of the flume was at 335mm in the x direction from the position (0,0). This can be seen in figure 4.2-4.

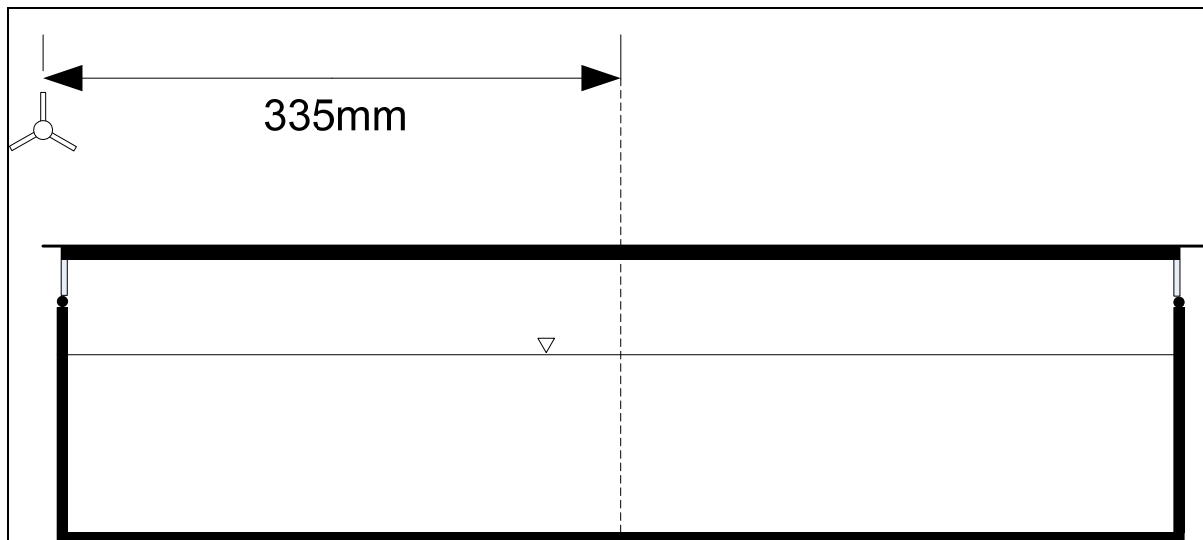


Figure 4.2-4 - Relative position of ADV to the flume.

The combination of the frame and the electrical movement system allows the ADV to be positioned at any $x y z$ coordinate within the system. There is a ruler along one side of the ADV which allows the z distance (distance in the downstream direction) to be measured accurately. This is shown in figures 4.2-5 - 4.2-7.

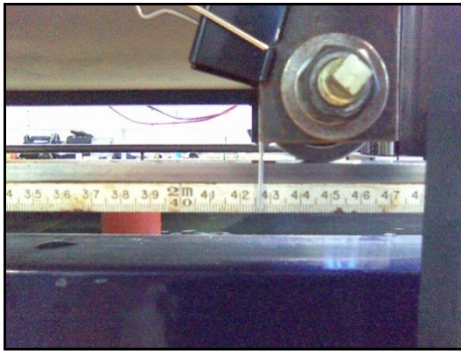


Figure 4.2-5 - Side rule on the flume

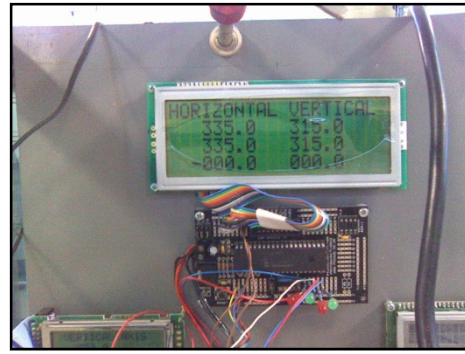


Figure 4.2-6 - Digital positioning system on the frame

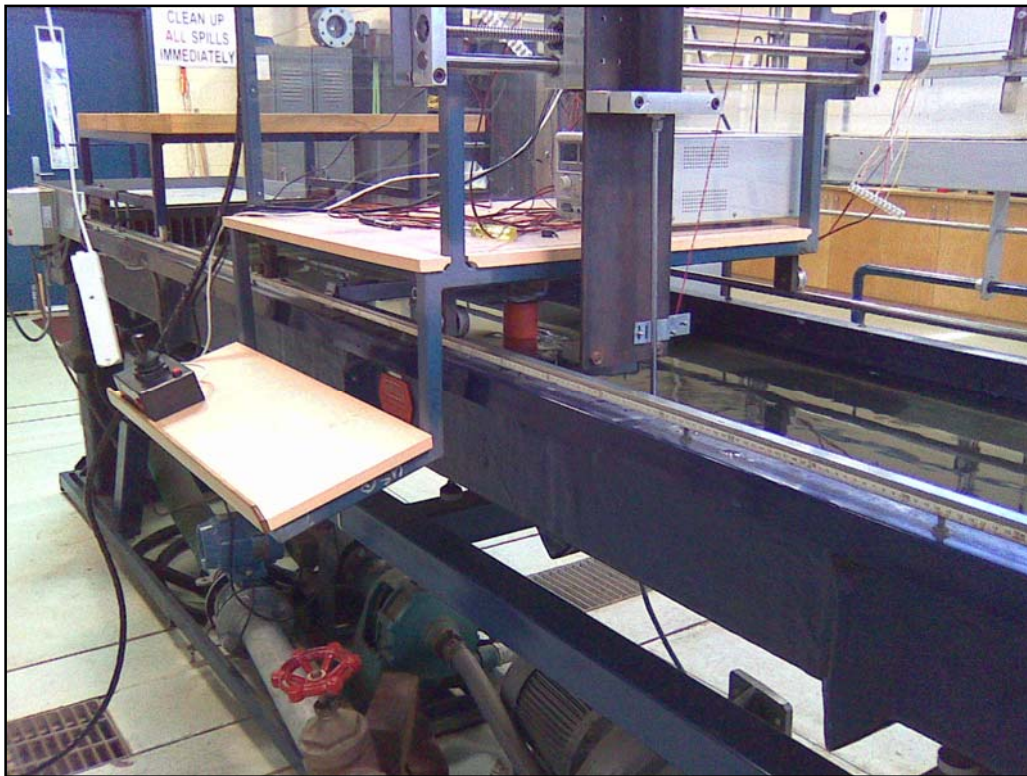


Figure 4.2-7 - Overall scope of the mechanical frame working on the flume.



4.3 DEVELOPMENT OF THE MODELS

To make this research more meaningful, the Bremer River Bridge was modelled. This would aid in determining whether or not the aerofoil shape pier can be useful in a real situation. The Bremer River Bridge is located on the Warrego Highway, approximately 7km North-east of Ipswich, QLD, AUSTRALIA.

Reason for selecting the Bremer River was because of the characteristics of the river bed. At the location of interest there is a wide base, which makes it easier to model in the laboratory. There was also substantial flow data and the bridge design files were accessible. Once this information was available, it was necessary to determine a flood event for which the piers will be tested (as the most destructive scour is caused in flooding conditions). The flow rate used was taken from the design files and based on a 1955 flood depth.

Flood statistics and a cross-sectional view of the Bremer River Bridge can be found in appendix G.

4.3.1 DIMENSIONAL ANALYSIS

The size of a river model is usually determined by the laboratory space available. In the case of a long river reach a natural model scale may result in such small flow depths that the depth and water elevations cannot be measured with sufficient accuracy, the flow in the model may become laminar, surface tension effects may become significant and sediment studies may be precluded because of the low tractive force. (Nalluri, 2001)

Dimensional analysis is a powerful tool for deriving the dimensionless relationships for a given system. The methodology has long been used by engineers and scientists, and the techniques have been progressively refined over the years. There are three main methods of dimensional analysis, (1) the indicial method, (2) Buckingham's method and (3) the matrix method. However it must be recolourised that all methods are absolutely dependent on the correct identification of all the factors which govern the physical events being analysed. The omission of a single factor may give quite misleading results (Borthwick, 2004).



In using physical scale models to predict the behaviour of prototype systems or designs it is rarely possible (except when only one force type is relevant) to achieve simultaneous equality of the various force ratios. The 'scaling laws' are then based on equality of the predominant force; strict dynamic similarity is thus not achieved resulting in the 'scale effect'.

Reynolds modelling is adopted for studies of flows without a free surface such as pipe flow and flow around submerged bodies, e.g. aircraft, submarines, vehicles and buildings.

The Froude number becomes the governing parameter in flows with a free surface since gravitational forces are predominant. Hydraulic structures, including spillways, weirs and stilling basins, rivers and estuaries, hydraulic turbines and pumps and wave-making resistance of ships are modelled according to the Froude law. (Nalluri, 2001)

For this research the Froude scaling method has been applied.

4.3.2 FROUDE SCALING METHOD

Plans of the Bremer River Bridge have shown depths of flow relative to the piers. For ease of modelling the piers in the flume, a segment of the flow has been selected. This segment can be seen in the appendix G.

The section chosen was one pier from the river. Flows around this pier would not have been affected by the neighbouring piers. This is because the hydraulic phenomenon's occurring at each pier have not affected, or been affected by their neighbouring pier.

According to design files and estimates from the designers of the bridge, the mean flow rate expected at a full flood (similar to the 1955 flood event) is 2.61m.s^{-1} . This velocity will be modelled in the flume. To comply with pump capacities and safety requirements (i.e. no spillage of water) the fluid in the model will be 100mm deep in a 120mm deep flume.

This dimensional analysis will determine what actual flow in the flume, will represent a flow of 2.61m.s^{-1} in the Bremer River.

A cross section of the flume is shown in figure 4.2-1.



Depth of flow for a flow rate of 2.61 m.s^{-1} is 45 feet. Converting this to metres and taking into account the average depth of flow this is 20.56m. This means that 20.56m will equal 0.1m depth in the flume.

Each of the piers in the river are 2.44m diameter, and the width of the section of interest is 21.95m. Hence the effective width of the section is $21.95 - 2.44 = 19.51 \text{ m}$.

Hence the vertical scale and horizontal scale become,

$$\frac{1}{\lambda_y} = \frac{\text{literal}}{\text{lab}} = \frac{20.56}{0.1} = 205.60 \quad \text{Hence; } \lambda_y = 0.00486 \quad \text{Equation 4.1}$$

$$\frac{1}{\lambda_x} = \frac{\text{literal}}{\text{lab}} = \frac{21.95 - 2.44}{0.61} = 31.27 \quad \text{Hence; } \lambda_x = 0.03198 \quad \text{Equation 4.2}$$

Known parameters of the Bremer River are;

$$V_{BR} = 2.61 \text{ m.s}^{-1} \quad Q_{BR} = VA = 2.61 \times 20.56 \times 19.51 = 1,046.9 \text{ m}^3 \cdot \text{s}^{-1} \quad A_{lab} = 0.61 \times 0.1 = 0.061$$

Velocity required in the flume;

$$V_{lab} = V_{BR} \sqrt{\lambda_y} = 2.61 \times \sqrt{0.00486} = 0.1819 \text{ m.s}^{-1} \quad \text{Equation 4.3}$$

Therefore;

$$\begin{aligned} \frac{Q_{lab}}{Q_{BR}} &= \frac{V_{lab}}{V_{BR}} \frac{(xy)m}{by} = \lambda_y^{\frac{3}{2}} \lambda_x \\ &= \left(\frac{1}{205.6} \right)^{\frac{3}{2}} \left(\frac{1}{31.27} \right) \\ &= 10.835 \times 10^{-6} \end{aligned} \quad \text{Equation 4.4}$$

Hence;

$$\begin{aligned} Q_{lab} &= Q_{BR} \lambda_y^{1.5} \lambda_x = 1046.9 \times 10.835 \times 10^{-6} \\ &= 0.01134 \text{ m}^3 \cdot \text{s}^{-1} \rightarrow 11.34 \text{ L.s}^{-1} \rightarrow 680 \text{ L.min}^{-1} \end{aligned} \quad \text{Equation 4.5}$$

Now that the flows required to simulate this are known, it is also necessary to determine whether or not the flow is turbulent.

$$R = \frac{A}{P} = \frac{0.061}{(2 \times 0.1 + 0.61)} = 0.0753 \quad \text{Equation 9}$$



$$Re = \frac{VR}{\nu} = \frac{0.1819 \times 0.0753}{1.13 \times 10^{-6}} = 1.212 \times 10^4$$

Equation 4.7

Therefore the flow will be well into the turbulent region. This will ideal for the experiment and the onset of vortex shedding.

Because the depth of flow under a bridge is relative to the width and size of the piers, it is important to subtract the width of the pier. This has been done in this dimensional analysis. The width of river being modelled is infact 21.95m and the width of pier is 2.44m. So by doing the dimensional analysis to model a river that is $21.95 - 2.44 = 19.51\text{m}$ wide, by adding a pier scaled to 2.44m to the section, flow regimes will be similar to that for a channel 21.95m wide.

Because flow is relative to the diameter of the pier, a pier 2.44m wide would be $2.44/31.27 = 0.078\text{m}$ in the lab model. Therefore construct experimental piers that are 78mm in diameter.

A schematic diagram of the channel is shown below.

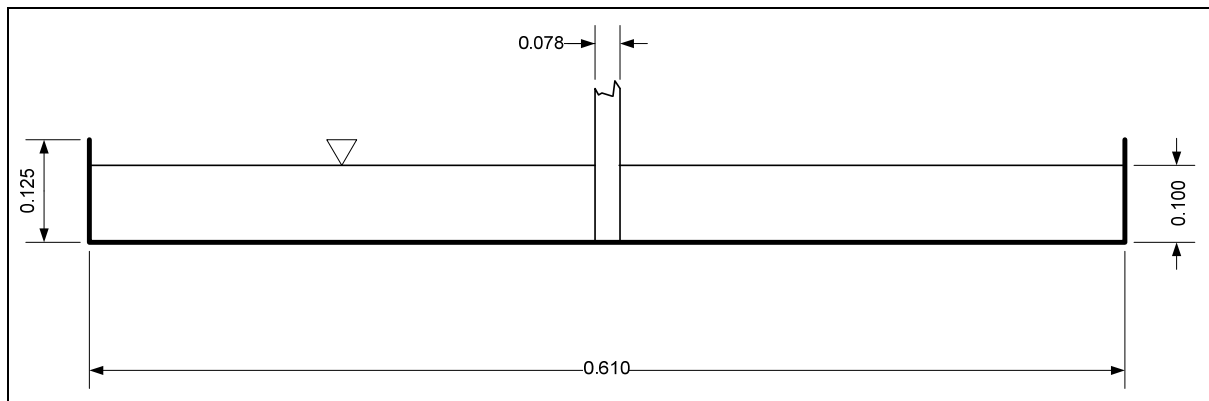


Figure 4.3-1 - Cross section of the channel with pier.

Due to some minor complications with the pump in the hydraulics flume it was not possible to accurately model the piers in a flow rate of 680L/min. However the system performed more accurately at 702L/min. By following the same method of dimensional analysis, it was possible to work backwards and conclude that this simulates a flow rate of 2.69m/s in the Bremer River (all other conditions remain the same, i.e. depth etc.). This also meant a velocity of 0.1918m/s in the flume.



$$\frac{Q_{lab}}{Q_{BR}} = \lambda_y^{1.5} \lambda_x \quad \text{Equation 4.8}$$

$$Q_{BR} = \frac{Q_{lab}}{\lambda_y^{1.5} \lambda_x} = \frac{702}{0.00486^{1.5} \times 0.03198} = 1079.8 m^3.s^{-1} \quad \text{Equation 4.9}$$

$$V_{BR} = \frac{Q_{BR}}{A_{BR}} = \frac{1079.8}{20.56 \times 19.51} = 2.69 m.s^{-1} \quad \text{Equation 4.10}$$

4.3.3 THE AEROFOIL PIER

The design of an aerofoil is much more complicated than simply putting a shape together, which is essentially what this research needed. The reasons for selecting the aerofoil shaped pier, is that the section of an aeroplane wing is designed to both minimise drag as much as possible in flying conditions and create drag as much as possible in landing conditions.

Traditionally an aerofoil is slightly ellipsoid at the front and has an uneven curvature throughout the section. A typical cross section of an aerofoil is shown in figure 4.3-2.

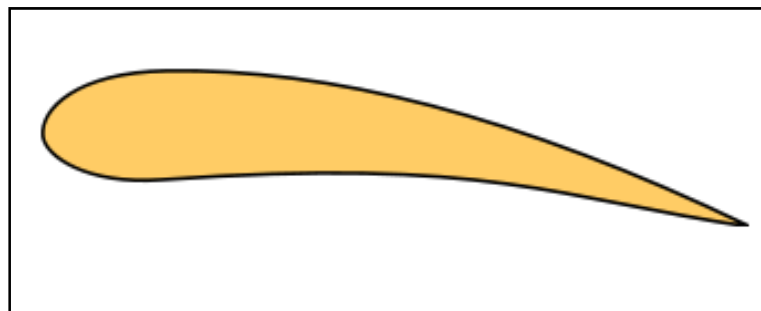


Figure 4.3-2 - Typical aerofoil design, with relevant features.

The aerofoil pier has been designed to that of a symmetrical aerofoil. The front of the pier has remained circular. This is for ease of comparison with the circular pier and keeps consistency with the dimensional analysis.

A symmetrical aerofoil section is shown in figure 4.3-3. This model has been slightly modified to meet the 78mm diameter circular front and can be seen in figure 4.3-4.

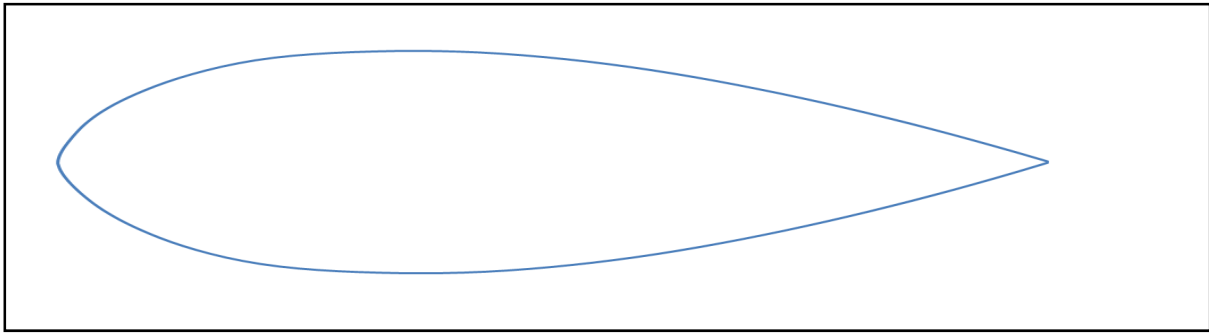


Figure 4.3-3 - Symmetrical aerofoil.

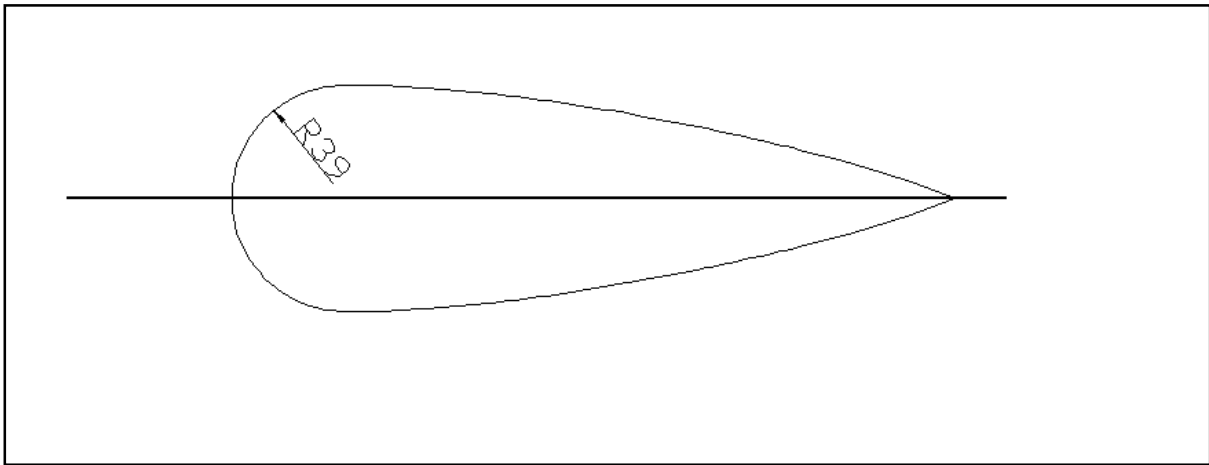


Figure 4.3-4 - Circular fronted aerofoil, based on a symmetrical aerofoil.

4.3.4 PIER CONSTRUCTION

The piers were constructed of HDPE material on a CNC milling machine at the University of Southern Queensland. This was done by the USQ Faculty of Engineering and Surveying Staff. The piers are shown in figures 4.3-5 and 4.3-6.



Figure 4.3-5 - Aerofoil Pier



Figure 4.3-6 - Circular Pier



4.4 EXPERIMENTAL METHOD

The size of the model piers has been determined, and the flow rates required to simulate the flows of the Bremer River have also been determined. The experimental method used to carry out the tests is similar to Herron's work (2007).

Model piers were positioned in the centre of the flume, so that side effects of the walls would not obstruct the flow. The piers were held in place with the holes in them and a frame made by the USQ staff (shown in fig 4.4-1). This meant that the only objects in the water were the ADV probe (downstream of the pier) and the pier being tested. The ADV was then positioned and velocities were recorded.

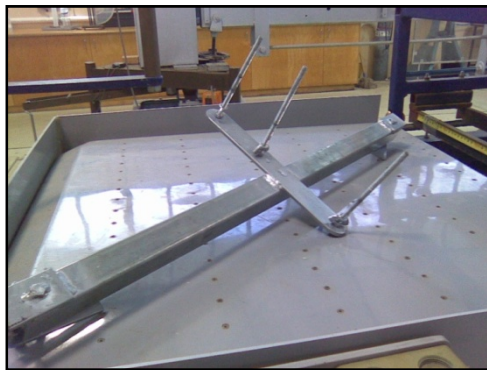


Figure 4.4-1- Frame used to hold piers in place, without obstructing flow

The probe was positioned 30mm to one side from the centre of the pier and 72mm downstream of the pier. (Ideally this would be less than 72mm, but due to physical limitations this was not possible). The probe was positioned and recorded velocities for a period of 50 seconds. This seemed an appropriate time for recoding of velocities behind the pier.

Once the 50 seconds had been recorded the probe was then moved back to 80mm behind the pier and the process continued. Once this was complete, a similar process continued up to 350mm downstream of the pier.

Once velocities were recorded up to 350mm, the probe was moved across stream 10mm and the same process continued.



The method of data acquisition can be seen in figure 4.4-1. This process was used for the aerofoil and circular pier.

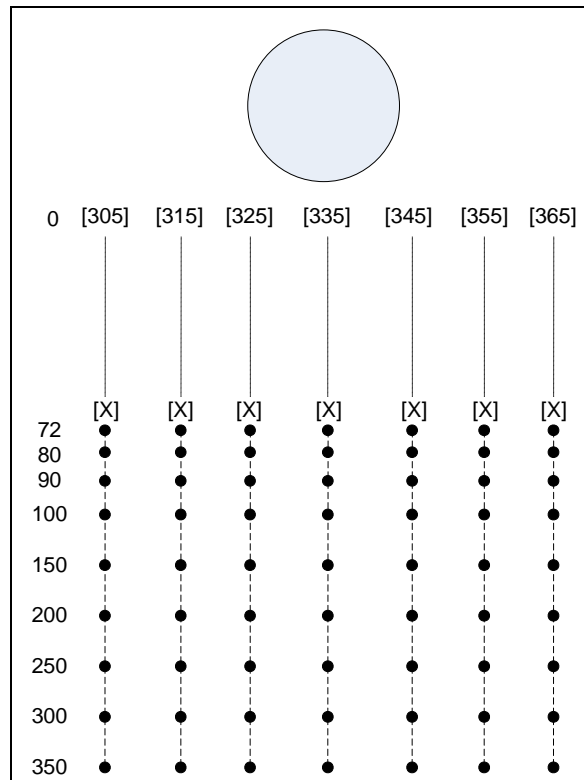


Figure 4.4-2 - Method used to record velocities at the pier.

4.5 SUMMARY

Experiments were performed so that the difference in vortex shedding between the aerofoil pier and the circular pier can be determined. These tests are important in relating theory and natural occurrences due to the highly unpredictable nature of fluid flow. These tests could shed important light on the future design of piers, particularly those shaped like aerofoils.



CHAPTER 5 - FLUENT™ AND GAMBIT™

5.1 OUTLINE

This chapter will outline the processes used to adequately describe the phenomenon's happening behind the piers. It will describe the mechanisms that FLUENT uses to calculate these phenomenon's and other programs used to assist with this. Results will be shown in appendix B. Measured velocities can be found in appendix E.

FLUENT is capable of solving three-dimensional and two-dimensional flow situations. However computational time, and time limitations allowed for only two-dimensional analysis to be carried out. Also due to bed conditions within the flume, three-dimensional flow in FLUENT would not accurately reproduce phenomenon's witnessed in the flume. This is because an equilibrium scour pattern could not be reached, hence vertical velocities in the flow are not an accurate representation of a real scenario.

5.2 GAMBIT™

The first step (and arguably the most important step) in a Computational Fluid Dynamics (CFD) solution is the generation of a grid that defines the cells on which flow variables (velocity, pressure, etc) are calculated throughout the computational domain. Modern commercial CFD codes come with their own grid generators, and third party grid generation programs are also available (Cimbala, Cengel, 2006). The grids used in this research are generated with FLUENT's grid generation package, GAMBIT.

GAMBIT is a Cad styled package that allows for a particular scenario to be developed and then a mesh applied to it. This is so that FLUENT can iterate through the equations of conservation at each point within the grid to arrive at a solution. These equations will be further discussed later in the chapter.



5.2.1 DEVELOPING THE MESH

So that FLUENT can accurately determine boundary layer phenomenon's around the walls and the pier in the flume, the mesh was developed so that it was very fine around the pier and walls. The section down stream of the pier was also made very fine so that the velocity movements could be accurately evaluated.

The flume was drawn in GAMBIT at a 1:1 scale. This can be seen in appendix D. The two types of piers, circular and aerofoil, were drawn and a mesh applied to them.

Once this was complete, the mesh was able to be exported into FLUENT for analysis.

5.3 FLUENT™

FLUENT is a computational fluid dynamics software that provides comprehensive modelling capabilities for a wide range of incompressible and compressible, laminar and turbulent fluid flow problems. Steady-state or transient analyses can be performed. In FLUENT, a broad range of mathematical models for transport phenomena (like heat transfer and chemical reactions) is combined with the ability to model complex geometries. Examples of FLUENT applications include laminar non-Newtonian flows in process equipment; conjugate heat transfer in turbomachinery and automotive engine components; pulverised coal combustion in utility boilers; external hydrodynamics; flow through compressors, pumps, and fans; and multiphase flows in bubble columns and fluidised beds. (FLUENT, v6.3 Documentation)

5.3.1 THE PRINCIPLES OF FLUENT

For all flows, FLUENT solves conservation equations for mass and momentum. For flows involving heat transfer or compressibility, an additional equation for energy conservation is solved. For flows involving species mixing or reactions, a species conservation equation is solved or, if the non-premixed combustion model is used, conservation equations for the mixture fraction and it's variance are solved. Additional transport equations are also solved when the flow is turbulent. (FLUENT, v6.3 Documentation)



5.3.2 THE EQUATIONS OF MOTION

The main motion equations that are solved throughout FLUENT are continuity, momentum in the x-direction, the y-direction, and the z-direction. For 2D analysis, only x and y momentum equations are solved. These equations apply for steady, incompressible fluid flow, for Newtonian fluids.

Continuity

$$\frac{\partial u}{\partial x} + \frac{\partial v}{\partial y} + \frac{\partial w}{\partial z} = 0 \quad \text{Equation 5.1}$$

x-momentum

$$u \frac{\partial u}{\partial x} + v \frac{\partial u}{\partial y} + w \frac{\partial u}{\partial z} = -\frac{1}{\rho} \frac{\partial P'}{\partial x} + \nu \left(\frac{\partial^2 u}{\partial x^2} + \frac{\partial^2 u}{\partial y^2} + \frac{\partial^2 u}{\partial z^2} \right) \quad \text{Equation 5.2}$$

y-momentum

$$u \frac{\partial v}{\partial x} + v \frac{\partial v}{\partial y} + w \frac{\partial v}{\partial z} = -\frac{1}{\rho} \frac{\partial P'}{\partial y} + \nu \left(\frac{\partial^2 v}{\partial x^2} + \frac{\partial^2 v}{\partial y^2} + \frac{\partial^2 v}{\partial z^2} \right) \quad \text{Equation 5.3}$$

z-momentum

$$u \frac{\partial w}{\partial x} + v \frac{\partial w}{\partial y} + w \frac{\partial w}{\partial z} = -\frac{1}{\rho} \frac{\partial P'}{\partial z} + \nu \left(\frac{\partial^2 w}{\partial x^2} + \frac{\partial^2 w}{\partial y^2} + \frac{\partial^2 w}{\partial z^2} \right) \quad \text{Equation 5.4}$$

5.4 FLUENT ANALYSIS

For this particular research the FLUENT boundary conditions are shown below. The same conditions were used for both piers.

$$V_i = 0.1918 \text{ m.s}^{-1} \quad \rightarrow \quad \text{Velocity at inlet, upstream of the pier.}$$

$$P_o = 1 \text{ Bar} \quad \rightarrow \quad \text{Pressure at the outlet was 1 atmosphere.}$$

$$\phi = 0.078 \text{ m} \quad \rightarrow \quad \text{Diameter of the piers was 78mm}$$



The mesh shown in figure 5.4-1 was used for the analysis. The circular pier was set to stationary non-slip boundary condition, as were the side walls of the flume. The left hand side of the mesh is defined as a velocity inlet. The right hand side of the mesh is defined as a pressure outlet. This was used because it was not possible to confirm the velocities at the outlet.

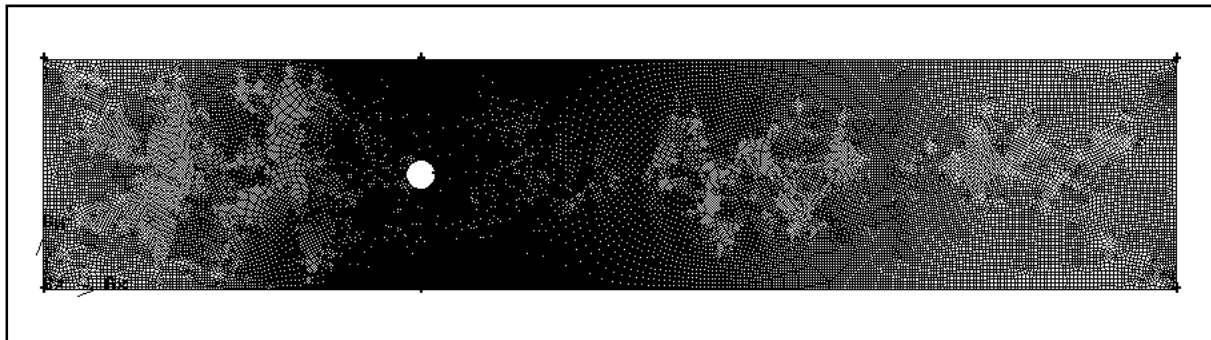


Figure 5.4-1 - Mesh developed in GAMBIT and used in FLUENT.

The set up of the aerofoil mesh was exactly the same as for the circular pier. A detailed case summary (for modelling in FLUENT) for each pier type can be seen in appendix C.

5.5 FLUENT RESULTS

The velocities obtained using FLUENT coincide with measured velocities down stream of the piers. The drag coefficients of the circular pier also match published drag coefficients (within reason) which indicates that the FLUENT model is a good representation of the experiment. The aerofoil however has a higher coefficient than published results (shown in figure 1.4-1). Reasons for this would be that the front of the pier is infact a semi-circle, and the l/d ratio is smaller than that of traditional aerofoils (traditional aerofoils l/d ratio is 5:1).

Note: The fluid model used for this analysis is laminar. Other researchers (Salaheldin T, Imran J, Chaudhry M, 2004) have used Reynolds averaged stress equations to simulate turbulent flows. These models have however been three-dimensional.

When modelled in FLUENT under Reynolds-averaged Navier Stokes (RANS) the software did not produce a realistic result, neither did other turbulence models within the software. Simulation under laminar flow was the only model to produce meaningful results.



CHAPTER 6 - ANALYSIS AND DISCUSSION OF RESULTS

6.1 OUTLINE

This chapter contains an analysis of the results from the experiments carried out in the USQ Hydraulics Laboratory. The results presented are a comparison between the CFD results and measured velocities within the flume.

The phenomenon of vortex shedding from both piers will be compared and analysed.

6.2 EXPERIMENTS

The phenomenon of vortex shedding was observed and recorded at various points behind the two piers. Also as an initial check velocities were recorded behind a 65mm diameter pier in the same flow rate as Herron (2007), and then compared to recorded results.

Velocities were recorded using the CollectV software, and then plotted using Microsoft Excel, this provided velocities at different points behind the piers, and allowed for confirmation of velocities within the FLUENT results. (i.e. confirming that FLUENT produced meaningful results).

6.3 QUALITY ASSURANCE OF THE SYSTEM

Herron (2007) confirmed that a 65mm circular pier in a flow of 305L/min would have a depth of 0.06m in the 610mm wide flume at USQ. Resulting in a theoretical velocity of 0.138m/s.

Part of Herron's results are shown here in figure 6.3-1, when compared with figure 6.3-2 it can be seen that the velocities are within reasonable range. When comparing this information, it is imperative that the type of flow being observed is considered. The analysis of turbulence behind a pier is both predictable and unpredictable. Meaning that it is possible to accurately evaluate or determine what frequency or magnitude the phenomenon's will occur at, however replicating these phenomenon's is somewhat impossible. Thus proving the un-steady state of flow. This is due to the unpredictability of fluid flow, particularly with turbulent situations. Hence the velocities being within a reasonable range (± 5 cm/s) is considered acceptable.

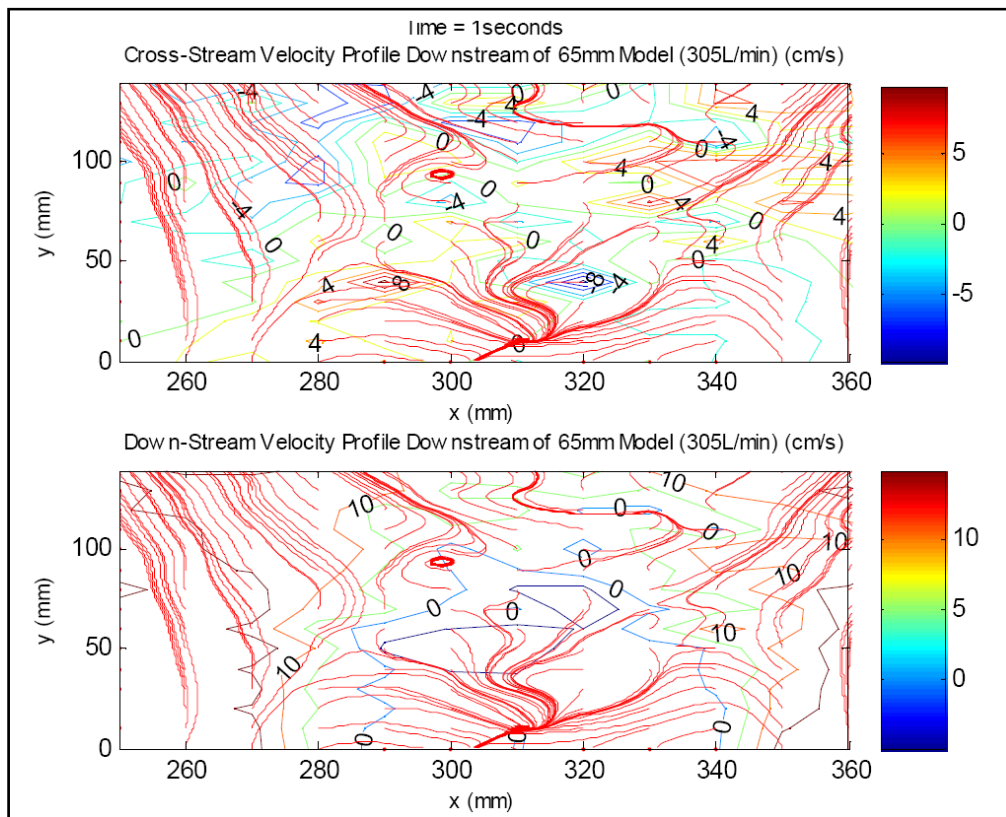


Figure 6.3-1 - Velocity contours downstream of the 65mm pier. $Q = 305\text{L/min}$. Lines represent velocity contours. (Herron, 2007)

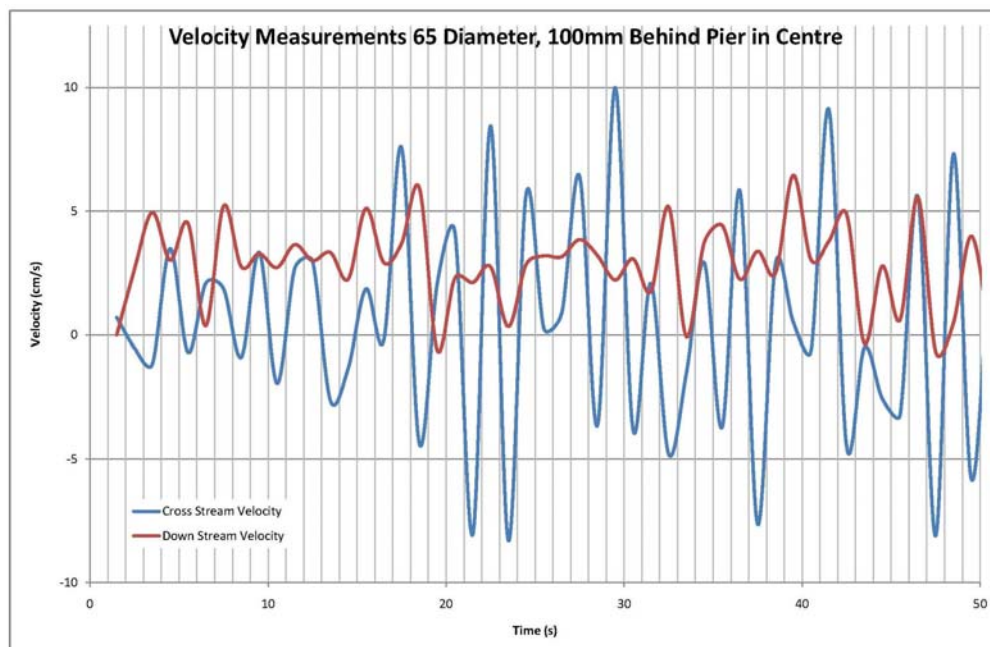


Figure 6.3-2 - Measured Velocities 100mm (in the centre) behind 65mm pier. Blue = Cross Stream Velocity, Red = Downstream Velocity.



Note that the measured velocities have been taken (relative to Herron's results shown in figure 6.3-2) at coordinate (310,100). Cross-stream velocities vary considerably, as expected due to the unsteady nature of the flow. The down stream velocities at this point remain rather small with small fluctuations. All velocity v time plots taken behind the 65mm pier can be found in appendix F.

It was also found that in Herron's work (Vortex Shedding on Bridge Piers, 2007), bricks were used within the flume to hold a 5mm thick grid in place. This could explain the slight differences in recorded velocities, the bricks and slight raise in the bed would have caused an increase in velocity around the piers; hence the slightly higher velocities.

6.4 THE CIRCULAR PIER

The circular pier was tested in the 100mm deep flow, with a theoretical velocity of 0.1918m/s. The phenomenon of vortex shedding occurred as expected and velocities were recorded. Plots of velocities against time can be found in the appendix E. The experiment was then modelled using FLUENT, the results from FLUENT can be seen in appendix B.

FLUENT claimed that the pier had a drag coefficient of 0.45 which coincides with published results reasonably well (Refer to fig 1.4-1, with $Re\ 1.212 \times 10^4$). The drag with respect to time is shown in figure 6.4-1. Oscillations in the drag coefficient are due to the movement of the fluid behind the pier.

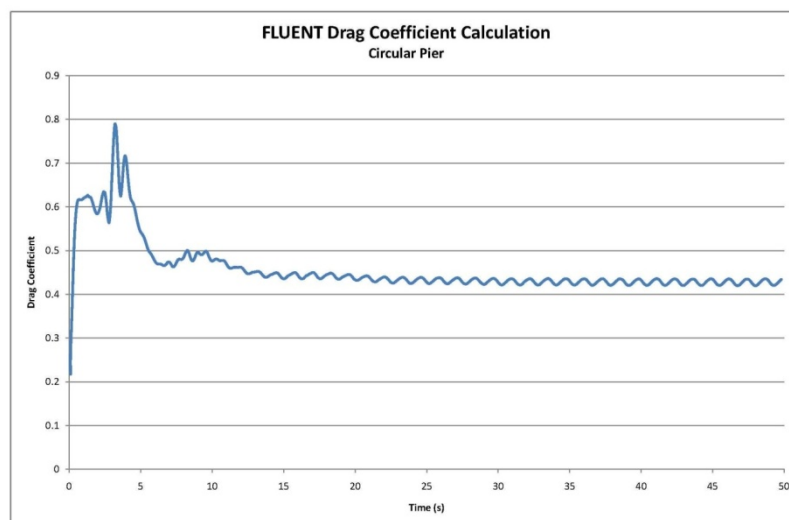


Figure 6.4-1 - Plot showing progress of FLUENT drag coefficient calculations with respect to time.



From this the lift force and drag force can be determined. The front of the aerofoil is still circular; hence the lift forces of the piers will not be compared because they are assumed to be the same for both cases.

Hence the drag force exerted on the pier would be;

$$\begin{aligned}
 F_{D_circle} &= \frac{C_d \rho V^2 YL}{2000} \\
 &= \frac{0.45 \times 998.2 \times 0.1918^2 \times 0.1 \times 0.078}{2000} \\
 &= 6.444 \times 10^{-5} \text{ kN}
 \end{aligned}
 \tag{Equation 6.1}$$

The scour pattern that would be expected in the flume can also be determined.

$$\begin{aligned}
 d_{sp_circle} &= 2.0 Y_2 K_{1P} K_{2P} K_{3P} \left(\frac{b_p}{Y_2} \right)^{0.65} \left(\frac{V_2}{\sqrt{g Y_2}} \right)^{0.43} \\
 &= 2.0 \times 0.1 \times 1.0 \times 1.0 \times 10 \times \left(\frac{0.078}{0.1} \right)^{0.65} \left(\frac{0.1918}{\sqrt{9.81 \times 0.1}} \right)^{0.43} \\
 &= 0.084 \text{ m}
 \end{aligned}
 \tag{Equation 6.2}$$

Hence the expected depth of scour in the flume would be around 85mm deep. This is assuming no bed material or movement. Which in reality is not possible. This has been determined purely as an example.

It is also possible to determine a theoretical shedding frequency using Strouhals number. Using equation 2.9 and 2.10 .

$$\begin{aligned}
 St &= 0.198 \left(1 - \frac{19.7}{Re} \right) \\
 &= 0.198 \left(1 - \frac{19.7}{\frac{0.1918 \times 0.078}{1.13 \times 10^{-6}}} \right) \\
 &= 0.1977
 \end{aligned}
 \tag{Equation 6.3}$$

$$\begin{aligned}
 St &= \frac{fL}{V} \\
 f &= \frac{0.1977 \times 0.1918}{0.078} \\
 f &= 0.486
 \end{aligned}
 \tag{Equation 6.4}$$

Hence a vortice will be shed approximately every 2 seconds. Results shown in appendix B confirm this.



The phenomenon of vortex shedding from the circular pier has been defined. An initial estimate for the expected scour pattern has also been provided.

6.5 THE AEROFOIL PIER

The aerofoil pier was tested in the 100mm same flow conditions as the circular pier. The phenomenon of vortex shedding was significantly reduced. Downstream turbulence was observed, however the magnitude and intensity of the turbulence was reduced considerably. Velocities were recorded behind the pier. Plots of velocity against time can be found in appendix E. The experiment was then modelled using FLUENT. These results are also published in the appendix B.

FLUENT determined that the pier had a drag coefficient of 0.33 which did not coincide with published results. The main reason for this is because the aerofoil shape of the pier is not a traditional 'aerofoil' shape. The length to width ratio of the pier is 3.2:1, meaning that the length of the pier is 3.2 times the width. Also the front of the pier is rounded, exactly the same as the circular pier. This was done for ease of construction of the models, and made comparison between the piers simpler (i.e. the result of reduction in down stream turbulence is because of the downstream part of the pier, since the upstream effects of the pier have remained the same as the circular pier).

The drag with respect to time is shown in figure 6.5-1.

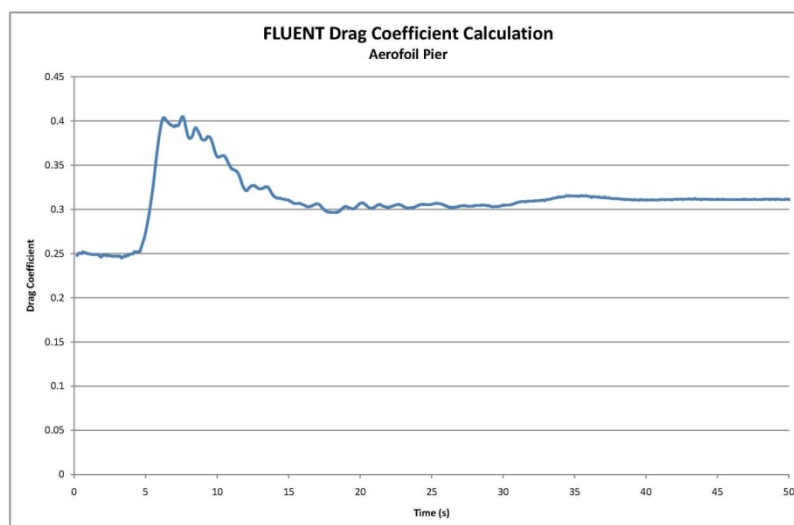


Figure 6.5-1 - Plot showing progress of FLUENT drag coefficient calculations with respect to time.



From this the drag force can be determined.

$$\begin{aligned}
 F_{D_aerofoil} &= \frac{C_d \rho V^2 YL}{2000} \\
 &= \frac{0.33 \times 998.2 \times 0.1918^2 \times 0.1 \times 0.078}{2000} \\
 &= 4.725 \times 10^{-5} \text{ kN}
 \end{aligned}
 \tag{Equation 6.5}$$

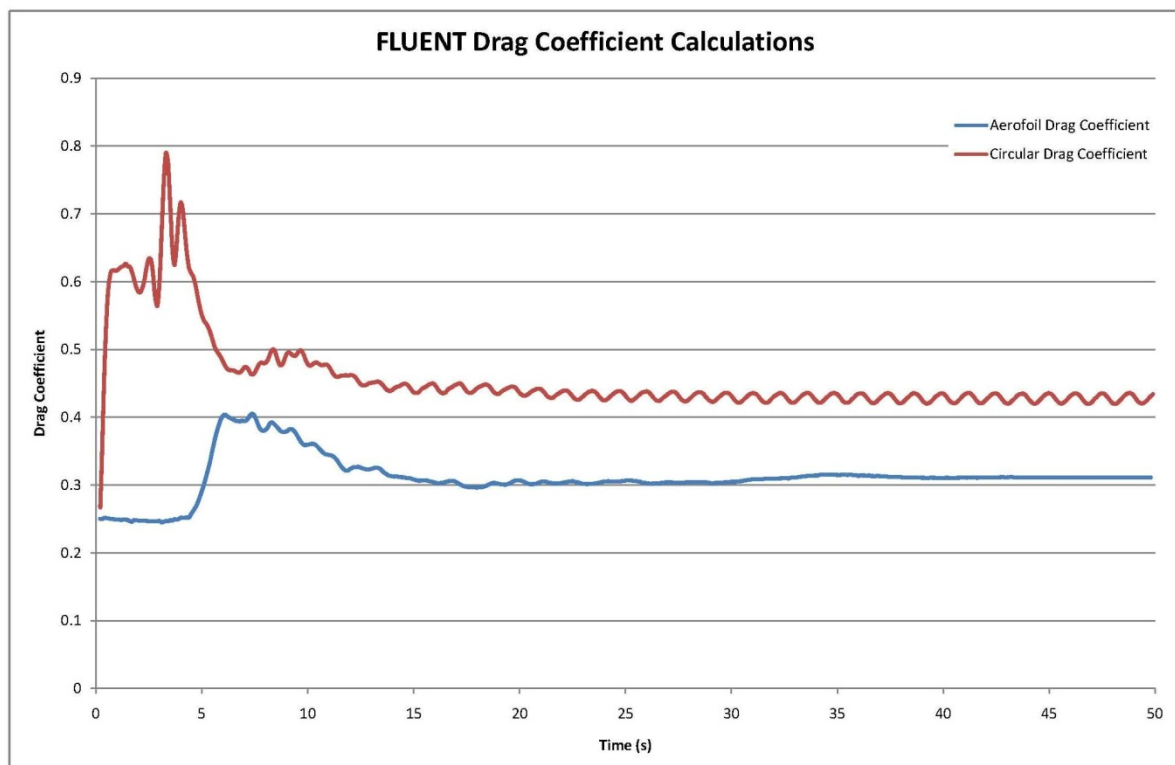
These results allow for a comparative view on the drag that the piers would exert.

$$\Delta F_D = 1 - \frac{4.725 \times 10^{-5}}{6.444 \times 10^{-5}} = 26.675\%
 \tag{Equation 6.6}$$

Therefore the aerofoil pier has produced a 26% reduction in drag forces on the pier.

The reduction in drag force is lower than expected (when compared to traditional aerofoils), this is because of the higher drag coefficient. CFD results show this also. The only cause for the higher than expected drag coefficient of the pier is because of the circular front, and the shortened length.

Figure 6.5-2 shown below is a comparative view of the drag coefficients for the two piers.



6.5-2 - Drag coefficient comparison. Red = Circular pier, Blue = Aerofoil pier

6.6 COMPARATIVE CONCLUSIONS

The FLUENT modelling of both piers has been successful and provided a good representation of the flows witnessed in the USQ Hydraulics Laboratory. Figure 6.6-1 shows vectors of velocity behind the circular pier at 50 seconds.

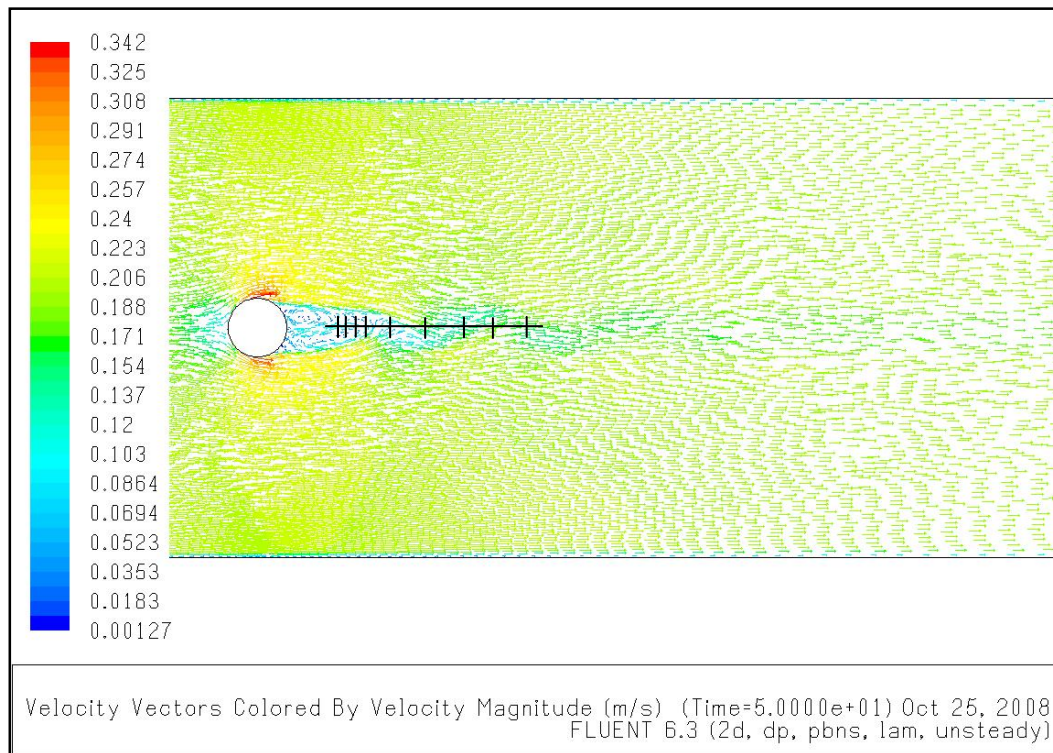


Figure 6.6-1 - Velocity vectors produce by FLUENT. The circular pier is 78mm diameter. Marked points show where velocities were recorded.

This is a specific snap-shot of an instance in time. The plot shows vortices occurring immediately behind the pier and the wake forming downstream of the pier. The velocities behind the pier match the measured velocities within ± 2 cm/s. The markers on the diagram show where velocities were measured. Table 6.6-1 shows the range in measured velocities over time in comparison with FLUENT results.

Absolute Values	Distance Behind Pier (mm)							
	72	80	90	100	150	200	250	300
Measured Velocity Range (cm/s)	0 - 10	0 - 15	0 - 14	0 - 19	0 - 20	0 - 15	4 - 18	6 - 18
FLUENT Velocity (cm/s)	0 - 12	0 - 13	0 - 13	0 - 17	0 - 20	0 - 17	4 - 18	6 - 18

Table 6.6-1 - Comparison of measured velocity magnitudes and FLUENT velocity magnitudes for the circular pier.

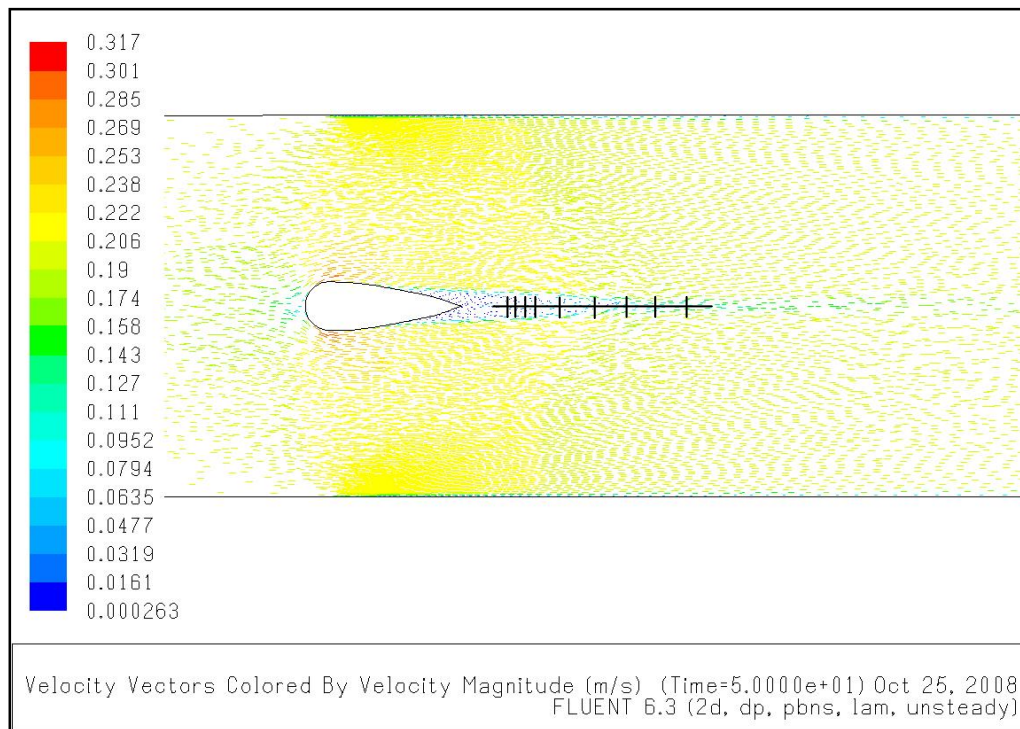


Figure 6.6-2 - Velocity vectors produce by FLUENT. The circular pier is 78mm diameter. The dense patches on either side of the pier are due to the mesh used for the analysis. This mesh has not affected the flow around the pier and can be ignored. Marked points show where velocities were recorded.

Again figure 6.6-2 is a specific snap-shot of an instance in time. The plot shows vortices occurring immediately behind the pier. The velocities behind the pier match the measured velocities within reason. These can be seen in table 6.6-2. The drag that was discovered in section 6.5 is shown here also. It is important to recognise that the vectors behind the pier, are very small in magnitude. This indicates that the moving behind the pier is moving slowly, and having very little impact on the flow around the pier.

Absolute Values	Distance Behind Pier (mm)								
	72	80	90	100	150	200	250	300	350
Measured Velocity Range (cm/s)	0 - 3	0 - 3	0 - 3.5	0 - 2.5	0 - 2	0 - 1.5	0 - 1.5	12 - 18	14 - 19
FLUENT Velocity (cm/s)	0 - 4	0 - 4	0 - 4.7	0 - 4	0 - 4.7	0 - 2	0 - 14.3	11 - 19	12.7 - 20.6

Table 6.6-2 - Comparison of measured velocity magnitudes and FLUENT velocity magnitudes for the aerofoil pier.

There is no fluctuation of velocities from side to side, as is expected for a circular pier. From this it can be concluded that the onset of vortex shedding has been significantly reduced, and the pier is having minimal effect on the flow.

As for as the matter of scour, it is difficult to say with confidence that there will be no scour. This is because of the region behind the pier where velocities are disrupted. However, the

scour would be significantly smaller than that of the circular pier. This is because of the symmetry associated with the flow. Further testing is required in this area.

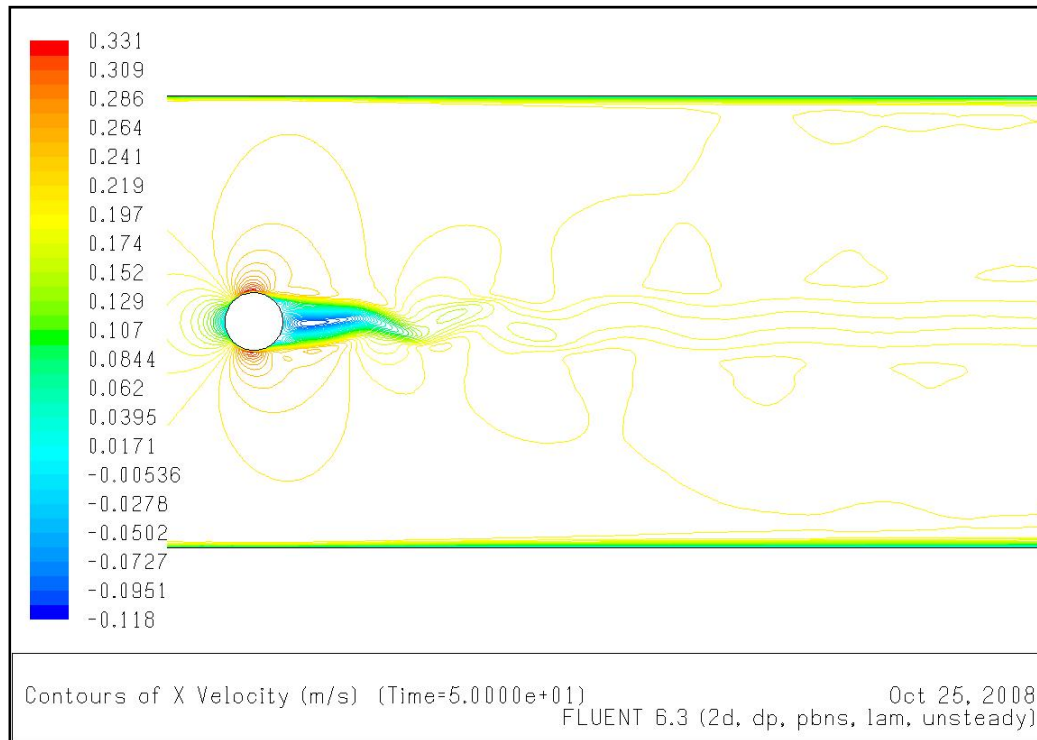


Figure 6.6-3 - Down stream velocity contours produce by FLUENT.

Figure 6.6-3 shows the down stream velocity contours that occur around the pier in this flow situation. This plot accurately shows the velocity patterns that occur behind the circular pier, and match measured velocities reasonably well along with visual confirmation throughout the testing period.

When this is compared with the aerofoil pier, shown in figure 6.6-4 it is obvious that the onset of vortex shedding has been significantly reduced. The flow remains largely uninterrupted except for the low velocity region immediately behind the pier. The region has negative velocities within it, meaning that flow is moving back toward the pier, (indicating that there is some backwash occurring). However the magnitude of these velocities is so small it would have no significant effect on the flow. Recorded velocities have shown this.

Also note the flow pattern occurring upstream of the pier. It is very similar, to the flow pattern that occurred upstream of the circular pier. This confirms that the hydraulic phenomenon's upstream are the same, due to the circular front of the aerofoil shaped pier.

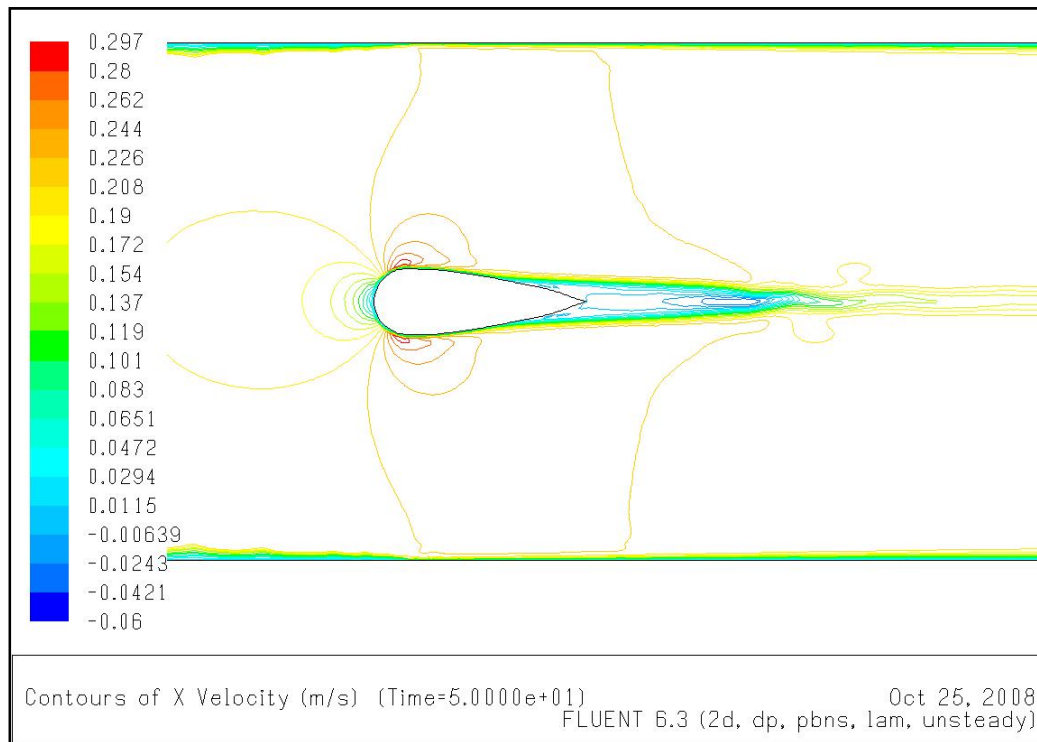


Figure 6.6-4 - Contours of downstream velocity produced by FLUENT.

From the results shown, it is plausible to say that the degree of scour formed from the aerofoil pier would be considerably smaller than that of the circular pier. Because of the 'uniqueness' of the pier shape, it is difficult (without further experiments, which will be discussed in the next chapter) to determine just what scour pattern will form behind the pier. However results from this research shed promising insight into the possibilities.

6.7 SUMMARY

Through modelling of the system in FLUENT, it is obvious that the onset of vortex shedding has been significantly reduced by the aerofoil shaped pier. The various plots used have aided in determining this, along with measured velocities.



The full details of the measured velocities can be found on the CD copy of this research. Key velocity measurements have been shown in the appendix, along with a variation of FLUENT results for the same flow situation. These will show how much the aerofoil shaped pier reduced downstream vortices and turbulence. From the reduction in turbulence, it is possible to conclude that the effect of scour would have also been significantly reduced.

CHAPTER 7 - FUTURE RESEARCH

This research has observed the phenomenon of vortex shedding from both a circular pier and an aerofoil pier. Results have shown that the aerofoil shaped pier has been effective in reducing the downstream vortices considerably. Through reviewed literature, development and testing of the piers several key areas for future research have been identified. These areas are;

- A detailed study into variations of the aerofoil shape. This research has examined only one pier as a starting point. The research would consider the front of the pier also, and look at different possibilities rather than the circular front used in this research.
- A study into construction possibilities for the pier. What materials could be used to construct such a pier, and will they meet the structural requirements.
- Carry out similar experiments on an erodible bed so that an actual scour pattern can be determined, rather than a theoretical estimate. This would also confirm the accuracy of this research.

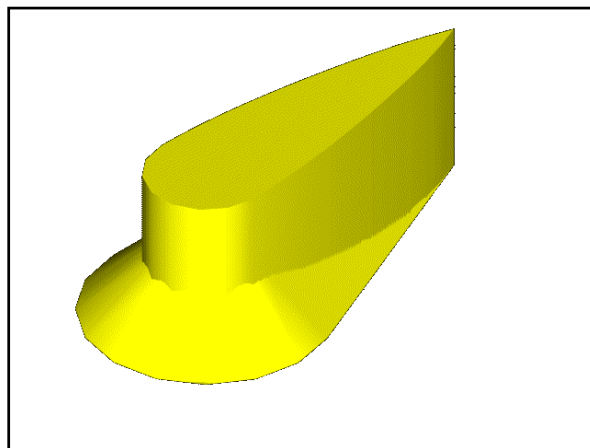


Figure 7.1 - Future possibility for aerofoil pier.

- Figure 7.1, shown above is what this research would consider the 'ideal' pier. The 45 degree incline on the front of the pier has shown good results in reducing the effects of horseshoe vortices, and this research has shown that the aerofoil pier has significantly reduced down stream shedding and turbulence. By combining the two



together it may be possible to reduce all vortices. Testing for this would be on an erodible bed so that the scour pattern can be observed.

- Further analysis with FLUENT software.



REFERENCES

1. Borthwick Martin, Chadwick Andrew, Morfett John 2004, *Hydraulics in Civil and Environmental Engineering*, Fourth Edition SPON Press, London.
2. Dargahi, B. 1990, *Controlling Mechanism of Local Scouring*, ASCE, 1990, 116(10): 1197 - 1214.
3. Farraday, R., Charlton. F., 1983, *Hydraulic Factors in Bridge Design*, Hydraulics Research Station Limited, Wallingford, Oxfordshire.
4. Featherstone R. E., Nalluri C. 2001, *Civil Engineering Hydraulics*, Fourth Edition, Blackwell Science, Carlton Victoria.
5. Hamill Les 1999, *Bridge Hydraulics*, E & FN SPON, London.
6. Herron, K., 2007, *Vortex Shedding on Bridge Piers*, University of Southern Queensland, Toowoomba.
7. Kirkil Gokhan, Constantinescu George, Ettema Robert n.d., *The Horseshoe Vortex System Around a Circular Bridge Pier on a Flat Bed*, The University of Iowa, Iowa City.
8. Overman, M. 1975, *Man, The Bridge Builder*, Priory Press, Hove, England.
9. Pope, Stephen B. 2000, *Turbulent Flows*, Cambridge University Press, Cambridge.
10. Roshko, A., 1976, *Structure of Turbulent Shear Flows - A New Look*, AIAA Journal, Vol. 14, 1349-1357
11. Schlichting H. Gersten K. 2000, *Boundary Layer Theory*, 8th rev. and enl. Ed., Springer, Berlin.
12. Transportation Association of Canada 2004, *Guide to Bridge Hydraulics*, Second Edition, Thomas Telford, London
13. Troitsky M. S. 1994, *Planning and Design of Bridges*, John Wiley and Sons, Toronto
14. Xanthoakos Petros P 1995, *Bridge Substructure and Foundation Design*, Prentice Hall PTR, New Jersey
15. Zhao, M., Hue, A., 2006, *Large-Eddy Simulation of Three-Dimensional Turbulent Flow Around a Circular Pier*, Journal of Hydrodynamics.
16. Zima Laura, Ackermann Norbert L., *Wave Generation in Open Channels by Vortex Shedding from Channel Obstructions*, Journal of Hydraulic Engineering, June 2002, pp596-203.



BIBLIOGRAPHY

1. Borthwick Martin, Chadwick Andrew, Morfett John 2004, *Hydraulics in Civil and Environmental Engineering*, Fourth Edition SPON Press, London.
2. Cao S, Tamura Y, *Flow Around a Circular Cylinder in Linear Shear Flows at Subcritical Reynolds Number*, Journal of Wind Engineering and Industrial Aerodynamics, 2008, doi:10.1016/j.jweia.2008.02.041
3. Cenedese A, Cerri G, Iannetta S, *L.D.V. Analysis of Wakes Behind Circular Cylinders and Airfoils*, CNR, December 1981.
4. Cimbala J, Çengel Y, 2006, *Fluid Mechanics: Fundamentals and Applications*, Mc Graw Hill.
5. Constantinescu George, Ettema Robert, Koken Mete, Muste Marian, *An Eddy-Resolving Technique to Predict the Unsteady Horseshoe Vortex and Wake of a Cylindrical Pier*, IIHR Hydrosience and Engineering, University of Iowa.
6. Daily, Harleman, 1966, *Fluid Dynamics*, Addison Wesley Publishing Company, USA
7. Dargahi, B. 1990, *Controlling Mechanism of Local Scouring*, ASCE, 1990, 116(10): 1197 - 1214.
8. Department of Main Roads, *Bremer River Duplication: Bridgesite Foundation Investigation*, 144/18A/14, 31 October 1989
9. Duan Jennifer G, 2005, *Two-Dimensional Model Simulation of Flow Field Around Bridge Piers*, ASCE Conf. Proc. 173, 449(2005)
10. Duan, G Jennifer, 2006, *Discussion of "Simulation of Flow and Mass Dispersion in Meandering Channels"*, ASCE, Journal of Hydraulic Engineering, March 2006.
11. Emori Richard, Schuring Dieterich, 1977, *Scale Models in Engineering*, Pergamon Press, London
12. Farraday, R., Charlton. F., 1983, *Hydraulic Factors in Bridge Design*, Hydraulics Research Station Limited, Wallingford, Oxfordshire.
13. Featherstone R. E., Nalluri C. 2001, *Civil Engineering Hydraulics*, Fourth Edition, Blackwell Science, Carlton Victoria.
14. Flavell D., 1981, *Bridge Scour in the Pilbara Region of Western Australia*, NAASRA BEL 1981 Seminar: Bridge Foundations, Australian Road Research Board, September 1981.



15. Goswami Indranil, Scanlan Robert H, Nicholas P Jones, *Vortex-Induced Vibration of Circular Cylinders I: Experimental Data*, Journal of Engineering Mechanics, Vol. 119, pp2270-2287
16. Hämäläinen Ville, 2001, *Implementing an Explicit Algebraic Reynolds Stress Model into the Three-Dimensional Finflo Flow Solver*, Report B-52, Helsinki University of Technology, Laboratory of Aerodynamics, 2001.
17. Hamill Les 1999, *Bridge Hydraulics*, E & FN SPON, London.
18. Herron, K., 2007, *Vortex Shedding on Bridge Piers*, University of Southern Queensland, Toowoomba.
19. Kirkil Gokhan, Constantinescu George, Ettema Robert n.d., *The Horseshoe Vortex System Around a Circular Bridge Pier on a Flat Bed*, The University of Iowa, Iowa City.
20. Li Xiangpeng, Zhou Hao, Cen Kefa, 2007, *Influences of Various Vortex Structures on the Dispersion and Deposition of Small Ash Particles*, Institute for Thermal Power Engineering, Zhejiang University, China, 2007.
21. Miao J M, Ho M H, 2006, *Effect of Flexure on Aerodynamic Propulsive Efficiency of Flapping Flexible Aerofoil*, Journal of Fluids and Structures #22 2006, Elsevier.
22. Neill R Charles, *Controlling Mechanism of Local Scouring - Journal Response #1 and Journal Response #2*, Northwest Hydr. Consultants, 4823-99 St., Edmonton, Alberta, ASCE, 1990, No. 10.
23. Overman, M. 1975, *Man, The Bridge Builder*, Priory Press, Hove, England.
24. Pope, Stephen B. 2000, *Turbulent Flows*, Cambridge University Press, Cambridge.
25. Roshko, A., 1976, *Structure of Turbulent Shear Flows - A New Look*, AIAA Journal, Vol. 14, 1349-1357
26. Sadeque A F M, Rajaratnam N, Loewen R M, 2008, *Flow Around Cylinders in Open Channels*, Journal of Engineering Mechanics, ASCE, January 2008.
27. Salaheldin Tarek, Imran Jasim, Chaudhry M Hanif, 2004, *Numerical Modelling of Three-Dimensional Flow Field Around Circular Piers*, Journal of Hydraulic Engineering, February 2004, pp91-100
28. Samchek Alan, Beckstead Gary, Zhou Joe, 2004, *Case Studies of Scour and Erosion at Water Crossings*, ASCE, 2004.
29. Schlichting H. Gersten K. 2000, *Boundary Layer Theory*, 8th rev. and enl. Ed., Springer, Berlin.



30. Sohankar A, *Large Eddy Simulation of Flow Past Rectangular-Section Cylinders: Side Ratio Effects*, Journal of Wind Engineering and Industrial Aerodynamics, 2008, doi:10.1016/j.jweia.2008.02.009
31. Suslov A S, *Two-Equation Model of Mean Flow Resonances in Subcritical Flow Systems*, Department of Mathematics and Computing, University of Southern Queensland, Toowoomba, Queensland 4350, Australia.
32. Thomas B., 1981, *Practical Aspects of Foundation Construction*, NAASRA BEL 1981 Seminar: Bridge Foundations, Australian Road Research Board, September 1981.
33. Thomas T G, Williams J J R, 1999, *Large Eddy Simulation of Vortex Shedding from Cubic Obstacle*, Journal of Aerospace Engineering 12, pp113-121, 1999.
34. Transportation Association of Canada 2004, *Guide to Bridge Hydraulics*, Second Edition, Thomas Telford, London
35. Troitsky M. S. 1994, *Planning and Design of Bridges*, John Wiley and Sons, Toronto
36. US Department of Transportation: Federal Highway Administration, 2001, *Evaluating Scour at Bridges*, Fourth Edition, National Highway Institute.
37. Xanthoakos Petros P 1995, *Bridge Substructure and Foundation Design*, Prentice Hall PTR, New Jersey
38. Yeo DongHun, Jones P Nicholas, *Investigation on 3D Characteristics of Flow Around a Yawed and Inclined Circular Cylinder*, Journal of Wind Engineering and Industrial Aerodynamics, 2008, doi:10.1016/j.jweia.2008.02.040
39. Zhao M., Hue, A., 2006, *Large-Eddy Simulation of Three-Dimensional Turbulent Flow Around a Circular Pier*, Journal of Hydrodynamics.
40. Zima Laura, Ackermann Norbert L., *Wave Generation in Open Channels by Vortex Shedding from Channel Obstructions*, Journal of Hydraulic Engineering, June 2002, pp596-203.



APPENDICES



APPENDIX A - PROJECT SPECIFICATION

ENG4111/4112 Research Project

PROJECT SPECIFICATION

TOPIC: THE EFFECTIVENESS OF AN AEROFOIL SHAPED PIER IN
REDUCING DOWN STREAM VORTICES AND TURBULENCE

SUPERVISOR: Mark Porter

ENROLMENT: ENG 4111 - Sem 1, DAY, 2008

ENG 4112 - Sem 2, DAY, 2008

PROJECT AIM: To determine how an aerofoil shaped pier will effect vortex shedding and downstream turbulence. The project will determine whether or not the pier type tested could be more useful than the traditional 'circular' piers used today.

PROGRAMME: REV B

1. Gain a good understanding of where bridge pier design currently stands.
2. Gather hydrological and design data from a river system (where a bridge has been constructed).
3. Perform dimensional analysis so that the flows are simulated in the USQ hydraulics laboratory. Allowing accurate data collection.
4. Design appropriate cross sections for bridge piers. In this case one possible aerofoil shape will be the primary objective.
5. Test the system with a circular pier. So that theoretical results may be compared with practical results. This will allow checking to see if the system is working correctly.
6. Perform testing on the model. This will be done by testing a circular pier and the aerofoil pier. This will allow for comparison.
7. Analyse collected data using FLUENT and compare aerofoil results to the results from the circular pier. Has the different shape reduced the effects of vortex shedding and downstream turbulence??
8. Critically appraise the work and recommend workings for the future.

As time permits;

9. Develop more than one aerofoil shape to see how these shapes affect the flow.

AGREED:

Student - Date:

26-10-08

Supervisor - Date:

Examiner/Co-Examiner - Date:



APPENDIX B - FLUENT RESULTS

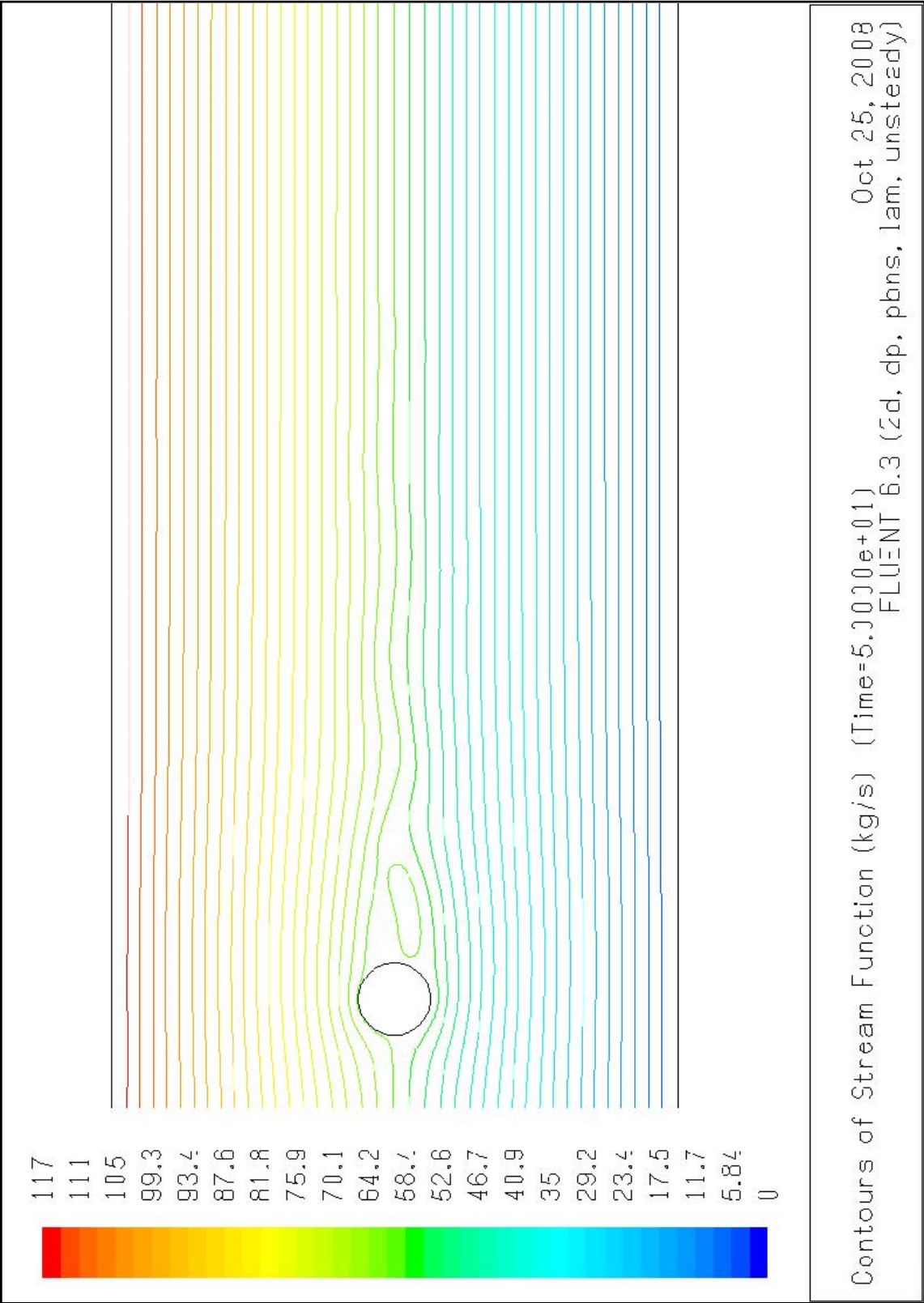


Figure B-1a - Snap shot in time of the stream function. Produced by FLUENT. Time is 50 seconds after flow has started.

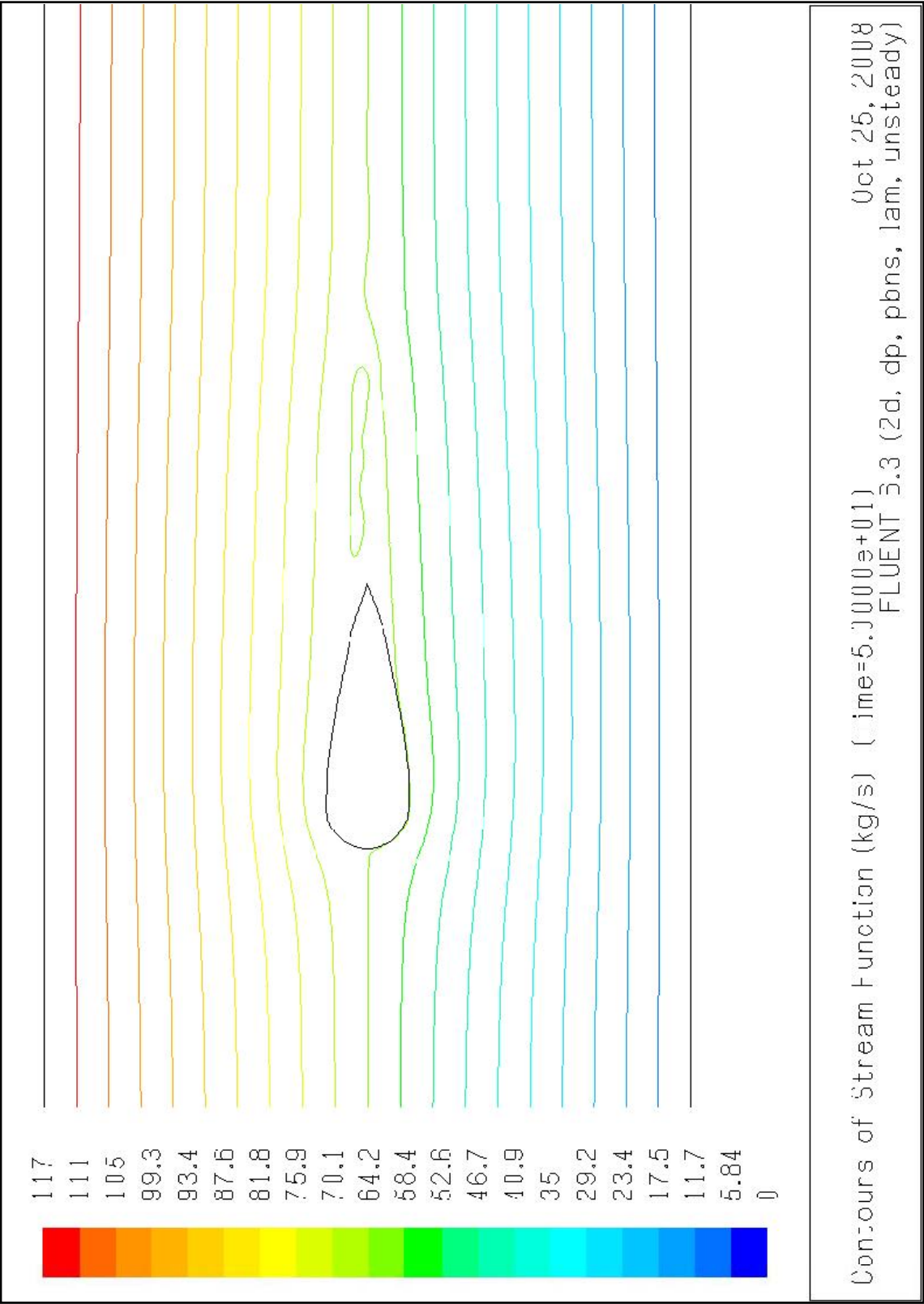


Figure B-1b - Snap shot in time of the stream function produced by FLUENT. Time is 50 seconds after flow has started.

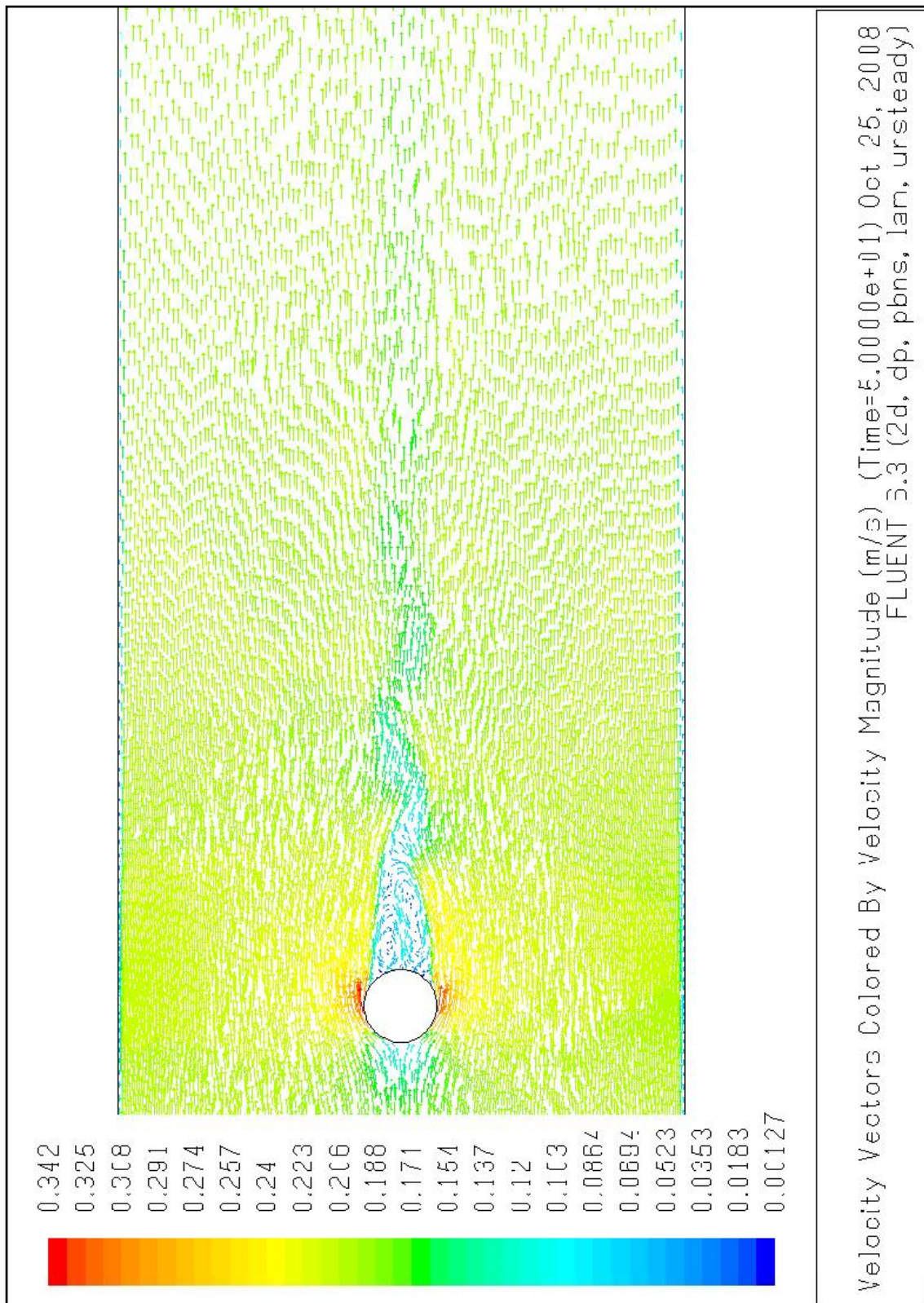


Figure B-2a - Vectors of velocity magnitude produced by FLUENT. Note the region behind the pier where velocities are flowing in a negative direction. Again this is a snap-shot in time.

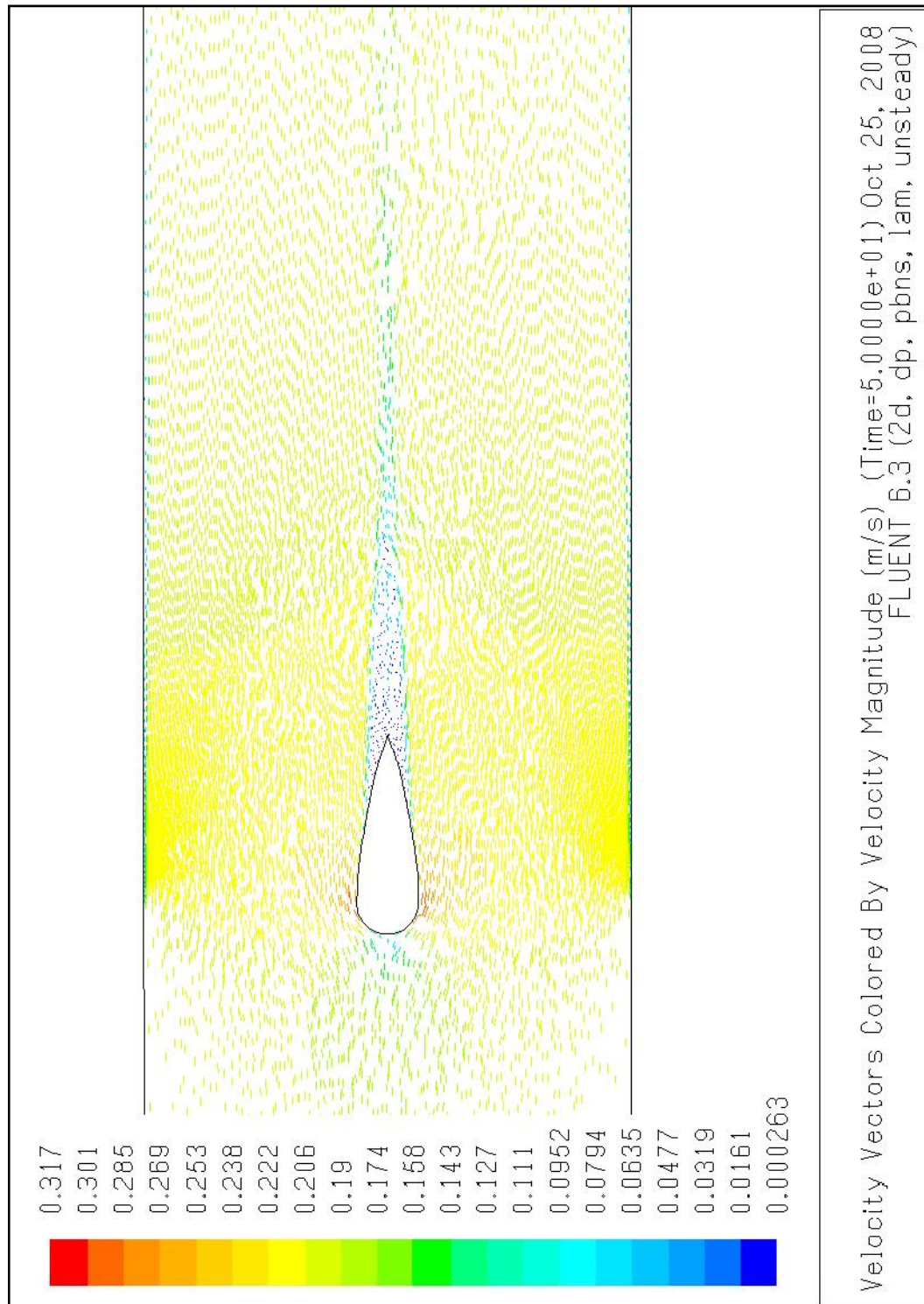


Figure B-2b - Vectors of velocity magnitude produced by FLUENT. Note the region behind the pier where velocities are flowing in a negative direction. There is a long low velocity area behind the pier. This indicates that there is some back flow, however what's important is the magnitude of this backflow. Note that the vectors are significantly smaller than that of the circular pier, and that the flow behind the pier is somewhat symmetrical.

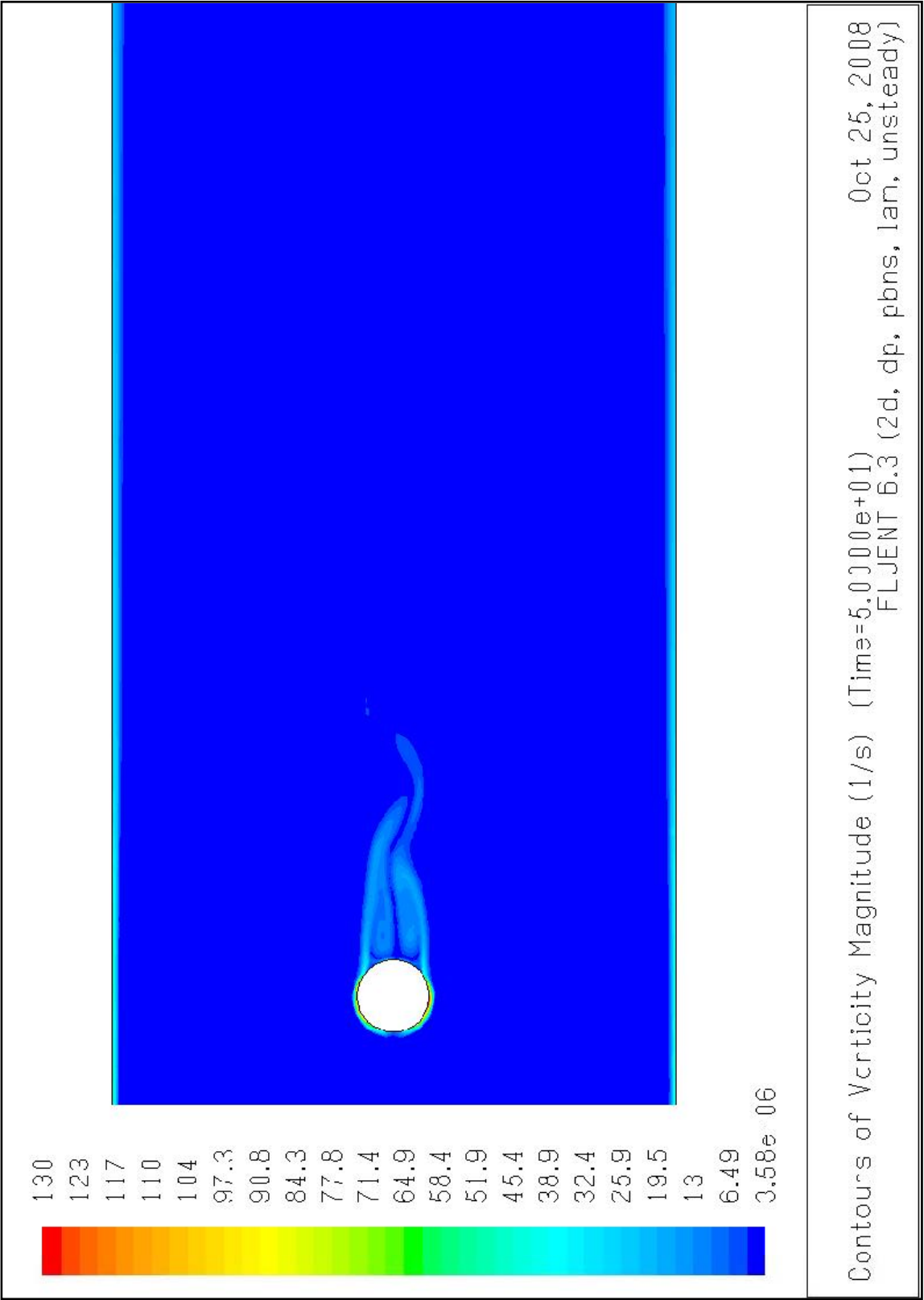


Figure B-3a - Contours of vorticity magnitude; Note the intensity of the vortices when compared with the aerofoil pier. The lighter regions indicate higher velocities.

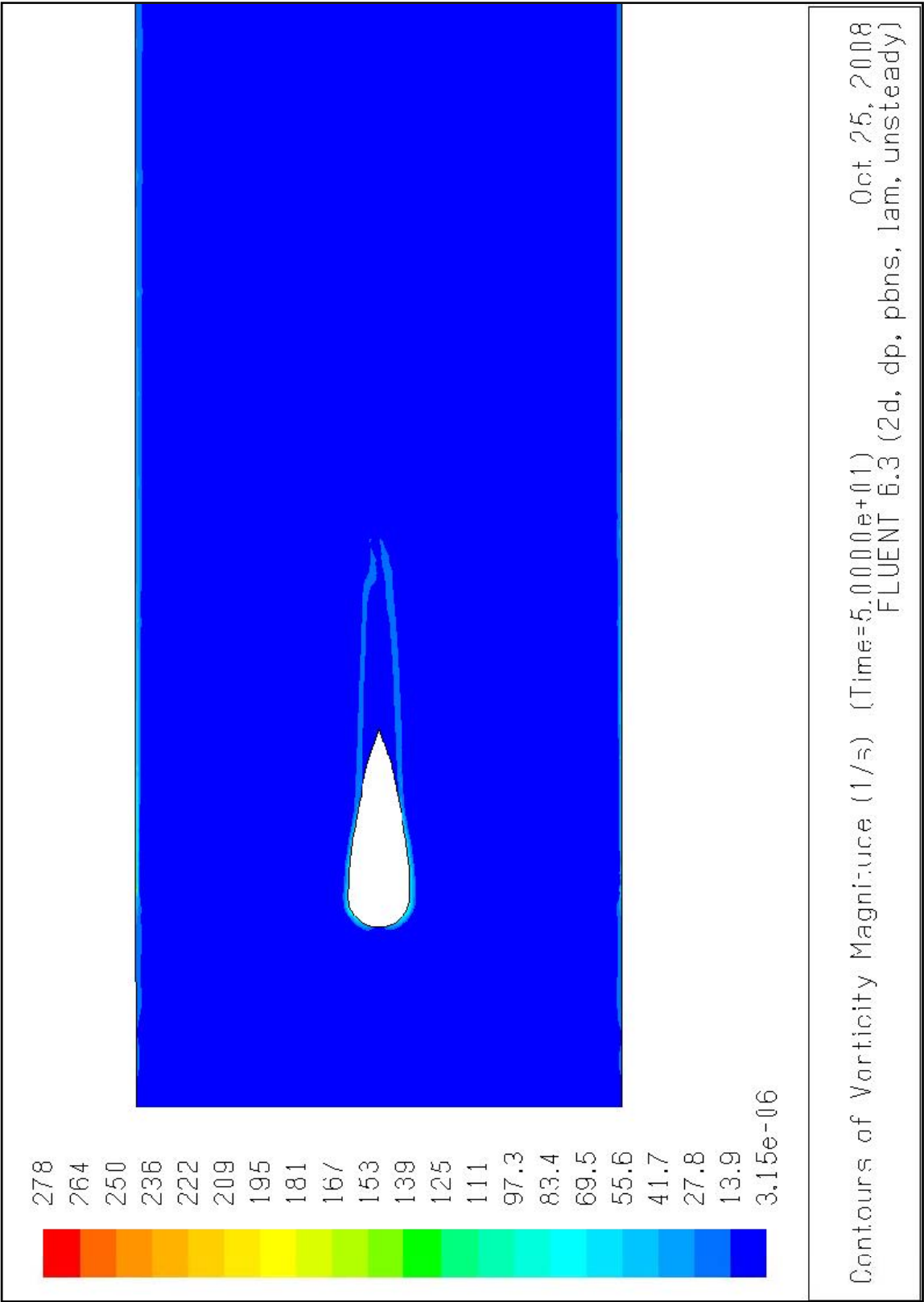


Figure B-3b - Contours of vorticity magnitude. The red regions indicate higher velocities.

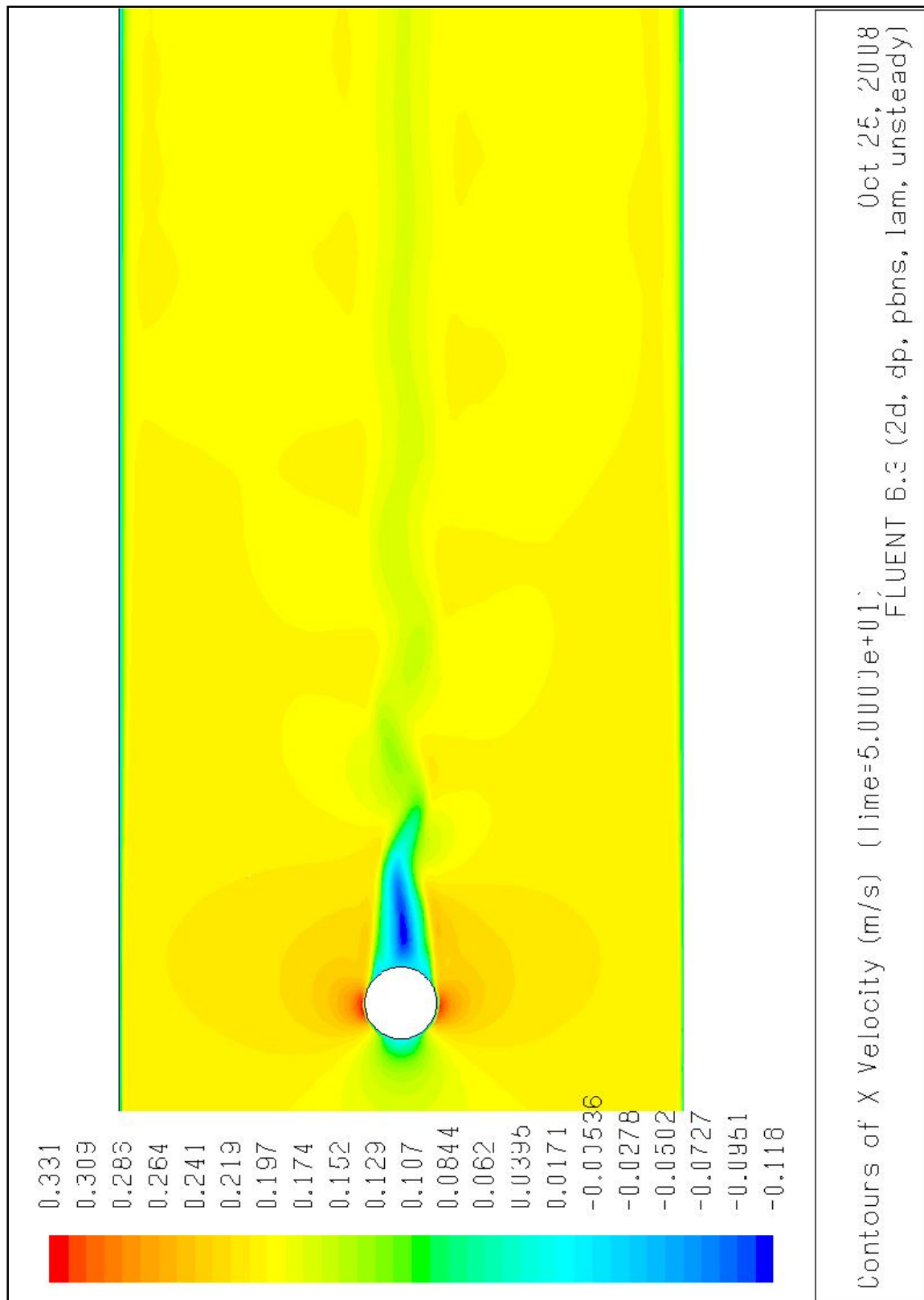


Figure B-4a - Contours of downstream velocity. This shows accurately the flow pattern at one instance in time, once the flow has stabilised. This flow pattern oscillates from side to side, hence the image is merely a snap shot in time.

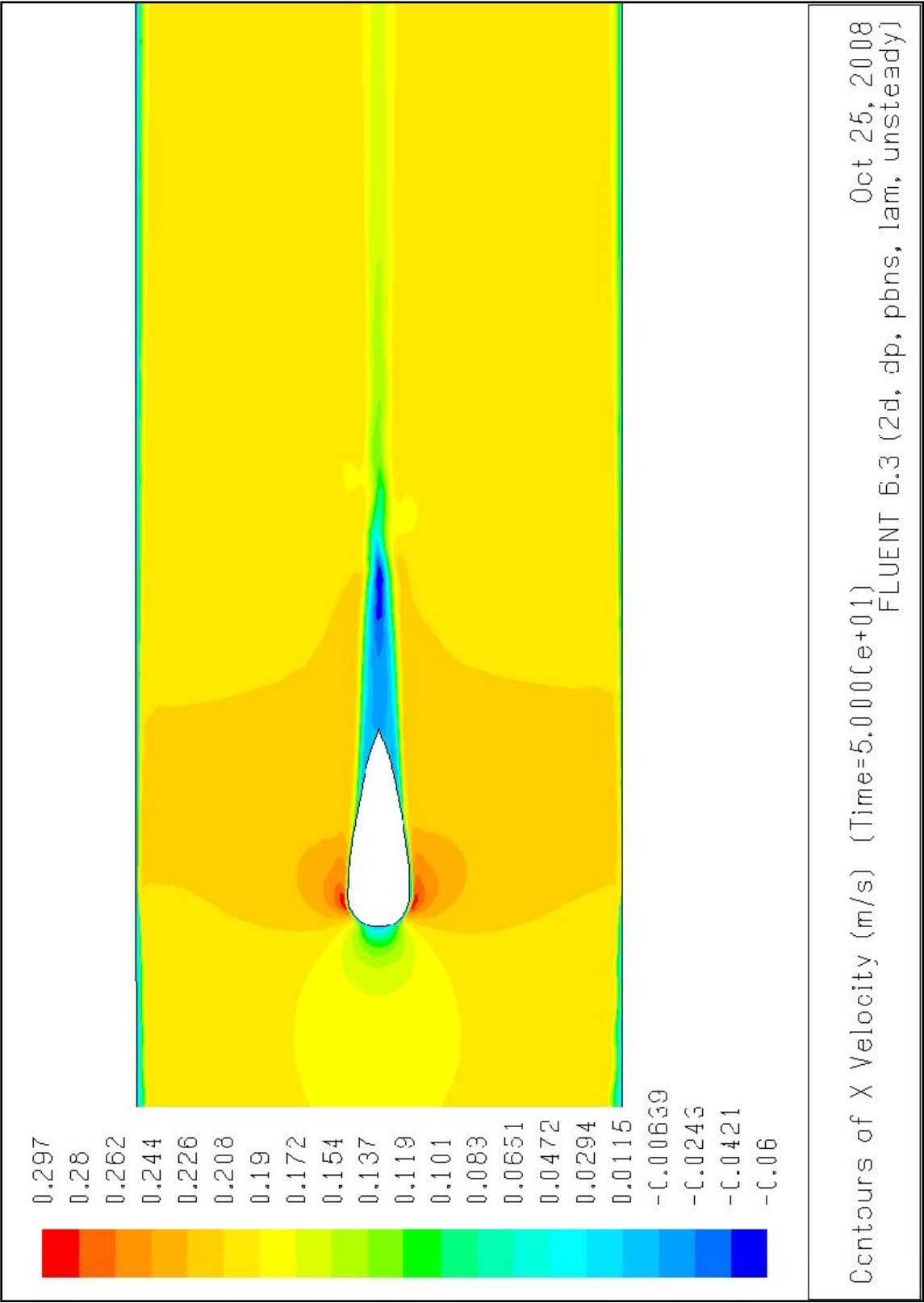


Figure B-4b - Contours of downstream velocity. This shows accurately the flow pattern at one instance in time, once the flow has stabilised. This flow pattern oscillates from side to side, hence the image is merely a snap shot in time.

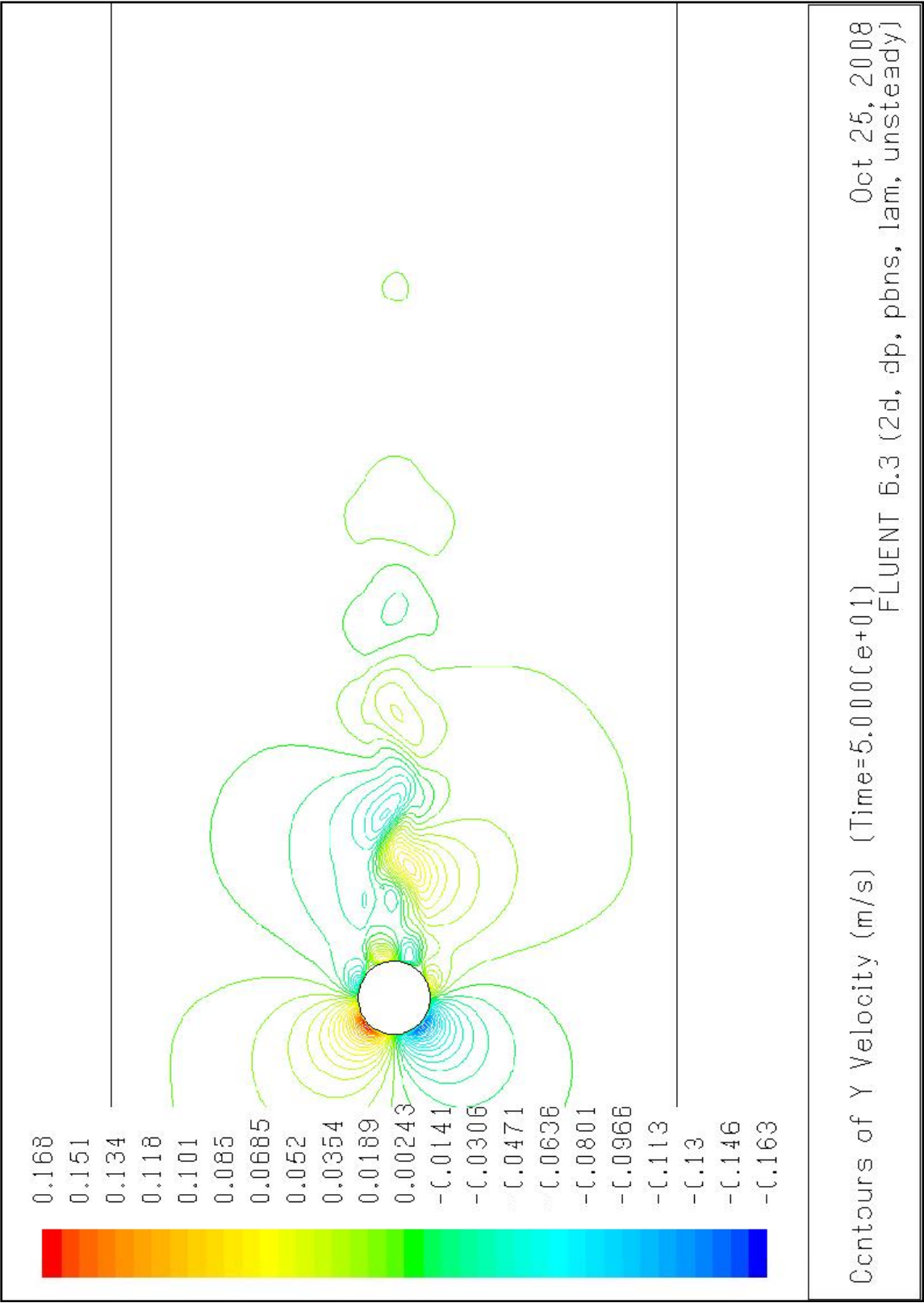


Figure B-5a - Contours of cross stream velocity. Because this is an instance in time, the velocities would oscillate from side to side with respect to time.

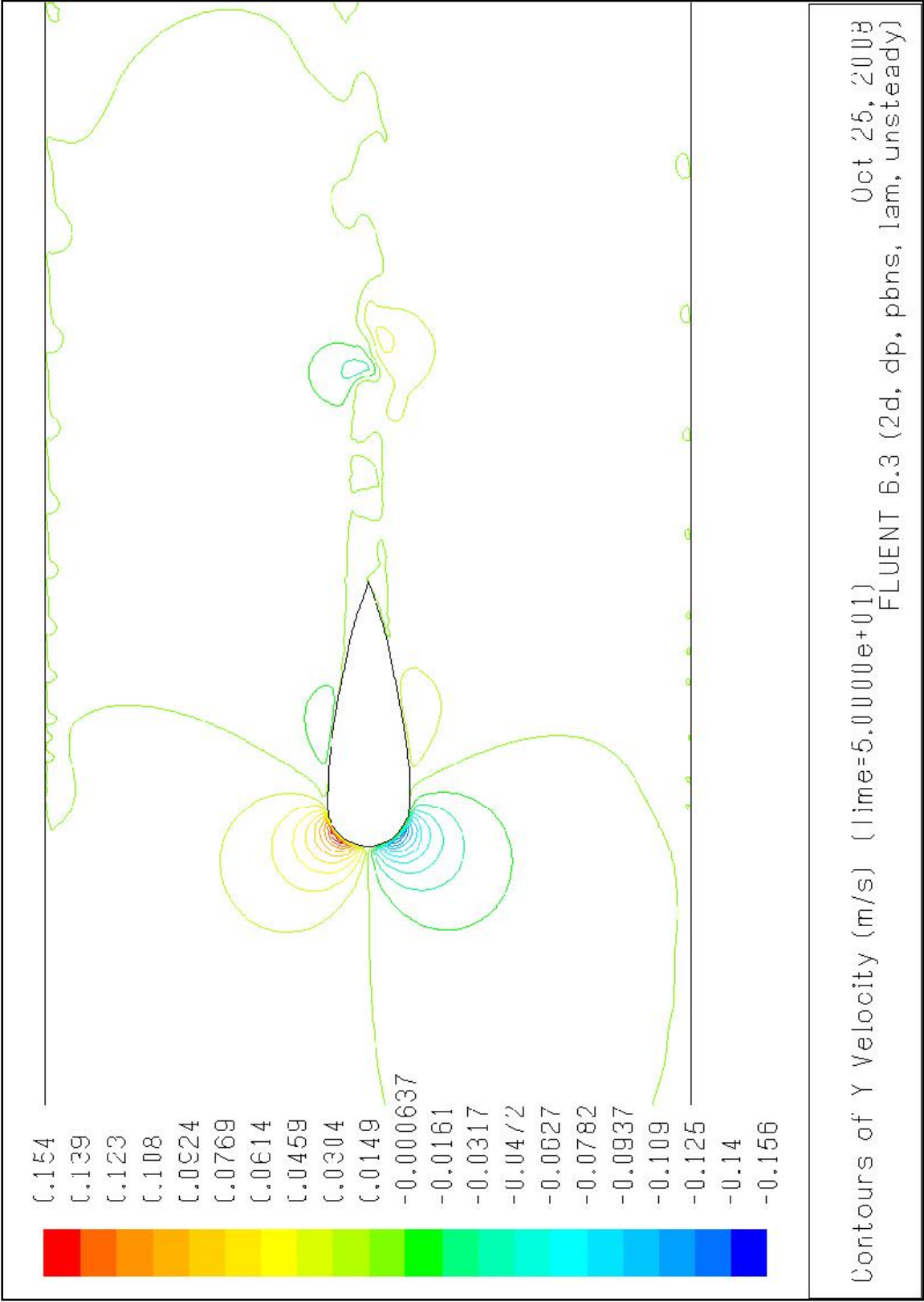


Figure B-5b - Contours of cross stream velocity. Because this is an instance in time, the velocities would oscillate from side to side with respect to time.

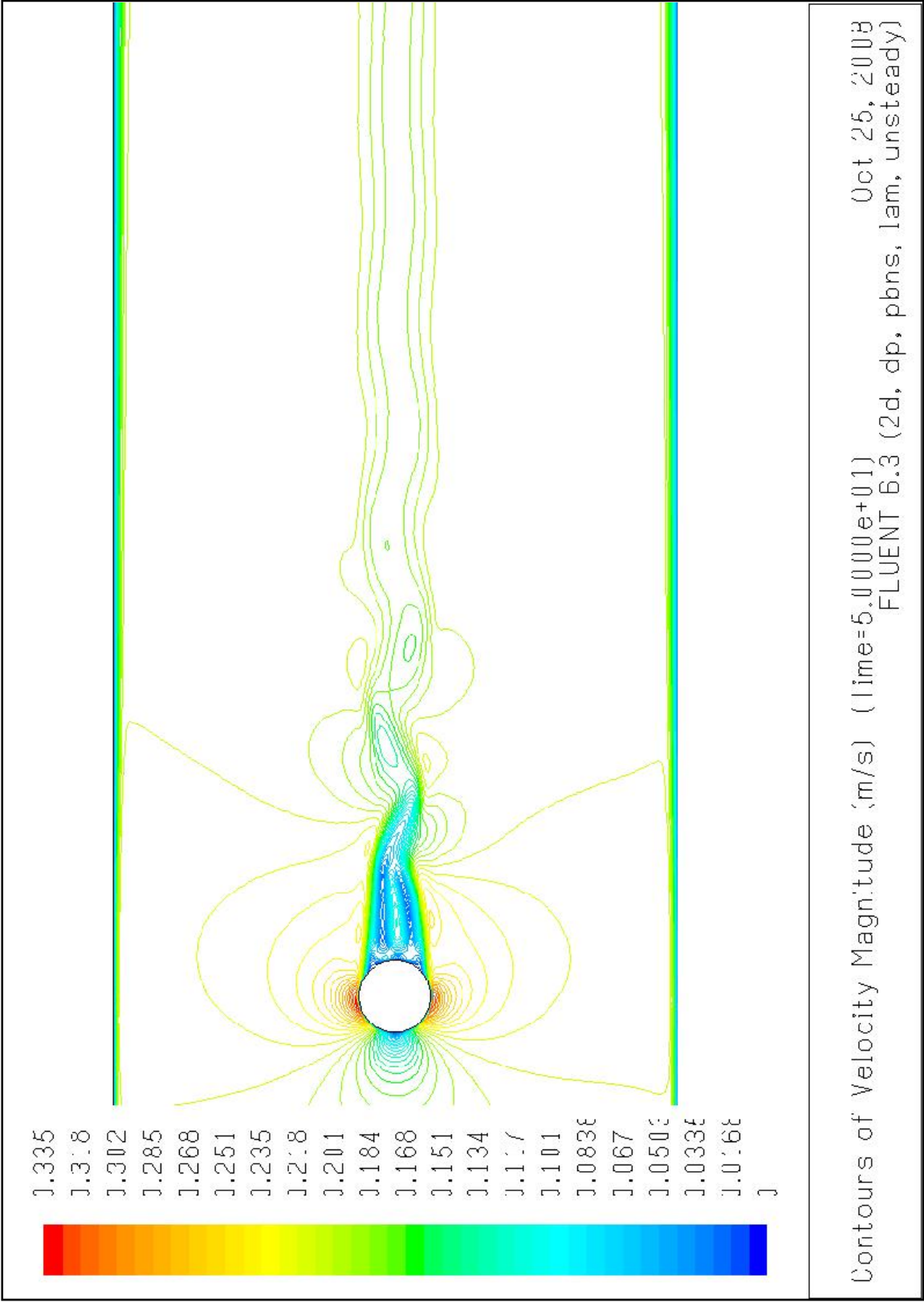


Figure B-6a - Contours of velocity magnitude. Note as the vortices move down stream, they increase in velocity.

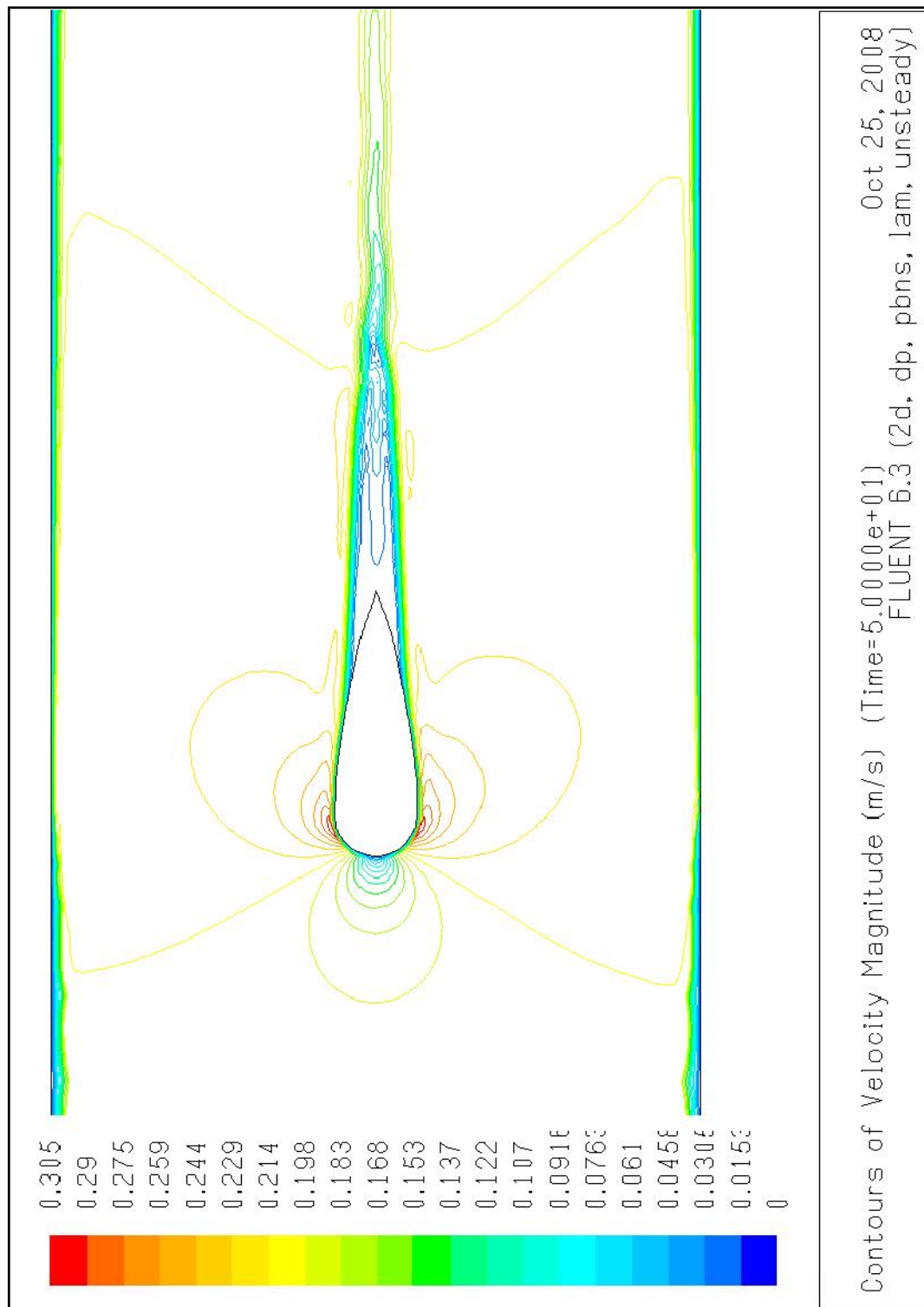
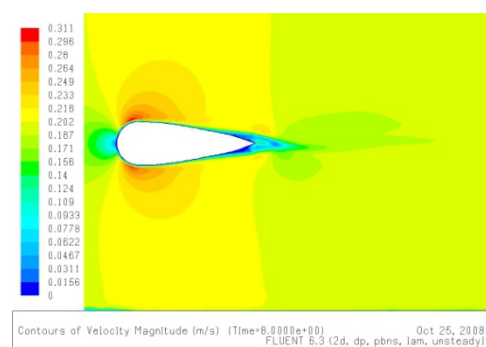
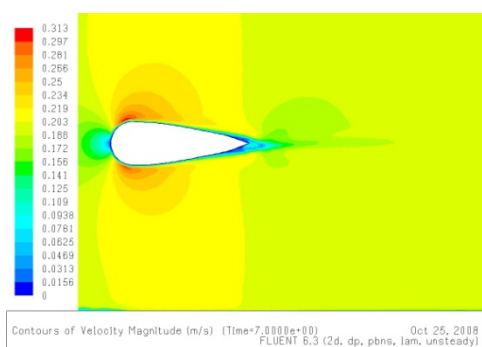
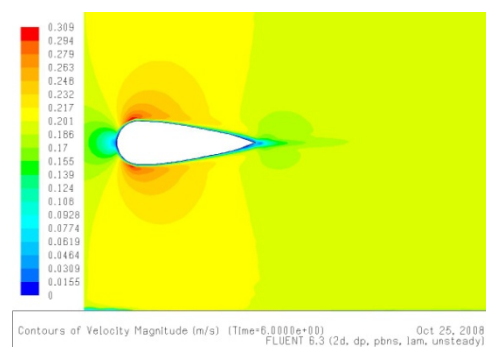
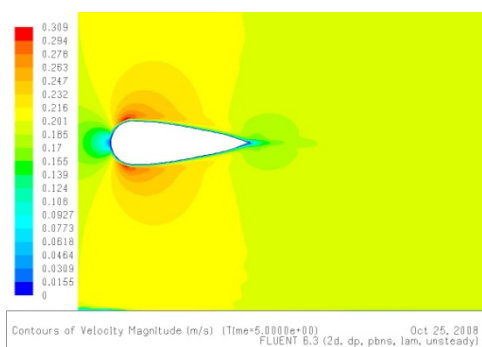
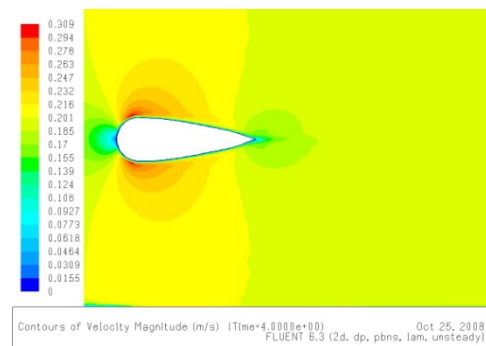
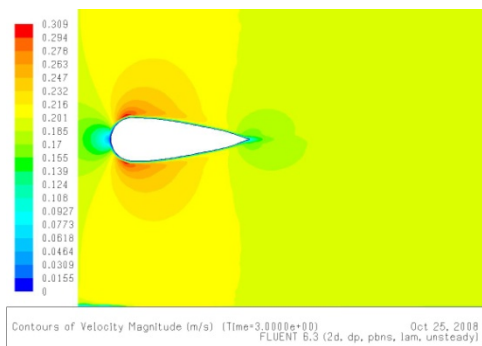
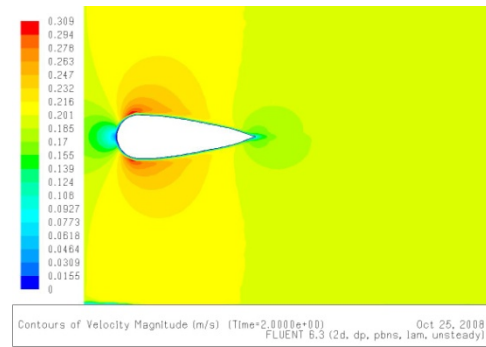
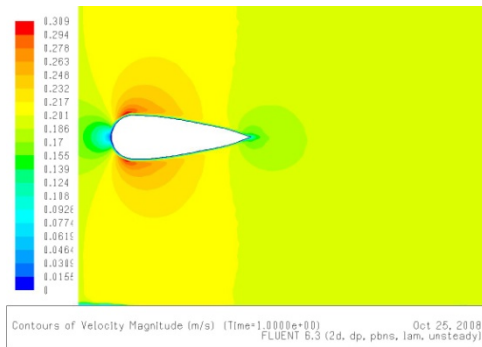


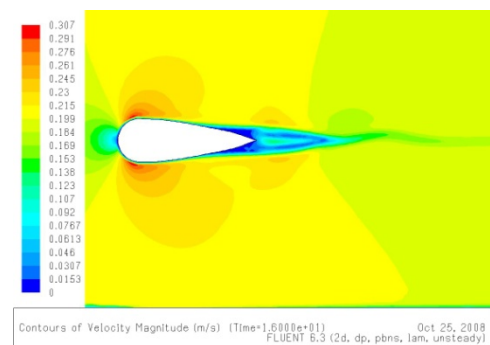
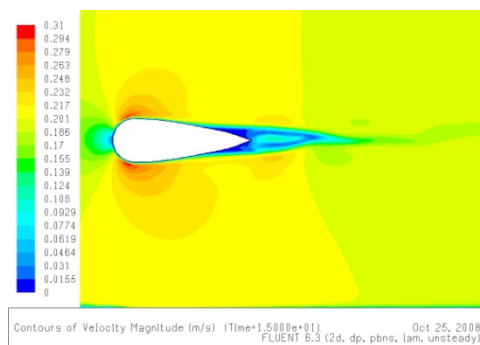
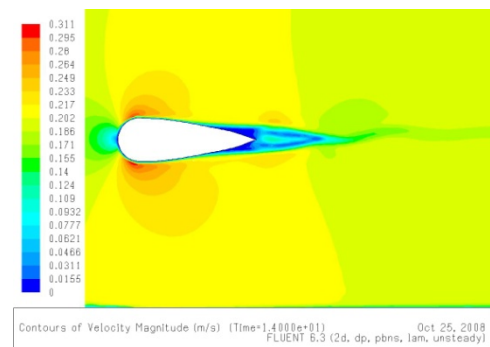
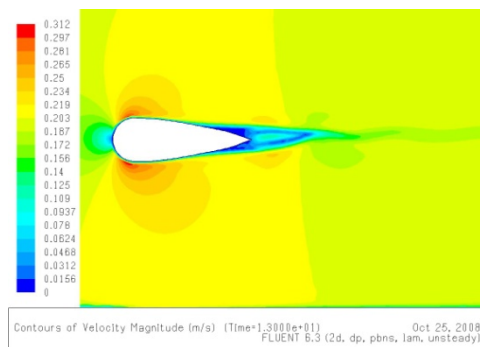
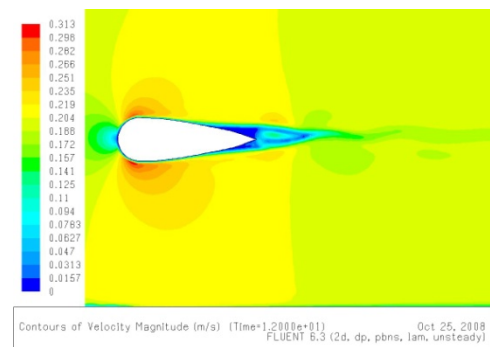
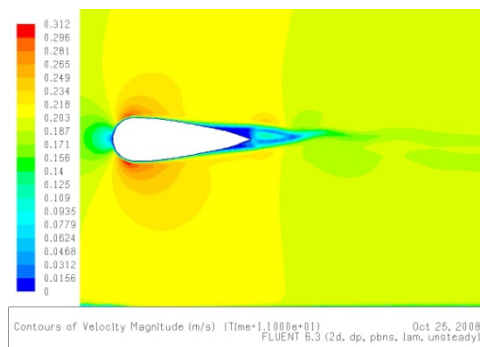
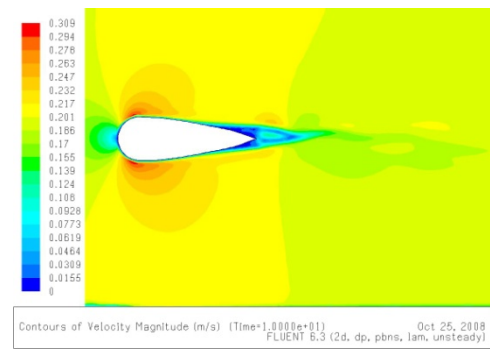
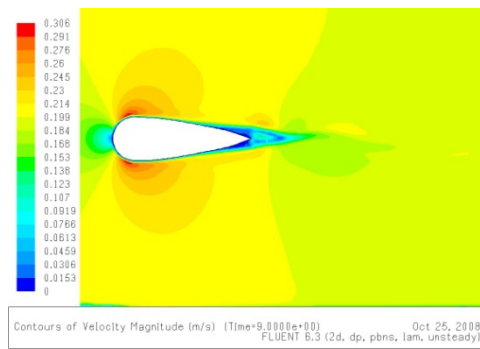
Figure B-6b - Contours of velocity magnitude. Note the pattern that evolves behind the pier. The oscillations are not violent. The velocity behind the pier is reduced, but vortices formed are significantly smaller and flow around the pier remains largely uninterrupted. Also oscillations are very small in comparison with the circular pier.

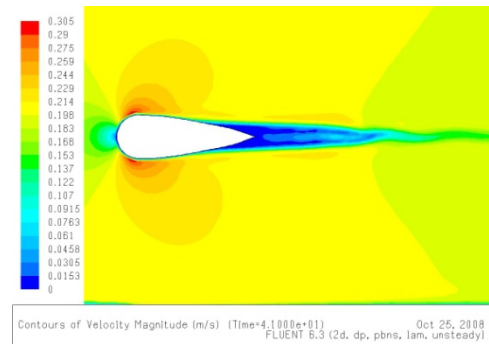
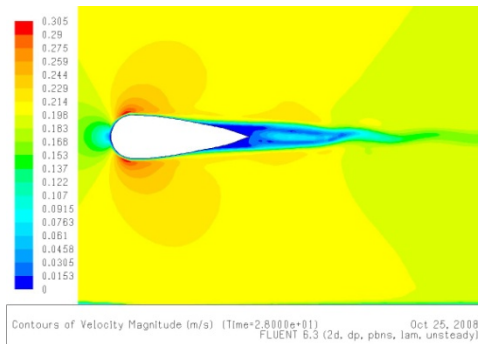
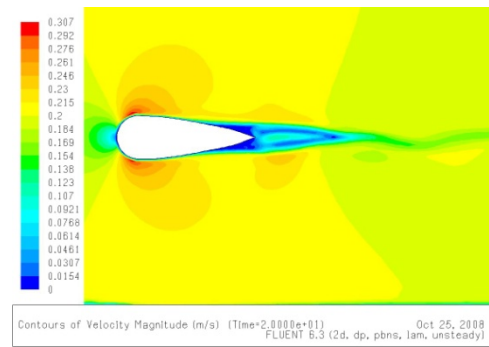
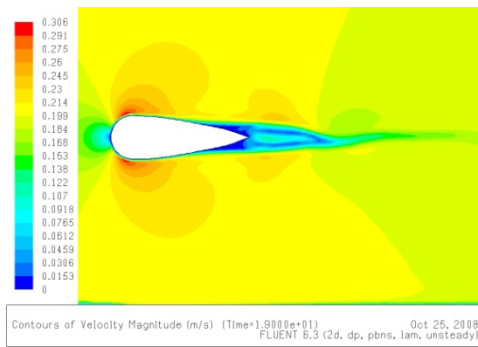
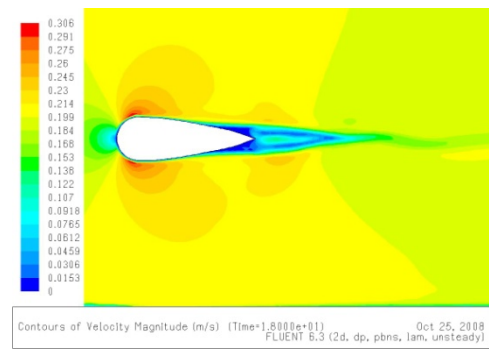
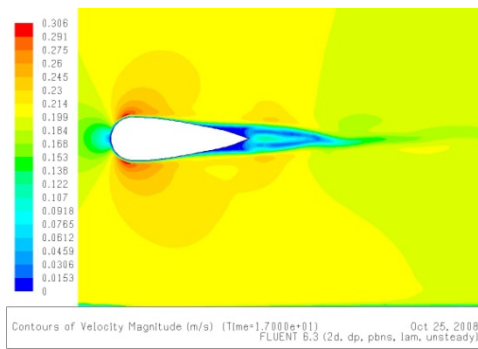


FLOW AROUND THE AEROFOIL PIER OVER A 20 SECOND PERIOD

Read the diagrams from left to right. Each image is taken at a 1 second interval. The last two images in the process are taken at 28 seconds and 41 seconds.



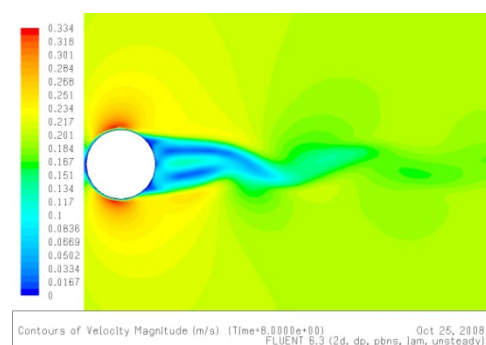
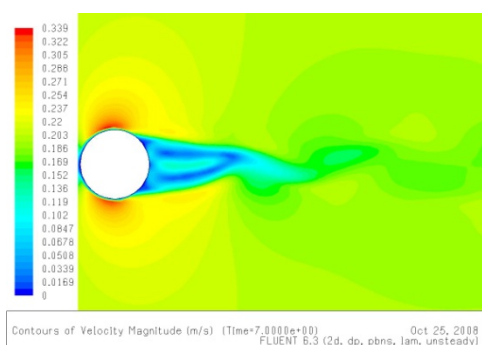
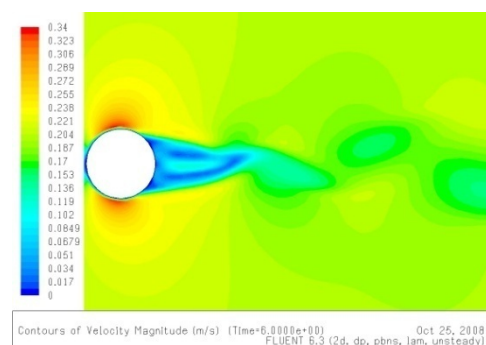
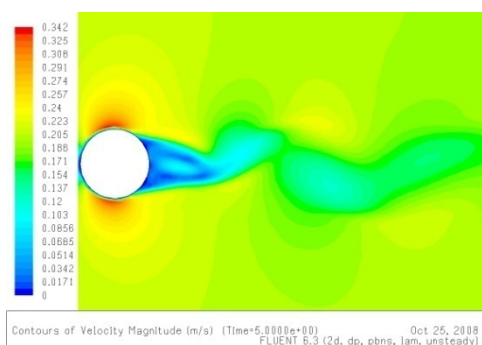
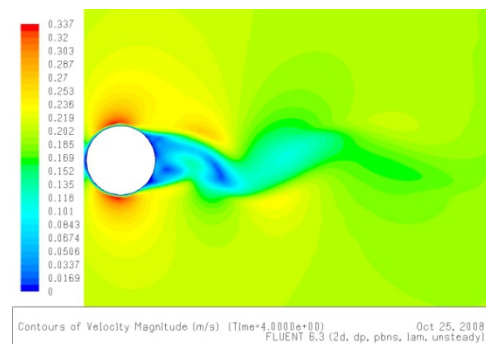
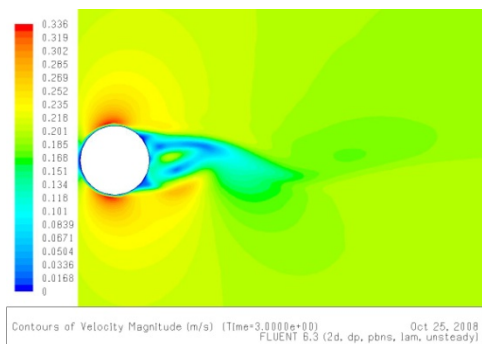
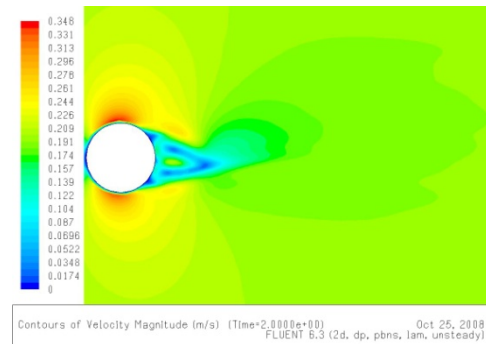
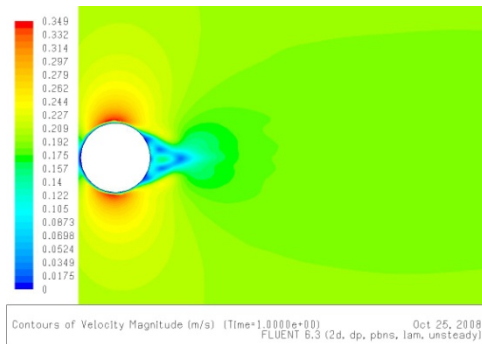


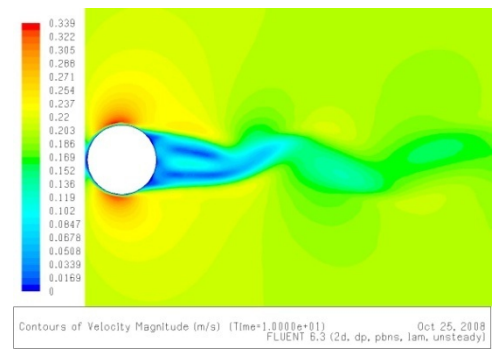
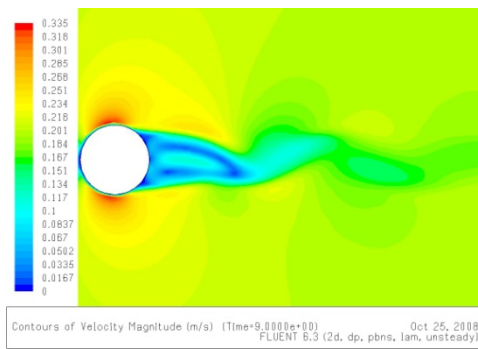




FLOW AROUND THE CIRCULAR PIER OVER A 10 SECOND PERIOD

Read the diagrams from left to right. Each image is taken at a 1 second interval. The circular profile is only 10 seconds because the phenomenon of vortex shedding establishes quickly.







APPENDIX C - FLUENT CASE SUMMARY

CIRCLE CASE SUMMARY

FLUENT
Version: 2d, dp, pbns, lam, unsteady (2d, double precision, pressure-based, laminar, unsteady)
Release: 6.3.26
Title:

Models

Model	Settings
Space	2D
Time	Unsteady, 1st-Order Implicit
Viscous	Laminar
Heat Transfer	Disabled
Solidification and Melting	Disabled
Species Transport	Disabled
Coupled Dispersed Phase	Disabled
Pollutants	Disabled
Pollutants	Disabled
Soot	Disabled

Boundary Conditions

Zones

name	id	type
water	2	fluid
cylinder	3	wall
outlet	4	pressure-outlet
inlet	5	velocity-inlet
wall	6	wall
default-interior	8	interior

Boundary Conditions

water	
Condition	Value
-----	-----
-----	-----
-----	-----
-----	-----
-----	-----
-----	-----



Material Name	water-liquid
Specify source terms?	no
Source Terms	((mass) (x-momentum) (y-momentum) (k) (epsilon) (uu-stress) (vv-stress) (ww-stress) (uv-stress))
Specify fixed values?	no
Fixed Values	((x-velocity (inactive . #f) (constant . 0) (profile)) (y-velocity (inactive . #f) (constant . 0) (profile)) (k (inactive . #f) (constant . 0) (profile)) (epsilon (inactive . #f) (constant . 0) (profile)) (uu-stress (inactive . #f) (constant . 0) (profile)) (vv-stress (inactive . #f) (constant . 0) (profile)) (ww-stress (inactive . #f) (constant . 0) (profile)) (uv-stress (inactive . #f) (constant . 0) (profile))))
Motion Type	0
X-Velocity Of Zone (m/s)	0
Y-Velocity Of Zone (m/s)	0
Rotation speed (rad/s)	0
X-Origin of Rotation-Axis (m)	0
Y-Origin of Rotation-Axis (m)	0
Deactivated Thread	no
Porous zone?	no
X-Component of Direction-1 Vector	1
Y-Component of Direction-1 Vector	0
Relative Velocity Resistance Formulation?	yes
Direction-1 Viscous Resistance (1/m2)	0
Direction-2 Viscous Resistance (1/m2)	0
Choose alternative formulation for inertial resistance?	no
Direction-1 Inertial Resistance (1/m)	0
Direction-2 Inertial Resistance (1/m)	0
C0 Coefficient for Power-Law	0
C1 Coefficient for Power-Law	0
Porosity	1

cylinder

Condition	Value
Wall Motion	0
Shear Boundary Condition	0
Define wall motion relative to adjacent cell zone?	yes
Apply a rotational velocity to this wall?	no
Velocity Magnitude (m/s)	0
X-Component of Wall Translation	1
Y-Component of Wall Translation	0
Define wall velocity components?	no
X-Component of Wall Translation (m/s)	0
Y-Component of Wall Translation (m/s)	0
Rotation Speed (rad/s)	0
X-Position of Rotation-Axis Origin (m)	0
Y-Position of Rotation-Axis Origin (m)	0
X-component of shear stress (pascal)	0
Y-component of shear stress (pascal)	0
Specularity Coefficient	0



outlet

Condition	Value
Gauge Pressure (pascal)	0
Backflow Direction Specification Method	1
X-Component of Flow Direction	1
Y-Component of Flow Direction	0
X-Component of Axis Direction	1
Y-Component of Axis Direction	0
Z-Component of Axis Direction	0
X-Coordinate of Axis Origin (m)	0
Y-Coordinate of Axis Origin (m)	0
Z-Coordinate of Axis Origin (m)	0
is zone used in mixing-plane model?	no
Specify targeted mass flow rate	no
Targeted mass flow (kg/s)	1

inlet

Condition	Value
Velocity Specification Method	2
Reference Frame	0
Velocity Magnitude (m/s)	0.1918
X-Velocity (m/s)	0
Y-Velocity (m/s)	0
X-Component of Flow Direction	1
Y-Component of Flow Direction	0
X-Component of Axis Direction	1
Y-Component of Axis Direction	0
Z-Component of Axis Direction	0
X-Coordinate of Axis Origin (m)	0
Y-Coordinate of Axis Origin (m)	0
Z-Coordinate of Axis Origin (m)	0
Angular velocity (rad/s)	0
is zone used in mixing-plane model?	no

wall

Condition	Value
Wall Motion	0
Shear Boundary Condition	0
Define wall motion relative to adjacent cell zone?	yes
Apply a rotational velocity to this wall?	no
Velocity Magnitude (m/s)	0
X-Component of Wall Translation	1
Y-Component of Wall Translation	0
Define wall velocity components?	no
X-Component of Wall Translation (m/s)	0
Y-Component of Wall Translation (m/s)	0
Rotation Speed (rad/s)	0
X-Position of Rotation-Axis Origin (m)	0
Y-Position of Rotation-Axis Origin (m)	0
X-component of shear stress (pascal)	0
Y-component of shear stress (pascal)	0
Specularity Coefficient	0



default-interior

Condition	Value

Solver Controls

Equations

Equation	Solved

Flow	yes

Numerics

Numeric	Enabled

Absolute Velocity Formulation	yes

Unsteady Calculation Parameters

Time Step (s)	0.1
Max. Iterations Per Time Step	1000

Relaxation

Variable	Relaxation Factor

Pressure	0.5
Density	1
Body Forces	1
Momentum	0.5

Linear Solver

Variable	Solver Type	Termination Criterion	Residual Reduction Tolerance

Pressure	V-Cycle	0.1	
X-Momentum	Flexible	0.1	0.7
Y-Momentum	Flexible	0.1	0.7

Pressure-Velocity Coupling

Parameter	Value

Type	SIMPLE

Discretization Scheme

Variable	Scheme

Pressure	PRESTO!
Momentum	Second Order Upwind



Solution Limits

Quantity	Limit
Minimum Absolute Pressure	1
Maximum Absolute Pressure	5e+10
Minimum Temperature	1
Maximum Temperature	5000

Material Properties

Material: water-liquid (fluid)

Property	Units	Method	Value(s)
Density	kg/m ³	constant	998.2
Cp (Specific Heat)	J/kg-K	constant	4182
Thermal Conductivity	W/m-K	constant	0.6
Viscosity	kg/m-s	constant	0.001003
Molecular Weight	kg/kgmol	constant	18.0152
L-J Characteristic Length	angstrom	constant	0
L-J Energy Parameter	K	constant	0
Thermal Expansion Coefficient	1/K	constant	0
Degrees of Freedom		constant	0
Speed of Sound	m/s	none	#f

Material: air (fluid)

Property	Units	Method	Value(s)
Density	kg/m ³	constant	1.225
Cp (Specific Heat)	J/kg-K	constant	1006.43
Thermal Conductivity	W/m-K	constant	0.0242
Viscosity	kg/m-s	constant	1.7894e-05
Molecular Weight	kg/kgmol	constant	28.966
L-J Characteristic Length	angstrom	constant	3.711
L-J Energy Parameter	K	constant	78.6
Thermal Expansion Coefficient	1/K	constant	0
Degrees of Freedom		constant	0
Speed of Sound	m/s	none	#f

Material: aluminum (solid)

Property	Units	Method	Value(s)
Density	kg/m ³	constant	2719
Cp (Specific Heat)	J/kg-K	constant	871
Thermal Conductivity	W/m-K	constant	202.4



AEROFOIL CASE SUMMARY

FLUENT

Version: 2d, dp, pbns, lam, unsteady (2d, double precision, pressure-based, laminar, unsteady)

Release: 6.3.26

Title:

Models

Model	Settings

Space	2D
Time	Unsteady, 1st-Order Implicit
Viscous	Laminar
Heat Transfer	Disabled
Solidification and Melting	Disabled
Species Transport	Disabled
Coupled Dispersed Phase	Disabled
Pollutants	Disabled
Pollutants	Disabled
Soot	Disabled

Boundary Conditions

Zones

name	id	type

fluid_space	2	fluid
pier	3	wall
outlet	4	pressure-outlet
inlet	5	velocity-inlet
wall	6	wall
default-interior	8	interior

Boundary Conditions

fluid_space

Condition	Value

Material Name	water-liquid
Specify source terms?	no
Source Terms	((mass)
(x-momentum) (y-momentum))	
Specify fixed values?	no
Fixed Values	((x-
velocity (inactive . #f) (constant . 0) (profile)) (y-velocity (inactive . #f) (constant . 0) (profile)))	
Motion Type	0
X-Velocity Of Zone (m/s)	0
Y-Velocity Of Zone (m/s)	0
Rotation speed (rad/s)	0



X-Origin of Rotation-Axis (m)	0
Y-Origin of Rotation-Axis (m)	0
Deactivated Thread	no
Porous zone?	no
X-Component of Direction-1 Vector	1
Y-Component of Direction-1 Vector	0
Relative Velocity Resistance Formulation?	yes
Direction-1 Viscous Resistance (1/m ²)	0
Direction-2 Viscous Resistance (1/m ²)	0
Choose alternative formulation for inertial resistance?	no
Direction-1 Inertial Resistance (1/m)	0
Direction-2 Inertial Resistance (1/m)	0
C0 Coefficient for Power-Law	0
C1 Coefficient for Power-Law	0
Porosity	1

pier

Condition	Value

Wall Motion	0
Shear Boundary Condition	0
Define wall motion relative to adjacent cell zone?	yes
Apply a rotational velocity to this wall?	no
Velocity Magnitude (m/s)	0
X-Component of Wall Translation	1
Y-Component of Wall Translation	0
Define wall velocity components?	no
X-Component of Wall Translation (m/s)	0
Y-Component of Wall Translation (m/s)	0
Rotation Speed (rad/s)	0
X-Position of Rotation-Axis Origin (m)	0
Y-Position of Rotation-Axis Origin (m)	0
X-component of shear stress (pascal)	0
Y-component of shear stress (pascal)	0
Specularity Coefficient	0

outlet

Condition	Value

Gauge Pressure (pascal)	0
Backflow Direction Specification Method	1
X-Component of Flow Direction	1
Y-Component of Flow Direction	0
X-Component of Axis Direction	1
Y-Component of Axis Direction	0
Z-Component of Axis Direction	0
X-Coordinate of Axis Origin (m)	0
Y-Coordinate of Axis Origin (m)	0
Z-Coordinate of Axis Origin (m)	0
is zone used in mixing-plane model?	no
Specify targeted mass flow rate	no
Targeted mass flow (kg/s)	1



inlet

Condition	Value
-----	-----
Velocity Specification Method	2
Reference Frame	0
Velocity Magnitude (m/s)	0.1918
X-Velocity (m/s)	0
Y-Velocity (m/s)	0
X-Component of Flow Direction	1
Y-Component of Flow Direction	0
X-Component of Axis Direction	1
Y-Component of Axis Direction	0
Z-Component of Axis Direction	0
X-Coordinate of Axis Origin (m)	0
Y-Coordinate of Axis Origin (m)	0
Z-Coordinate of Axis Origin (m)	0
Angular velocity (rad/s)	0
is zone used in mixing-plane model?	no

wall

Condition	Value
-----	-----
Wall Motion	0
Shear Boundary Condition	0
Define wall motion relative to adjacent cell zone?	yes
Apply a rotational velocity to this wall?	no
Velocity Magnitude (m/s)	0
X-Component of Wall Translation	1
Y-Component of Wall Translation	0
Define wall velocity components?	no
X-Component of Wall Translation (m/s)	0
Y-Component of Wall Translation (m/s)	0
Rotation Speed (rad/s)	0
X-Position of Rotation-Axis Origin (m)	0
Y-Position of Rotation-Axis Origin (m)	0
X-component of shear stress (pascal)	0
Y-component of shear stress (pascal)	0
Specularity Coefficient	0

default-interior

Condition	Value
-----	-----

Solver Controls

Equations

Equation	Solved
-----	-----
Flow	yes



Numerics

Numeric	Enabled

Absolute Velocity Formulation	yes

Unsteady Calculation Parameters

Time Step (s)	0.1
Max. Iterations Per Time Step	1000

Relaxation

Variable	Relaxation Factor

Pressure	0.5
Density	1
Body Forces	1
Momentum	0.5

Linear Solver

Variable	Solver Type	Termination Criterion	Residual Reduction Tolerance

Pressure	V-Cycle	0.1	
X-Momentum	Flexible	0.1	0.69999999
Y-Momentum	Flexible	0.1	0.69999999

Pressure-Velocity Coupling

Parameter	Value

Type	SIMPLE

Discretization Scheme

Variable	Scheme

Pressure	PRESTO!
Momentum	Second Order Upwind

Solution Limits

Quantity	Limit

Minimum Absolute Pressure	1
Maximum Absolute Pressure	5e+10
Minimum Temperature	1
Maximum Temperature	5000



Material Properties

Material: water-liquid (fluid)

Property	Units	Method	Value(s)
Density	kg/m ³	constant	998.2
Cp (Specific Heat)	J/kg-K	constant	4182
Thermal Conductivity	W/m-K	constant	0.6
Viscosity	kg/m-s	constant	0.001003
Molecular Weight	kg/kgmol	constant	18.0152
L-J Characteristic Length	angstrom	constant	0
L-J Energy Parameter	K	constant	0
Thermal Expansion Coefficient	1/K	constant	0
Degrees of Freedom		constant	0
Speed of Sound	m/s	none	#f

Material: air (fluid)

Property	Units	Method	Value(s)
Density	kg/m ³	constant	1.225
Cp (Specific Heat)	J/kg-K	constant	1006.43
Thermal Conductivity	W/m-K	constant	0.0242
Viscosity	kg/m-s	constant	1.7894e-05
Molecular Weight	kg/kgmol	constant	28.966
L-J Characteristic Length	angstrom	constant	3.711
L-J Energy Parameter	K	constant	78.6
Thermal Expansion Coefficient	1/K	constant	0
Degrees of Freedom		constant	0
Speed of Sound	m/s	none	#f

Material: aluminum (solid)

Property	Units	Method	Value(s)
Density	kg/m ³	constant	2719
Cp (Specific Heat)	J/kg-K	constant	871
Thermal Conductivity	W/m-K	constant	202.4

APPENDIX D - GAMBIT DESIGN

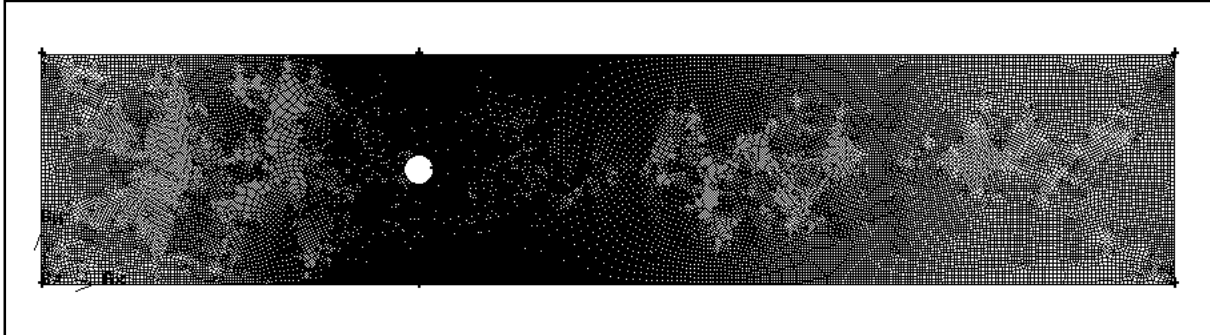


Figure D-1a - Mesh for the circular pier. Note in figure D-1b, the fine mesh around the pier. The pier is 78mm diameter as determined in dimensional analysis. The left hand boundary is the velocity-inlet and the right hand boundary is the pressure-outlet. All other boundaries are set to the 'wall' condition.

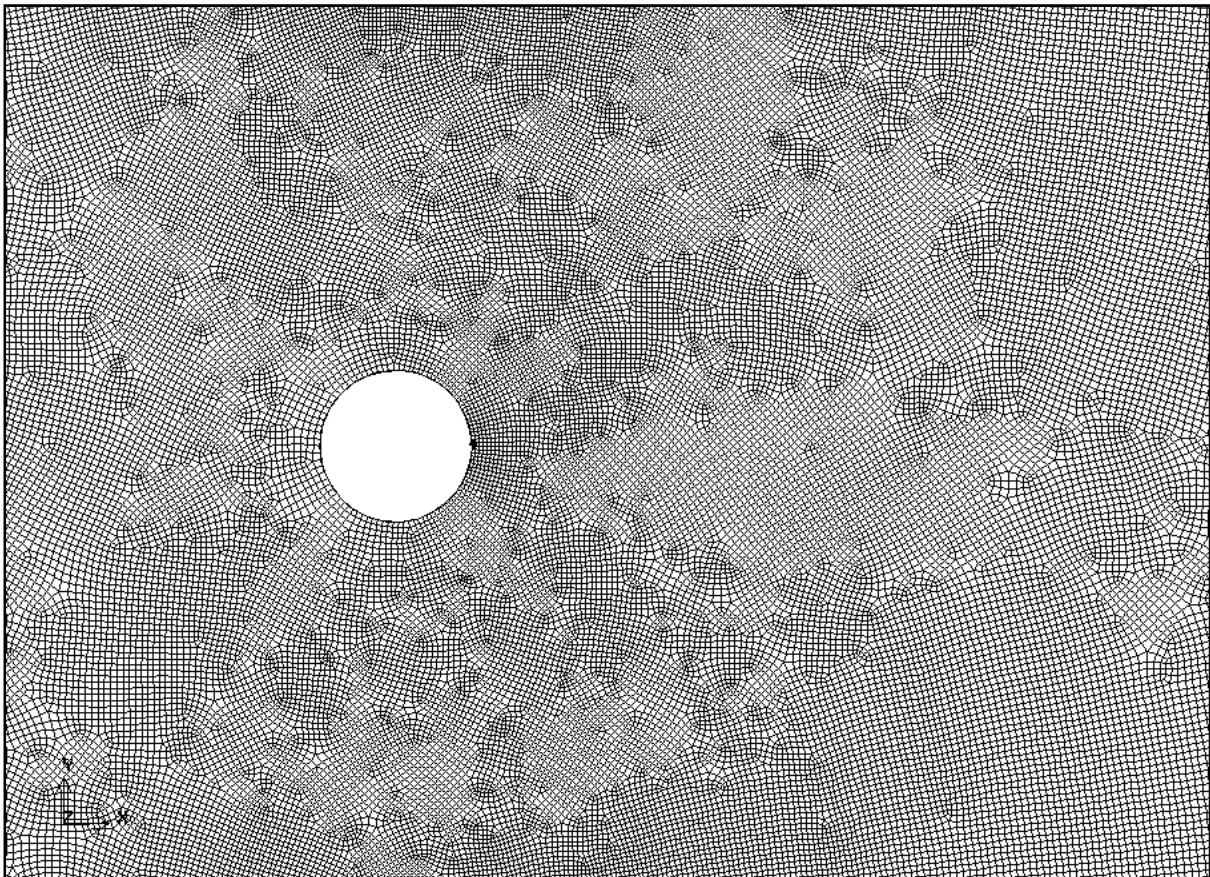


Figure D-1b - Finer mesh immediately around the pier.

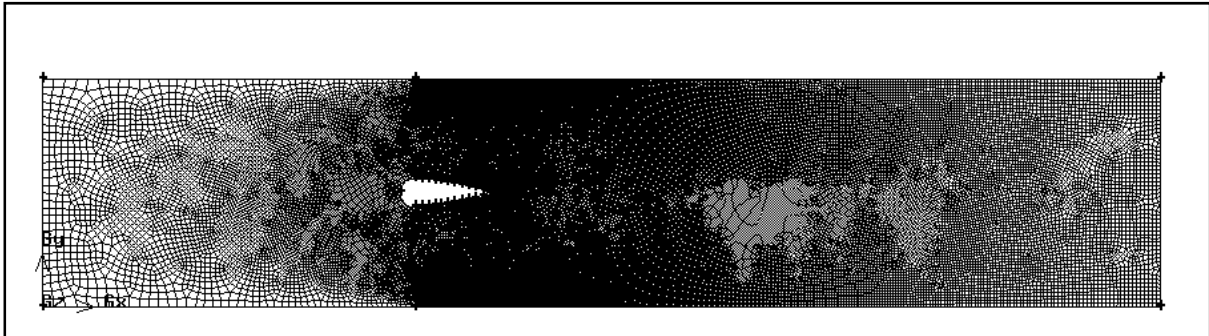


Figure D-2a - Mesh for the aerofoil pier. Note in figure D-2b, the fine mesh around the pier. The pier is 78mm diameter as determined in dimensional analysis. The left hand boundary is the velocity-inlet and the right hand boundary is the pressure-outlet. All other boundaries are set to the 'wall' condition.

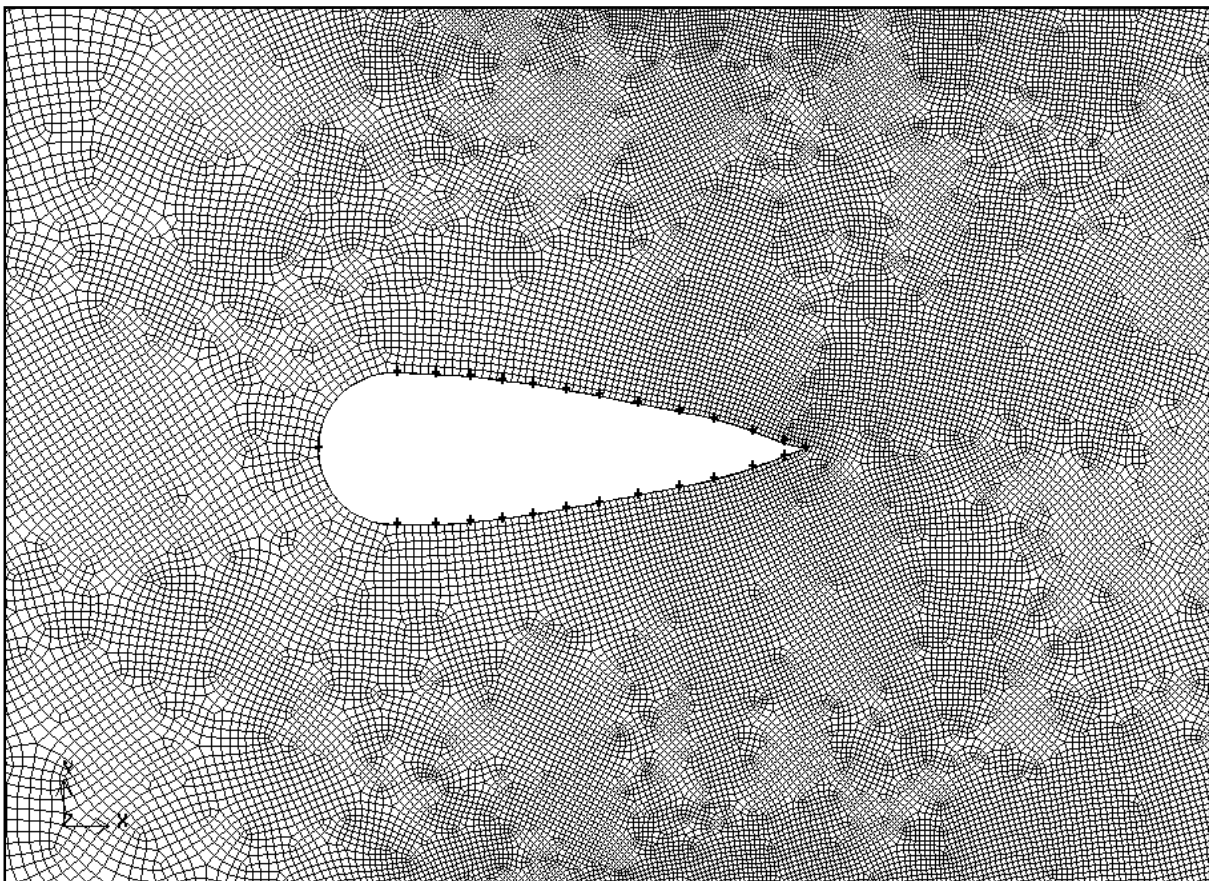


Figure D-2b - Finer mesh immediately around the pier.

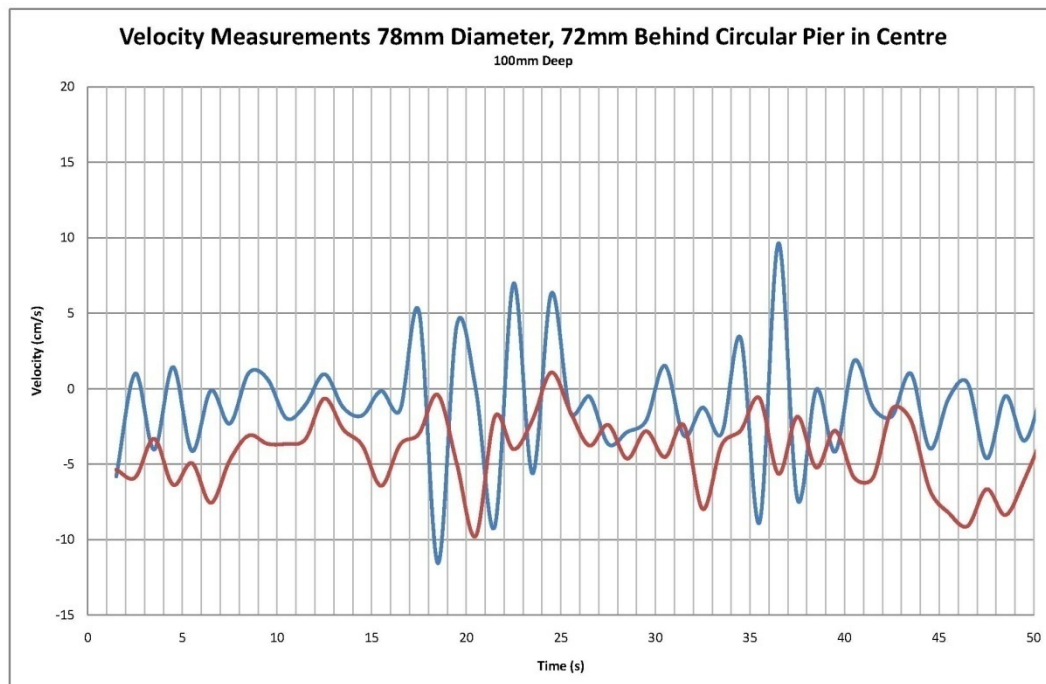
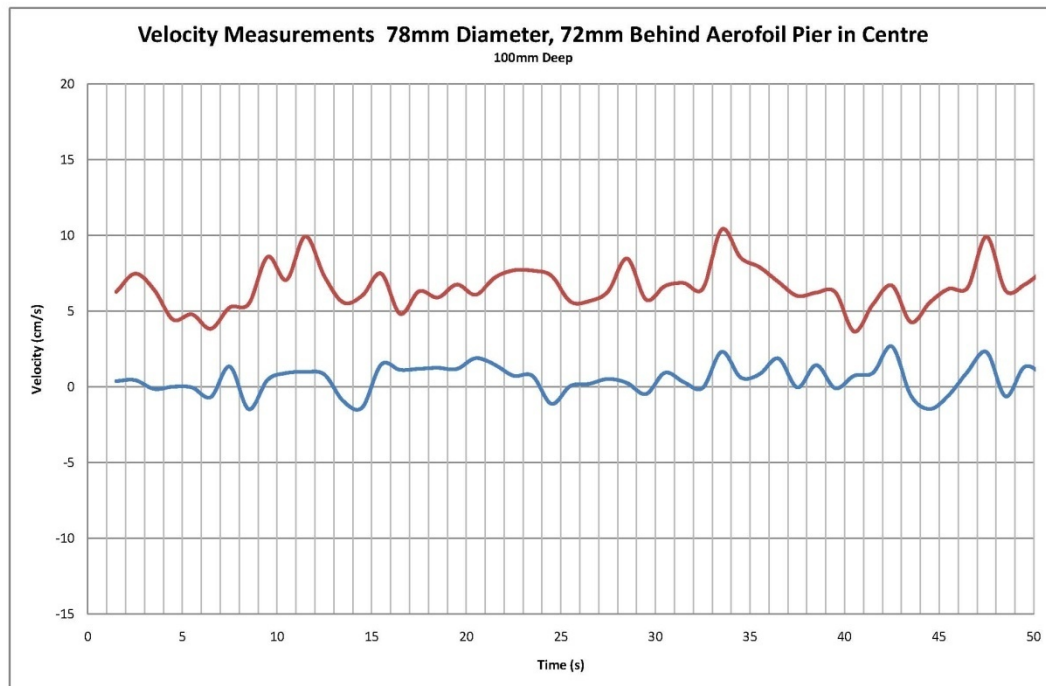


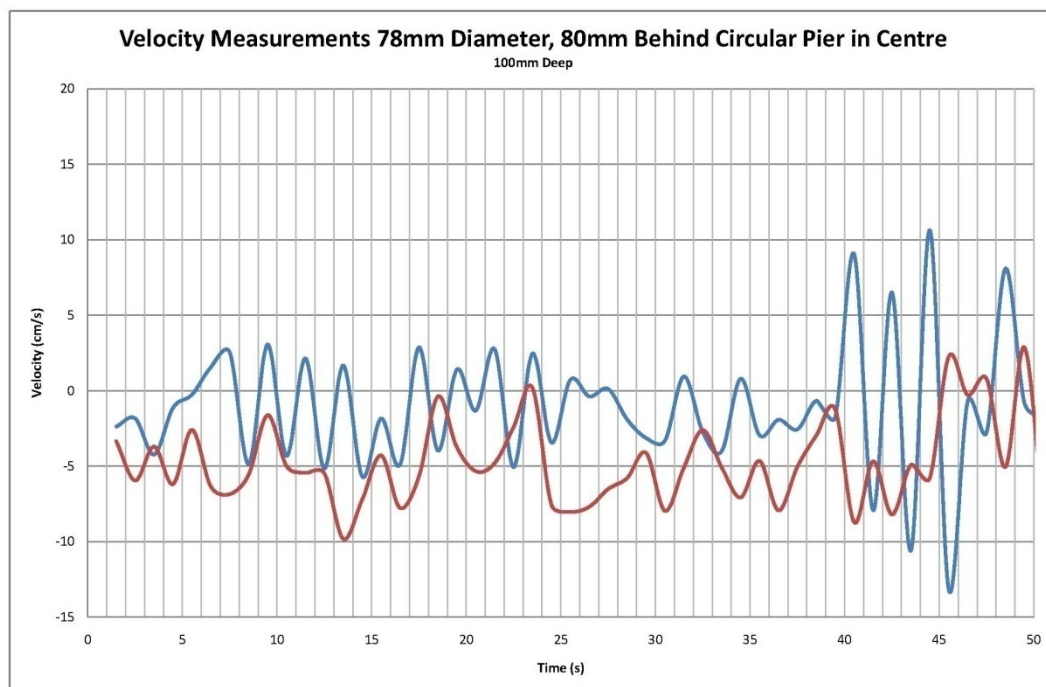
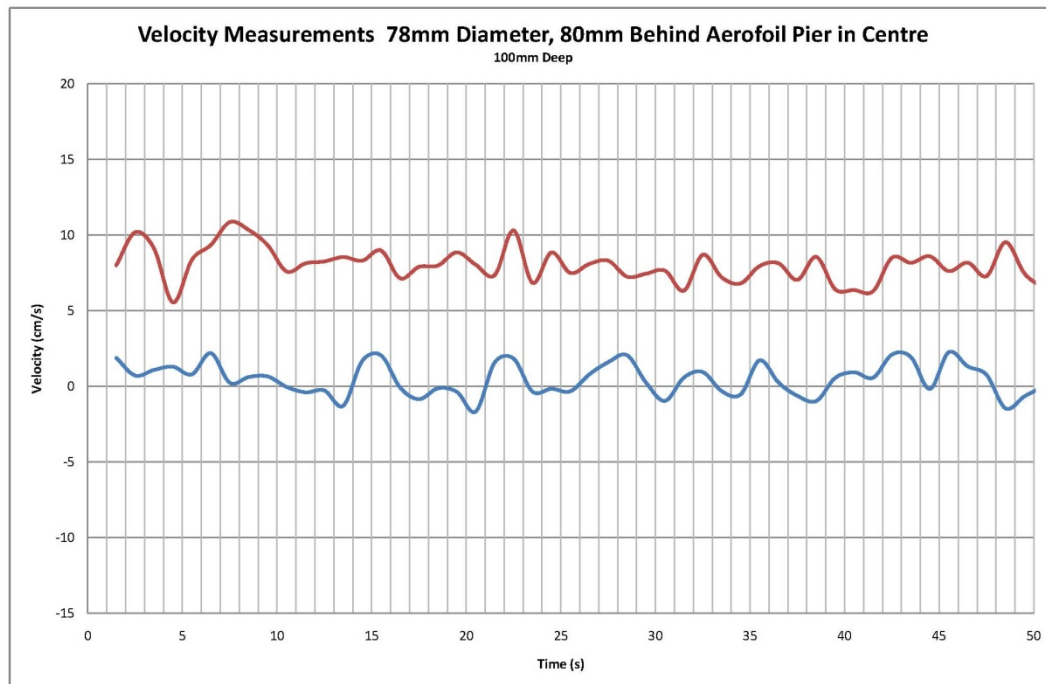
APPENDIX E - MEASURED VELOCITIES USING THE ADV

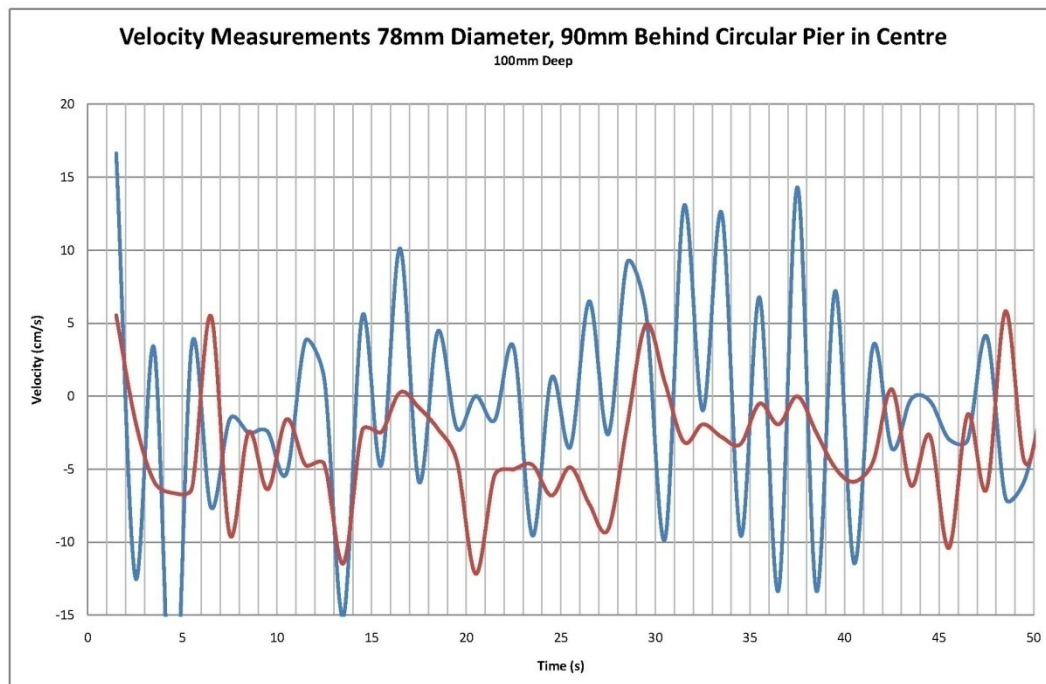
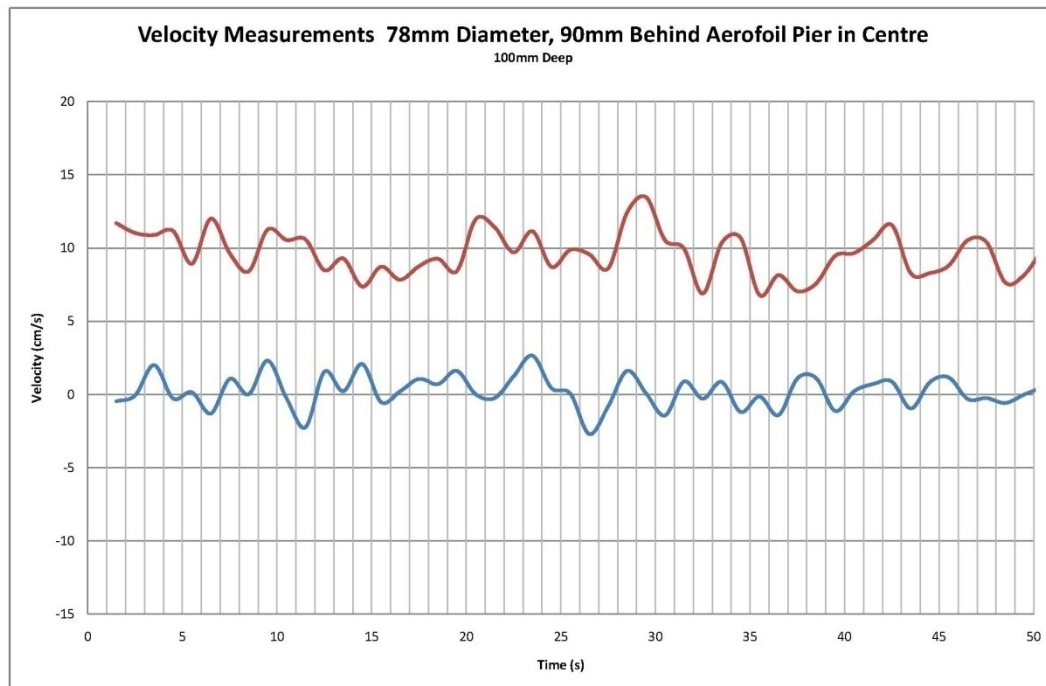
The plots shown here are a comparative view of measured velocities between the aerofoil pier and the circular pier. These velocities were taken from the centre of the pier, at the distances outlined on each graph. For further assistance with recorded velocities and plots please refer to the cd provided.

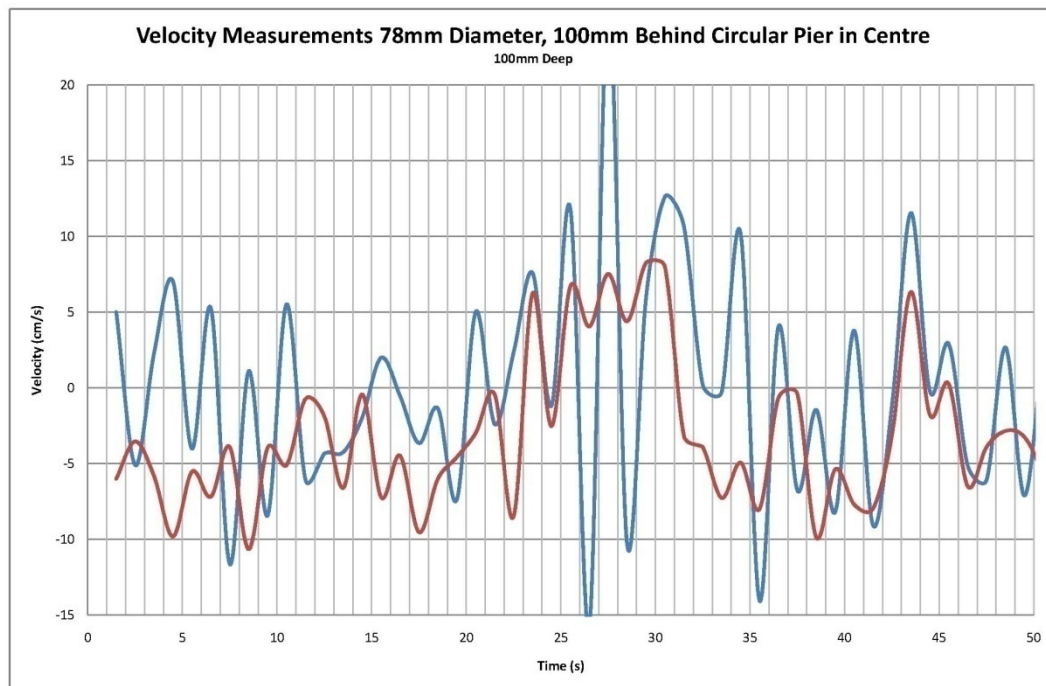
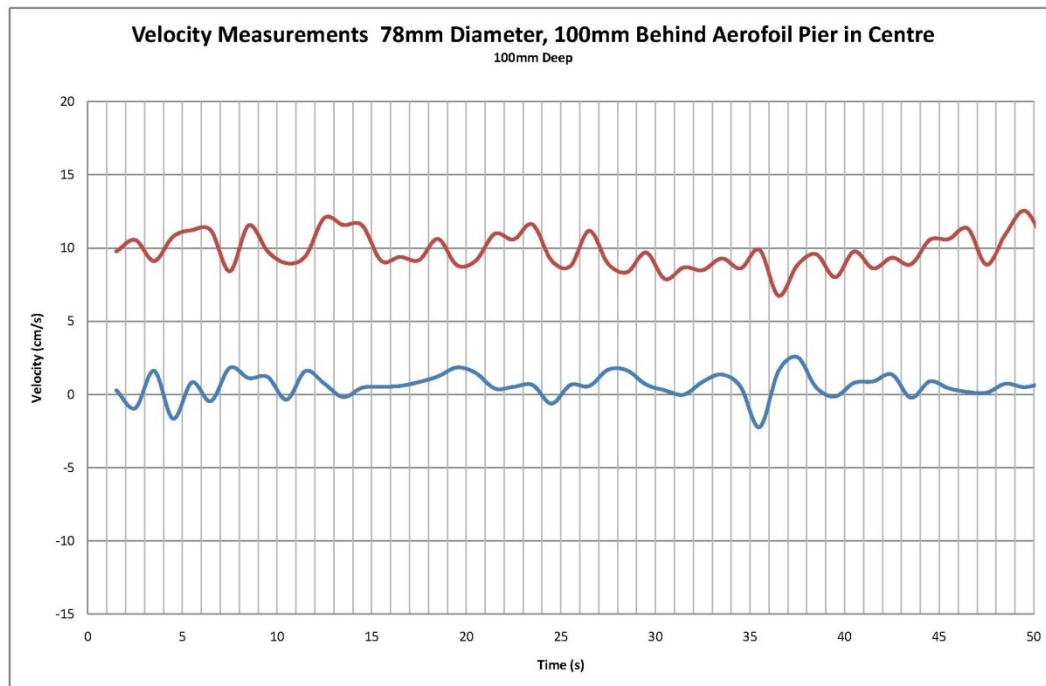
In each plot the red line represents down stream velocity, and the blue represents the cross stream velocity. Negative velocities in the down stream direction mean that the water is flowing in the upstream direction.

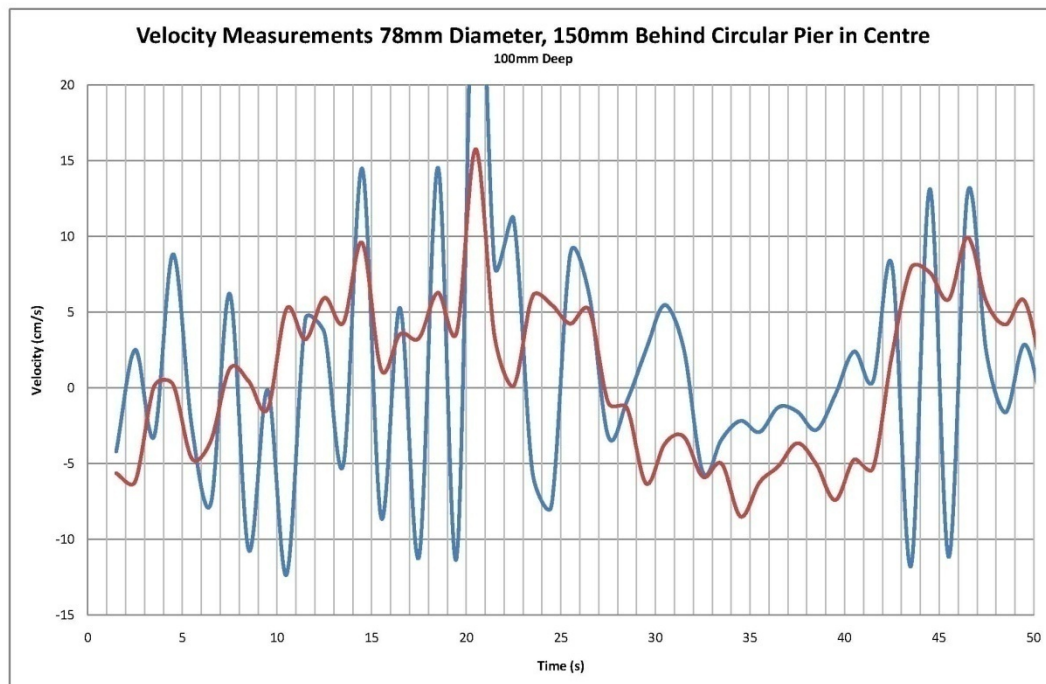
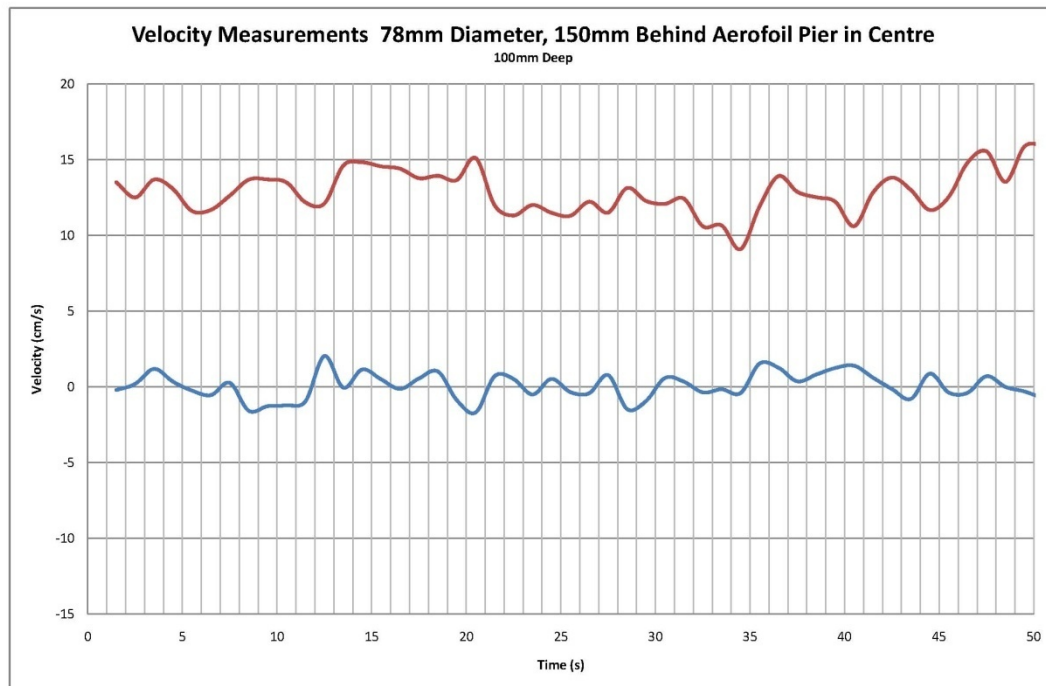
Also note that the cross-stream velocities with the aerofoil pier still fluctuate. This indicates that there is still the presence of turbulence, however the magnitude of the turbulence is still much smaller than the circular pier. This is confirmed with the FLUENT results also.

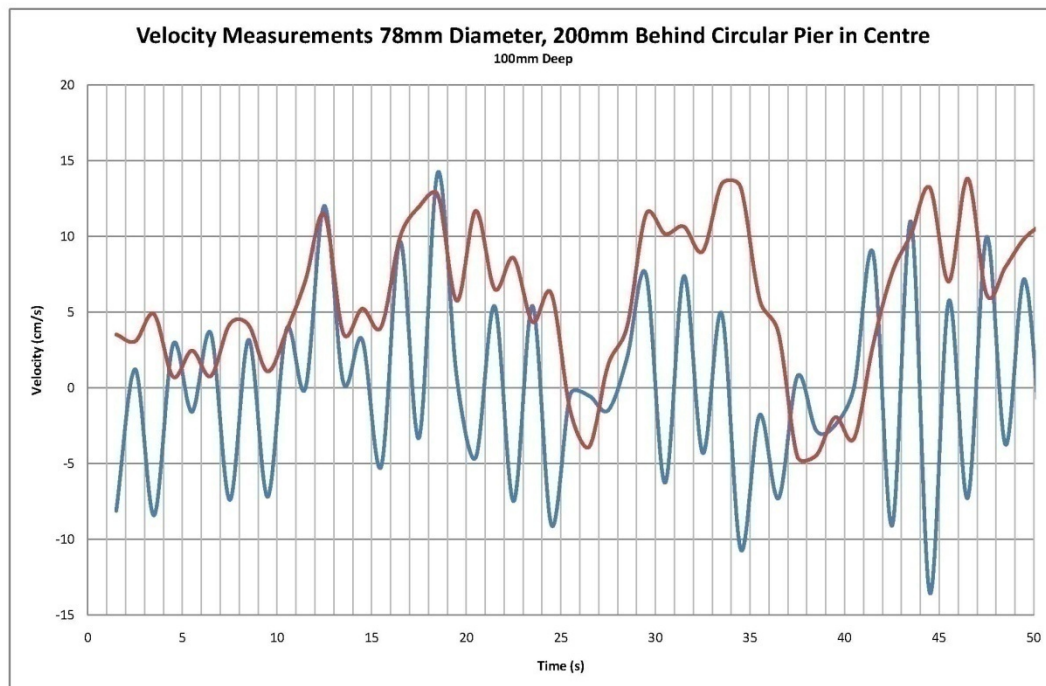
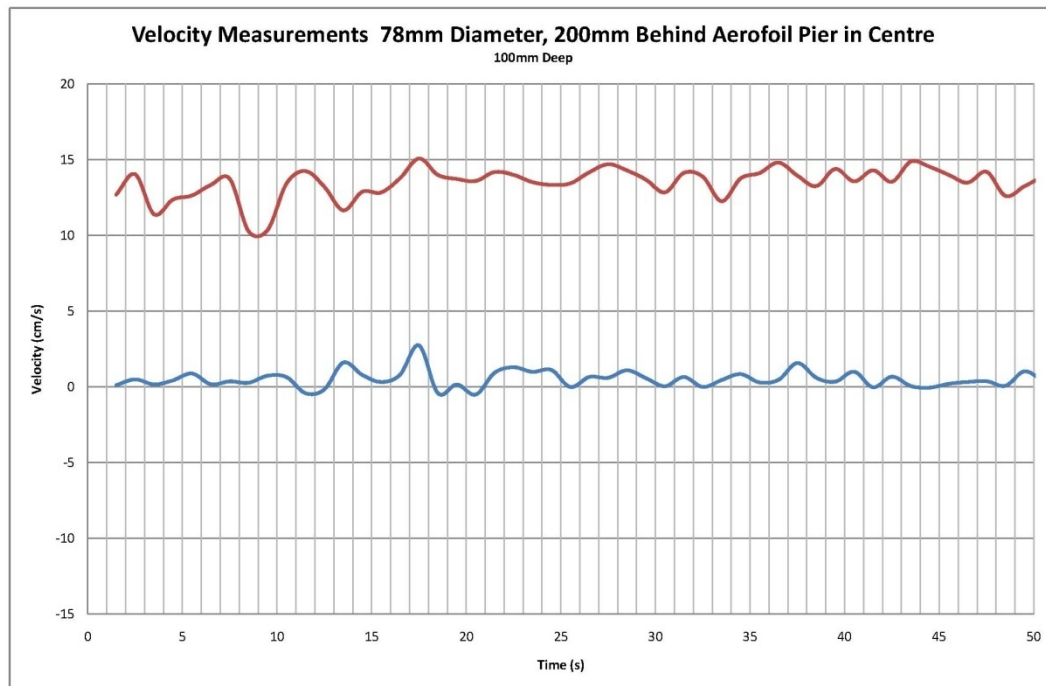


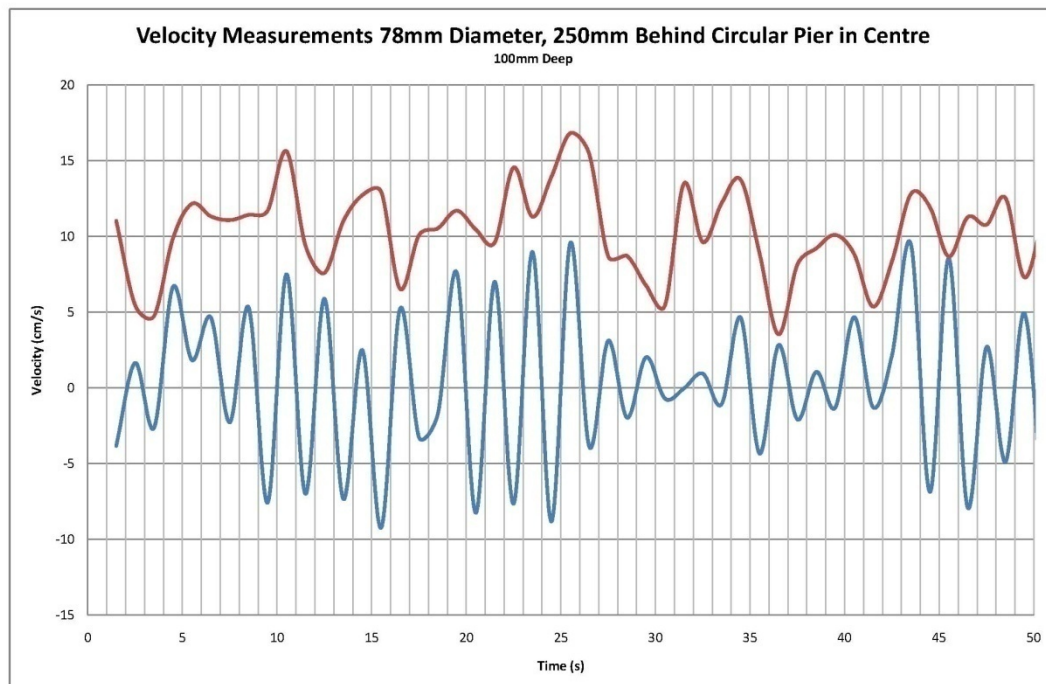
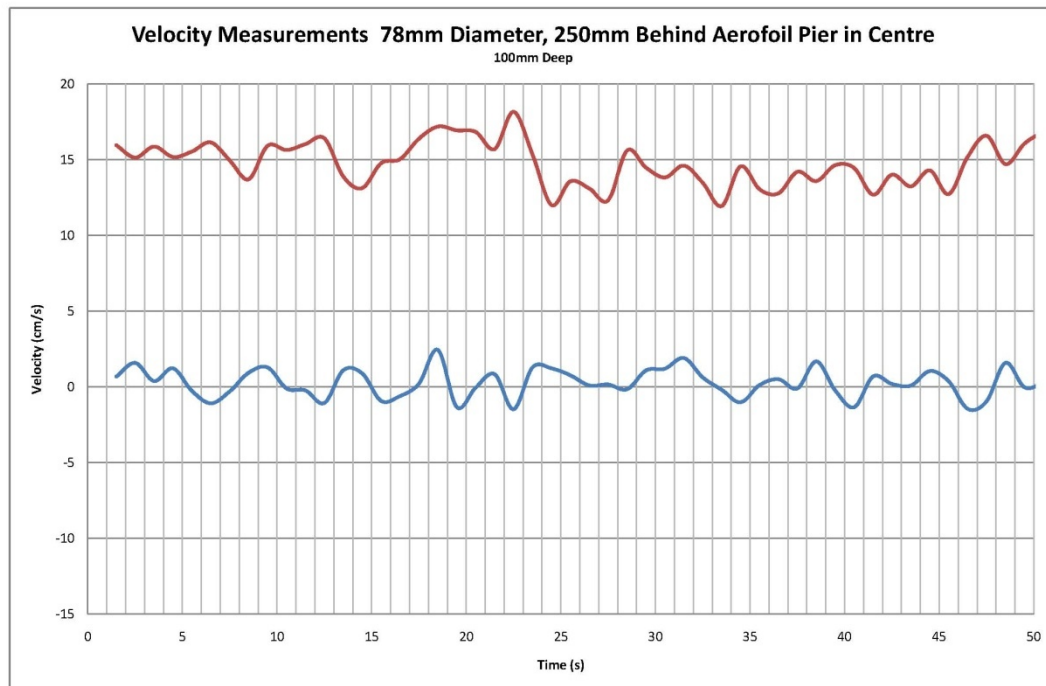


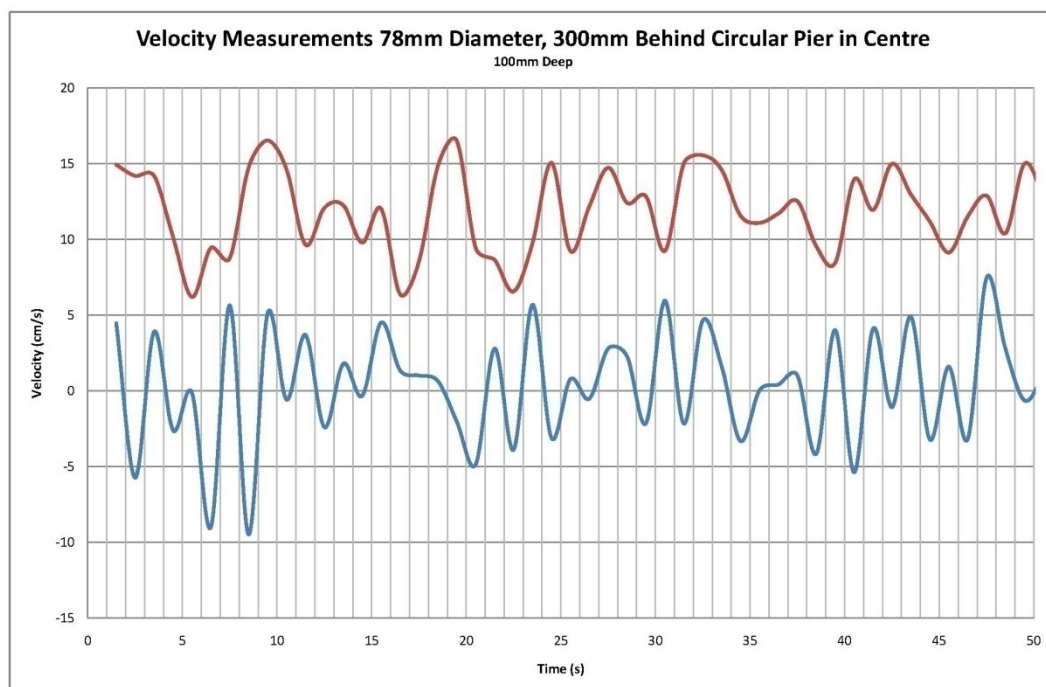
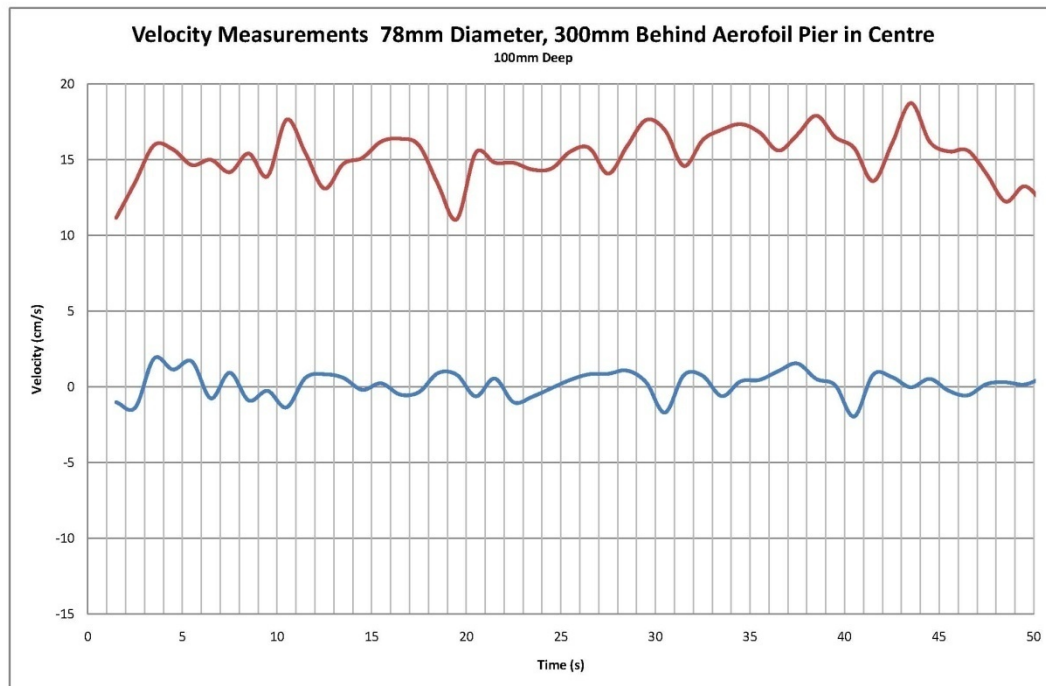


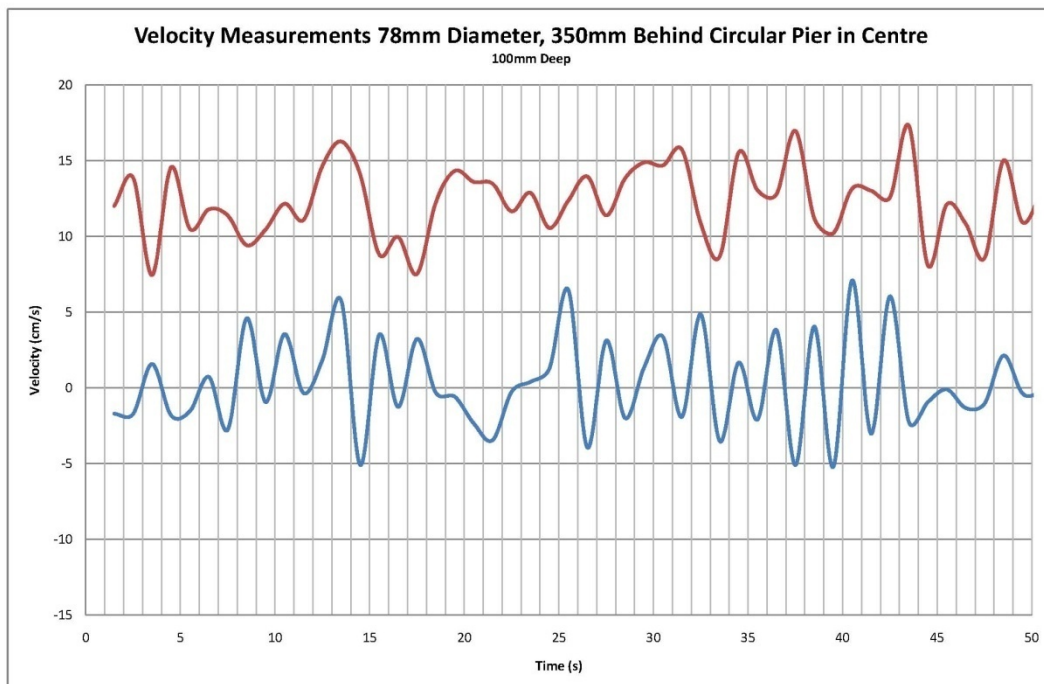
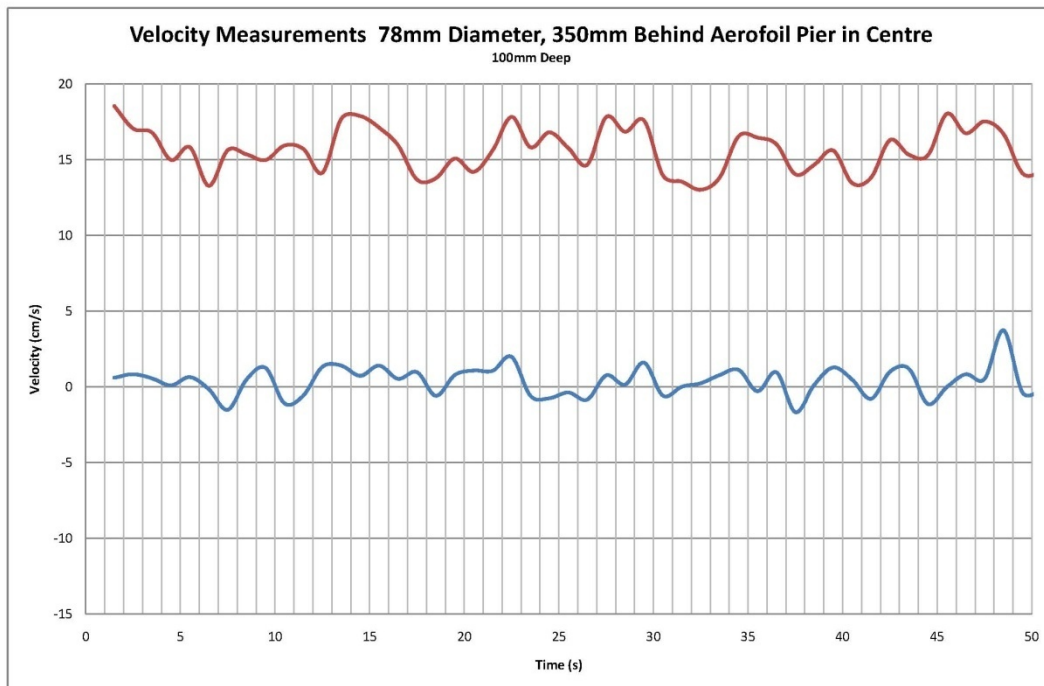








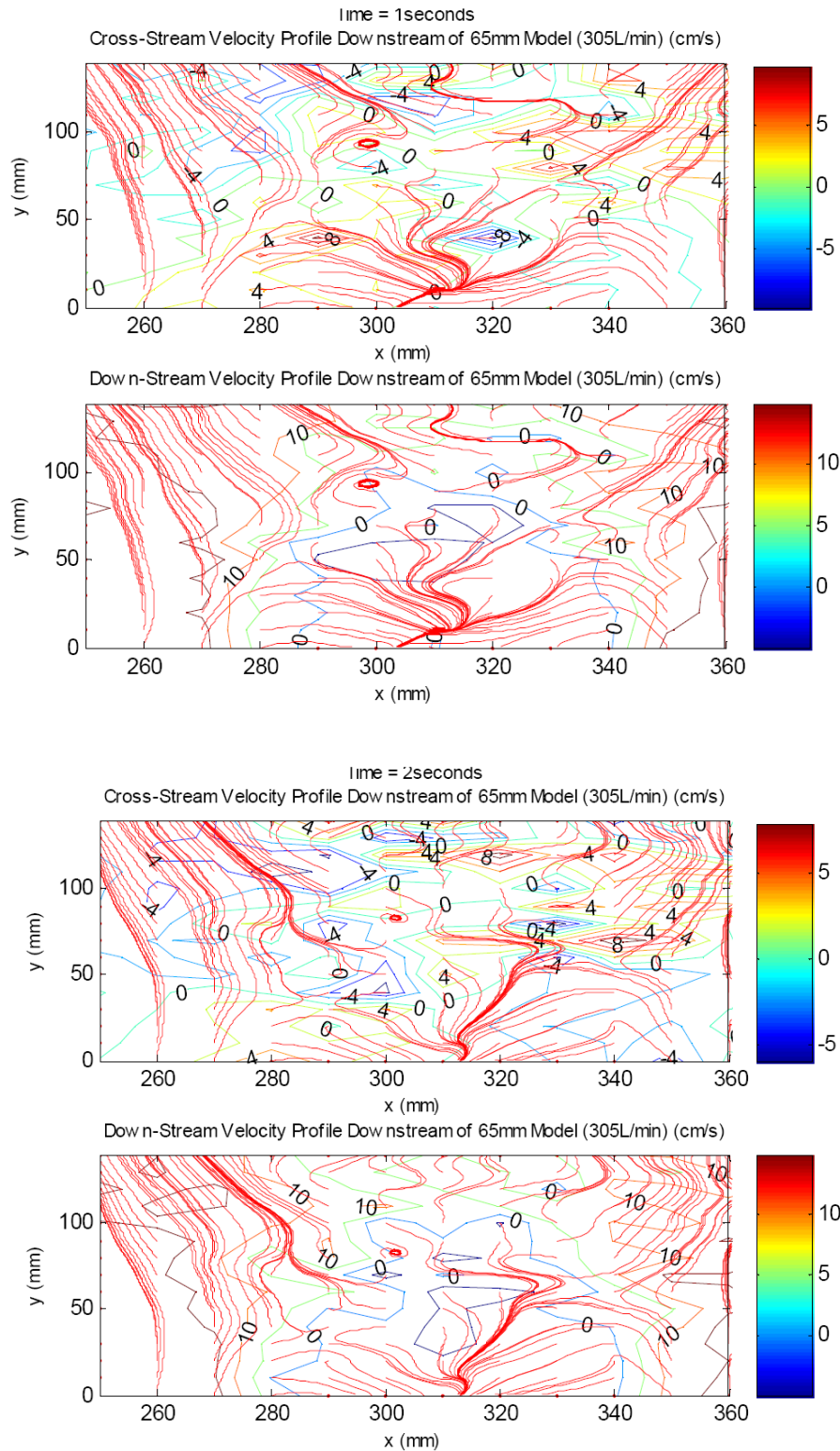


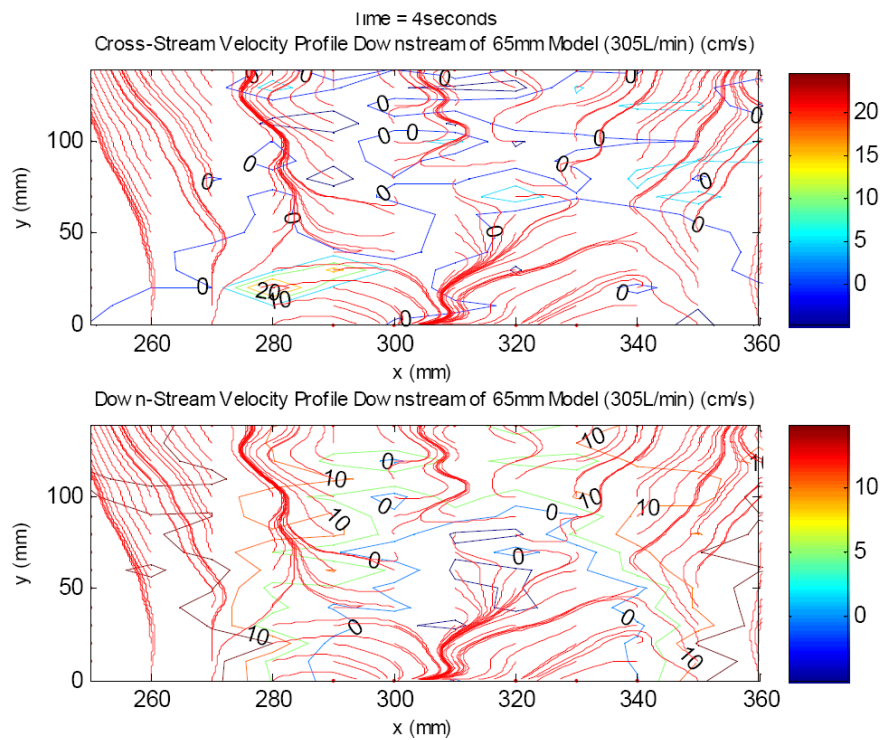
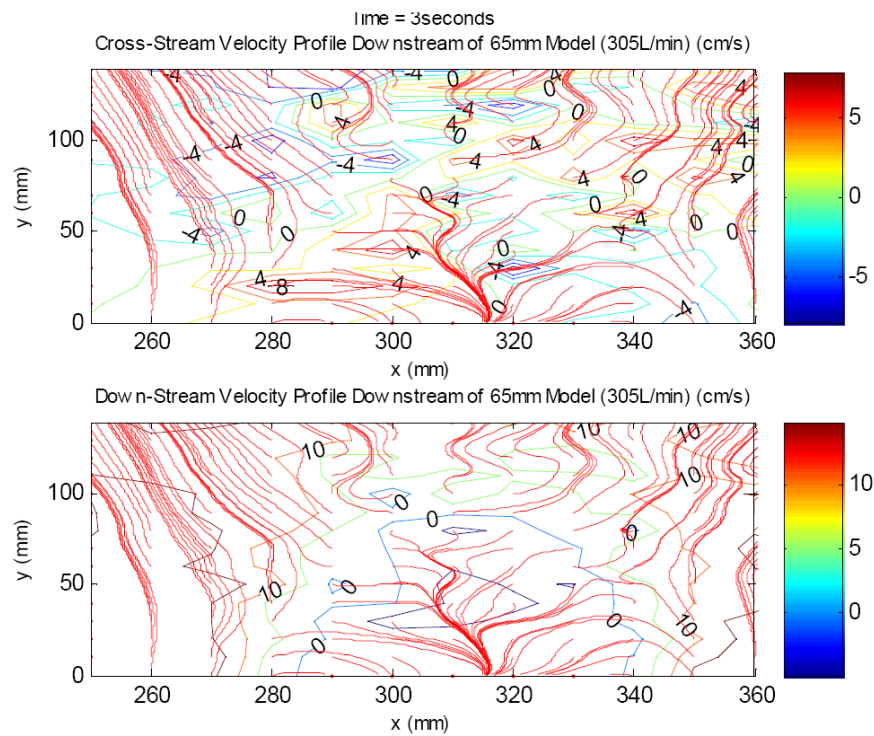


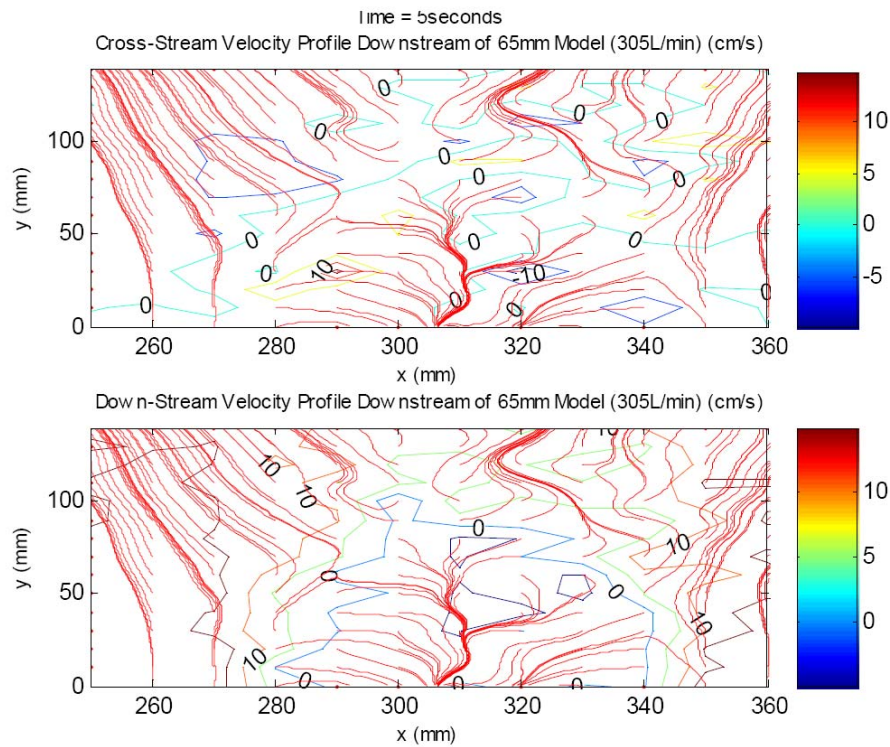


APPENDIX F - RECORDED VELOCITIES FOR THE 65MM PIER

HERRON'S RESULTS

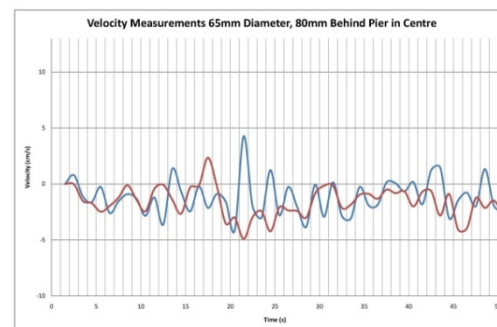
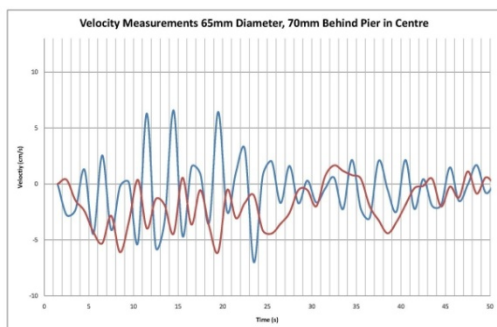
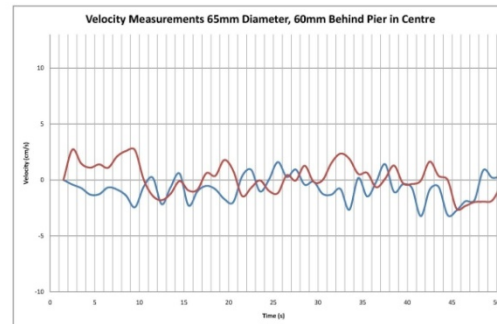
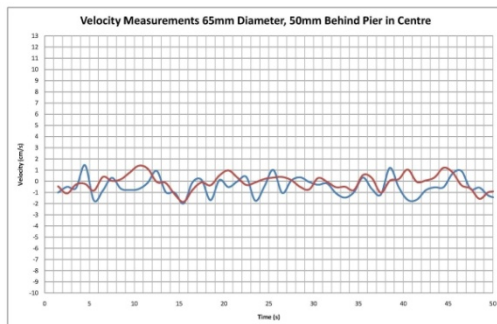


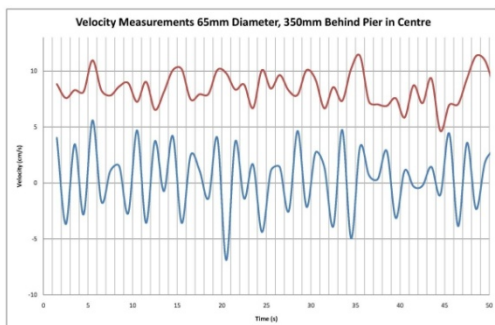
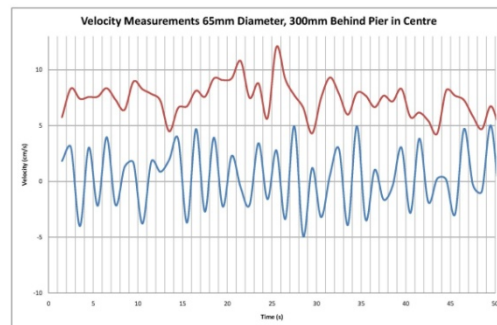
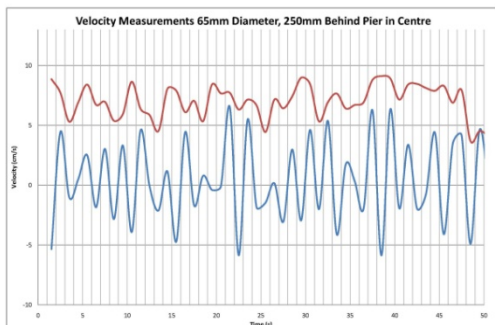
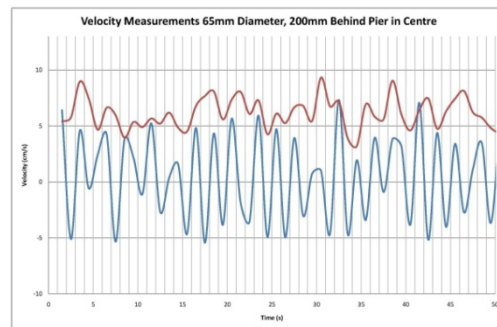
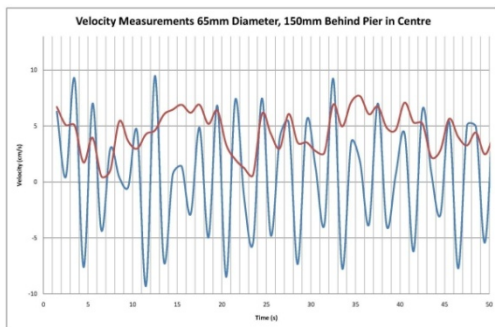
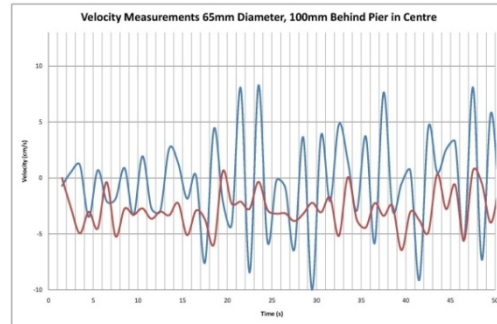
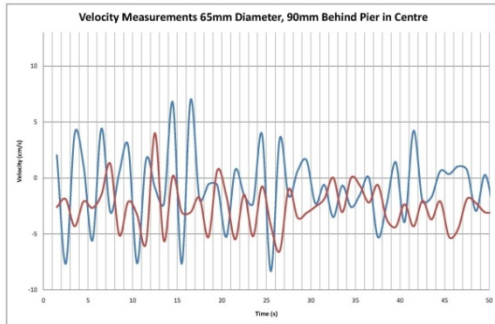




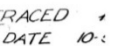
MEASURED VELOCITIES

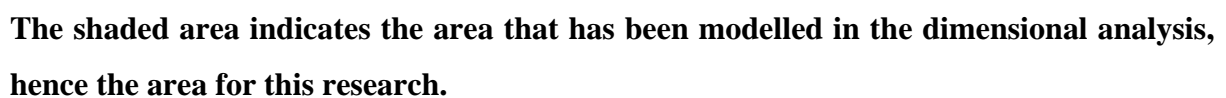
(Red = Down-stream Velocity, Blue = Cross-stream Velocity)





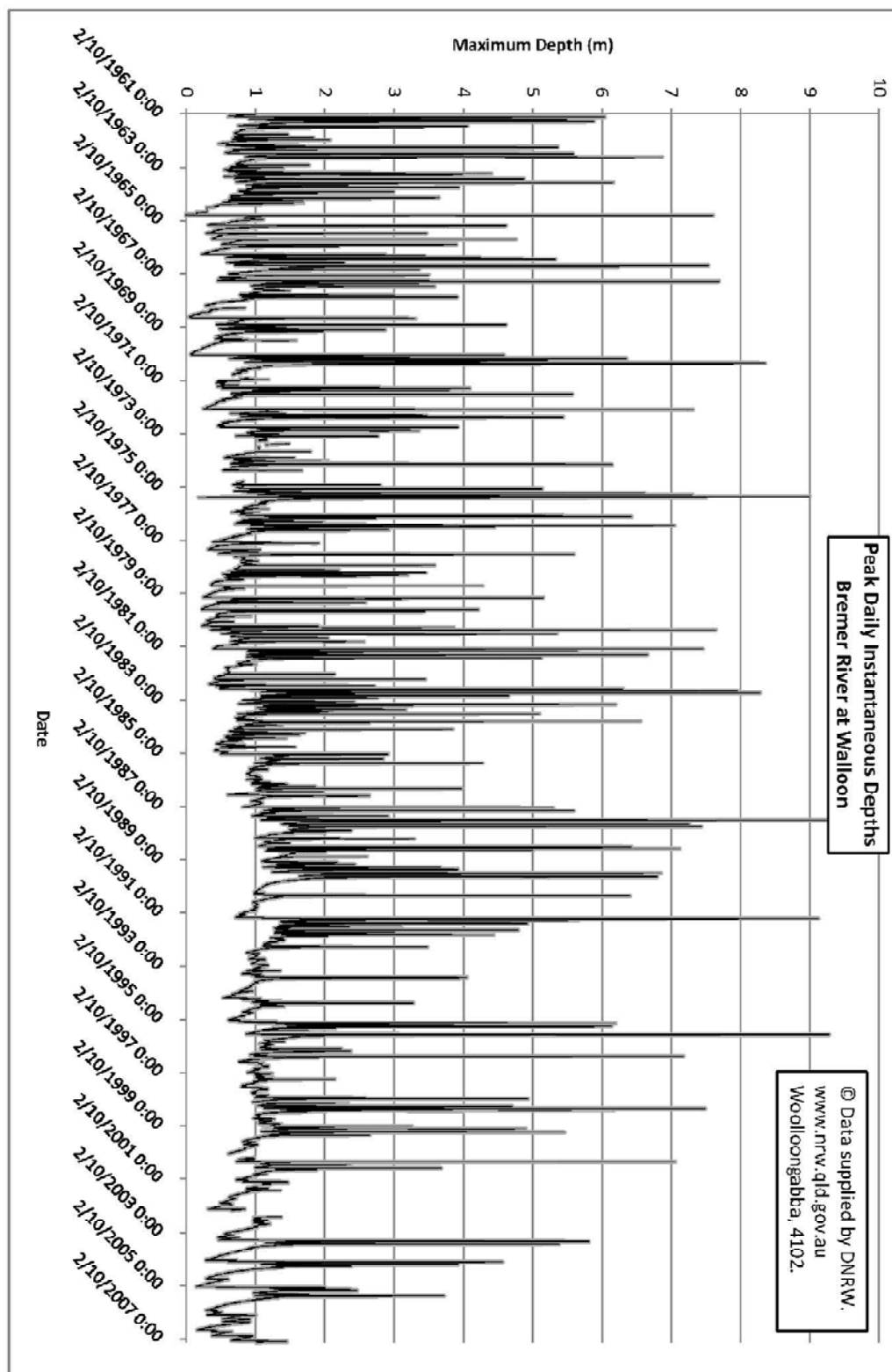
BREMER RIVER BRIDGE CROSS SECTION - COURTESY OF DMR QLD

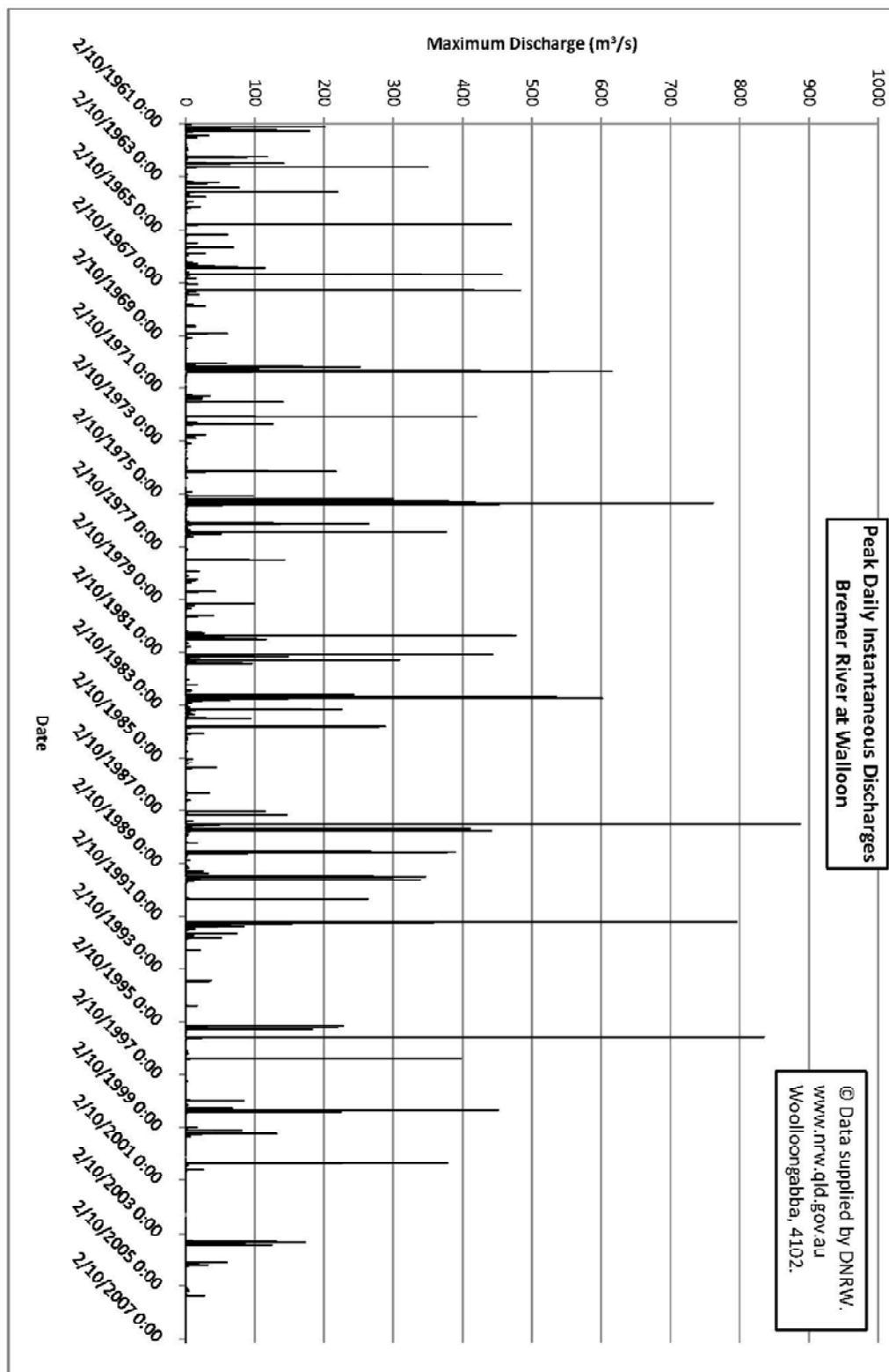






BREMER RIVER FLOW DATA - COURTESY OF DNRW QLD







BREMER RIVER DESIGN SHEETS - COURTESY OF DMR QLD

FROM MAIN ROADS BRASSALL

03.23.1992 14:10

NO. 4 P. 1



Queensland Department of Transport
Cnr White and Cotton Street Nerang
PO Box 442 Nerang 4211

Facsimile

To:

BILL SEMPLE
BRIDGE BRANCH

Fax number: (07 834 2065

Subject:

Our Reference: 85/18A/53

Your Reference:

Date: 23 10 3 1992

Number of pages following: 2

If problems occurred in the transmission of the documents, please contact:

Message

Please find attached, notes regarding
design velocities for
Bremer River Bridge.

Lonain.

From: S.L. BARTHELOT

Division/Branch/Section: KARALEE SITE OFFICE

Direct Phone: (07) 294 7112

Direct Fax: (07) 201 7585



IN ROADS BRASSALL

03.23.1992 14:11

NO. 4 P. 2

2065

Memorandum



Main Roads
Main Roads Department, Queensland

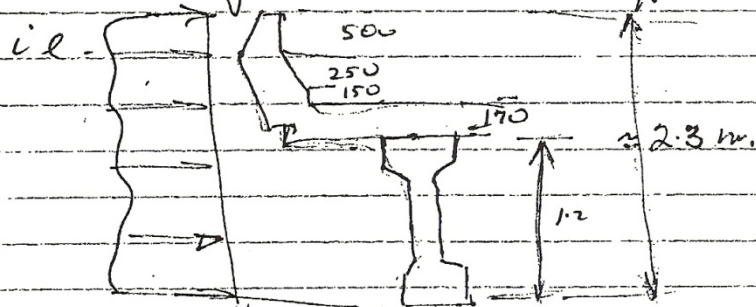
To L.B.
From P.R.
Subject Bremer River.
Reference
Enquiries
Extension
Date 21/6/89

After further discussion with JMF regarding design flood forces, the following should be considered.

Either

3m debris mat $\times (25+27)$ m wide
using surface velocity.
Drag factor 1.0. $\rightarrow (.52V^2)$ $\rightarrow 3.7$ Seismic
5.3 kN.

OR Flood force on exposed superstructure



using surface velocity and drag factor
of 2 $\rightarrow 2.2$ (refer Apelts work on
drag factors.) i.e. $(1.1V^2)$

For the second option F.S. of 1.5 on o/s.
shd be adequate.

see also attached notes



IN ROADS BRASSALL

03.23.1992 14:12

NO. 4 P. 3

DE
for information.

BREMER RIVER FLOODING

① Original Bridge Flood Loading

Main Channel - 1500 lbs/ft.
 { If factor of safety of 2 used
 this is equivalent to $3.7 \text{ m/s} \times \sqrt{2}$
 i.e. Ult velocity of 5.3 m/sec. + Load factor of 1.0 IMF.
 check both conditions. }
 Surface 3.7 m/sec
 { This would be based on 10 ft
 debris mat and surface
 velocity = 12.24 ft/sec
 Av. velocity = 8.57 ft/s
 (2.61 m/s) }
 Overflow Channel - 1000 lbs/ft.
 { Corresponds to
 3.05 m/s (surface)
 4.3 m/s (U/V) }
 { $V_{av} = 7 \text{ ft/sec}$
 (2.13 m/s) }

Recommend Debris loads as in original design.

Because: (1) Bridge has withstood overtopping floods

(2) There would have to be very good reasons
(not known) why lower velocities could
be adopted.

② Flood Levels

Deck Level of Exist. Bridge - RL 15.80m (15.85m S
A.H.D.)

1974 Flood at Exist. Bridge - RL 19.70m AHD.
(includes backwater from Brisbane River)

Bremer R. flooding only in 1974 - RL 19.0m AHD approx

See attached Paper by Eng. G. Heatherwick (Bureau of
Meteorology).

∴ Bremer River bridge will be substantially overtopped
even after Wivenhoe Dam and reduced floods in
Brisbane ~~Bremer~~ River.

M. Hee



APPENDIX H - SCHOHARIE CREEK BRIDGE FAILURE

THE COLLAPSE OF THE SCHOHARIE CREEK BRIDGE

Summarized from Storey and Delatte, *Lessons from the Collapse of the Schoharie Creek Bridge*, Proceedings of the 3rd ASCE Forensics Congress, October 19 - 21, 2003, San Diego, California

INTRODUCTION

The Schoharie Creek Bridge collapsed on the morning of April 5, 1987 after three decades of service. The collapse of pier three caused two spans to fall into the flooded creek. Five vehicles fell into the river, and ten occupants died.

Bridges across waterways must be designed structurally not only to carry their own weight and traffic loads, but also to resist the hydraulic forces imposed by rivers and other bodies of water. Moreover, the construction of the bridge abutments and piers alters the river's flow, and may lead to new patterns of erosion and deposition. The collapse of the Schoharie Creek Bridge illustrates the importance of designing bridge piers to resist scour. The case also illustrates the importance of the inspection and maintenance of bridges.

DESIGN AND CONSTRUCTION

The Schoharie Creek Bridge was one of several bridges constructed by the New York State Thruway Authority (NYSTA) for a 900 km (559-mile) superhighway across New York State in the early 1950's. The bridge was situated northwest of Albany in the Mohawk Valley (WJE Associates, 1987).

The 1949 edition of the American Association of State Highway Officials (AASHO – now the American Association of State Highway and Transportation Officials, AASHTO)



“Standard Specifications for Highway Bridges” was used for the design of the Schoharie Creek Bridge. The preliminary design for the bridge was contracted out to Madigan-Hyland Consulting Engineers (WJE Associates, 1987).

The design firm developed two designs for the crossing of the Schoharie creek. The preliminary designs were similar except for the lengths of spans, one 183 meters (600 feet) and the other 165 meters (540 feet). Both plans placed two piers on shallow footings in the Schoharie Creek and two piers on the creek banks to support the structure.

The New York State Department of Public Works (DPW), later named the New York State Department of Transportation (NYSDOT), approved the 165 meter (540-foot) bridge for the crossing of the Schoharie Creek. The final design was submitted in January 1952 and consisted of five simply supported spans with nominal lengths of 30.5, 33.5, 36.6, 33.5, and 30.5 meters (100, 110, 120, 110 and 100 feet). Concrete pier frames supported the bridge spans along with abutments at each end (figure 1).

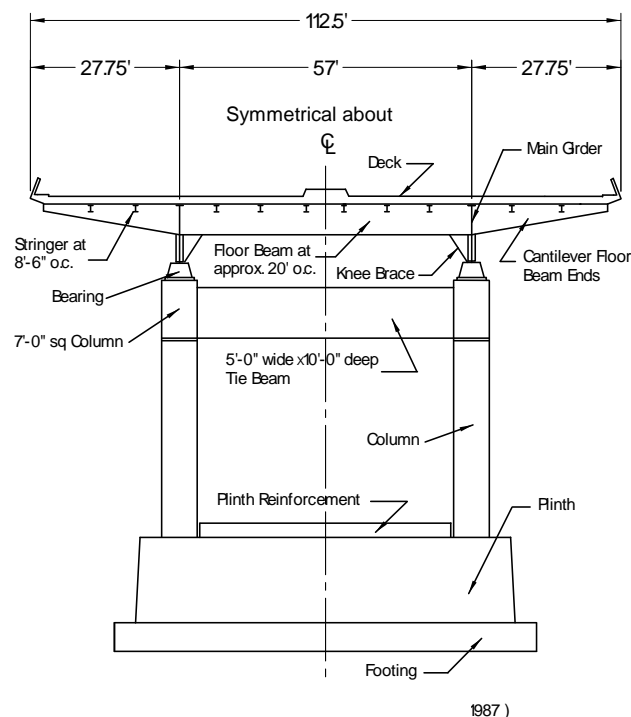


Figure 1. Pier Section



The pier frames were constructed of two slightly tapered columns and tie beams. The columns were fixed within a lightly reinforced plinth, which was positioned on a shallow reinforced spread footing. The spread footing was to be protected by a layer of dry riprap. The superstructure was made up of two longitudinal main girders with transverse floor beams. The skeleton of the 200 mm (eight-inch) thick bridge deck was comprised of steel stringers (WJE Associates, 1987). A plan of the bridge spans is shown in figure 2.

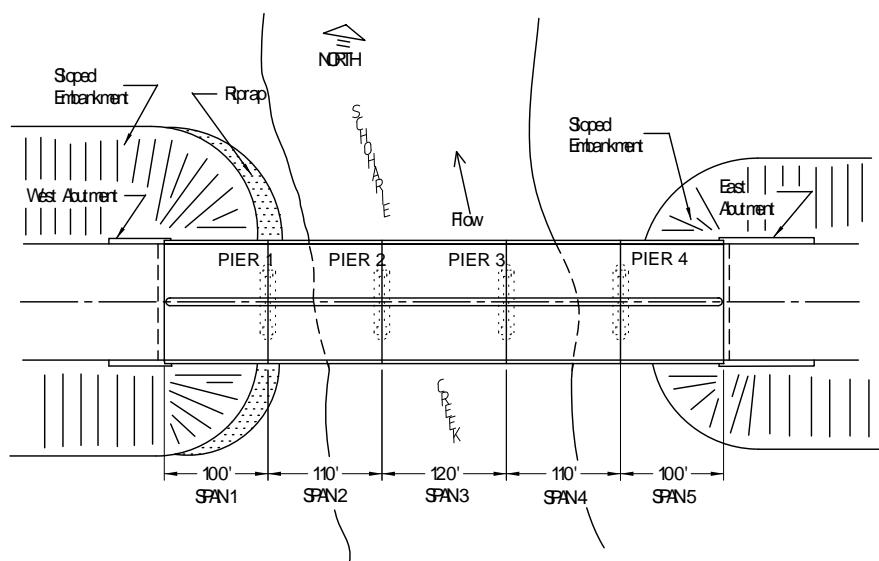


Figure 2 - Schematic plan of bridge (after "Collapse," 1987)

Figure 2. Schematic plan of bridge (after “Collapse,” 1987)

The construction contract for the bridge was awarded to B. Perini and Sons, Inc. on February 11, 1953, and construction began shortly thereafter. Madigan-Hyland Consulting Engineers performed construction inspection for the bridge in conjunction with DPW. The majority of the construction was completed and the bridge was opened to partial traffic during the summer of 1954. The Schoharie Creek Bridge was fully completed soon after October of 1954 (WJE Associates, 1987). Nearly a year later, the bridge successfully survived a 100 year flood, but the damage from the October 16, 1955 flood may have had a bearing on the collapse three decades later (NTSB, 1988).



The as-built plans did not reflect the true condition of the bridge. They showed that sheet piling had been left in place to protect the piers. However, it had been removed after construction (WJE Associates, 1987, NTSB, 1988).

PIER MODIFICATIONS

Shortly after construction was completed, in the spring and summer of 1955, the Schoharie Creek Bridge pier plinths (shown in figure 1) began to form vertical cracks. The cracks ranged from 3 to 5 mm (1/8 to 3/16 inches) in width and the locations of the cracks varied from pier to pier (WJE Associates, 1987). The cracks occurred due to the high tensile stresses in the concrete plinth. The plinth could not resist the bending stresses between the two columns. The original designs called for reinforcement to be placed in the bottom portion of the plinth only since designers had confidence that the concrete in tension could resist the bending stresses without reinforcement.

It was later determined that the upper portion of the pier plinths had a tensile stress of 1.4 MPa (200 psi) and there should have been more than 39,000 square mm “upwards of 60 square inches of steel in the upper face” of the plinth (WJE Associates, 1987). In 1957, plinth reinforcement was added to each of the four piers to correct the problem of vertical cracking.

The plinth may be seen as an upside down uniformly loaded beam, with the soil bearing pressure providing the uniform loading and the two columns acting as supports. It becomes obvious that the top of the plinth represents the tension face of the beam and requires reinforcement. However, to be properly anchored the tension reinforcement must be extended past the supports – in this case, into the columns (NTSB, 1988). Obviously, this was not done, and it would have been difficult to extend the reinforcement through the columns without replacing the columns. Ironically, because the added plinth reinforcement was not adequately anchored, it may have contributed to the brittle and sudden nature of the subsequent collapse, by supporting the plinth until most of it had been undermined (WJE Associates, 1987, Thornton-Tomasetti, P. C., 1987).

There were several other problems that occurred shortly after the completion of the bridge. Inspectors noticed that the expansion bearings were out-of-plumb, roadway approach



slabs had settled, roadway drainage was poor, and the supporting material for west embankment dry stone pavement was deficient. All of the problems mentioned and other minor problems were corrected by fall of 1957 (WJE Associates, 1987).

THE COLLAPSE

The Schoharie Creek Bridge collapsed on the morning of April 5, 1987 during the spring flood (Boorstin, 1987, Thornton et al., 1988). Rainfall totaling 150 mm (6 inches) combined with snowmelt to produce an estimated 50 year flood (WJE Associates, 1987).

The collapse was initiated by the toppling of pier three, which caused the progressive collapse of spans three and four into the flooded creek. The piers and spans are shown in Figure 2. One car and one tractor-semitrailer were on the bridge when it collapsed. Before the road could be blocked off, three more cars fell into the gap. The drivers of the other vehicles were probably too close to the bridge to stop in time when it fell. Over the next three weeks, nine bodies were recovered. One was never found. (NTSB, 1988).

Pier two and span two fell ninety minutes after span three dropped, and pier one and span one shifted two hours after that (Thornton-Tomasetti, P. C., 1987). The NTSB suggested that pier two collapsed because the wreckage of pier three and the two spans partially blocked the river, redirecting the water to pier two and increasing the stream velocity (NTSB, 1988). The missing span and the floodwaters may be seen at the following web sites:

- Scour Critical Bridges (2002)
http://www.nationalbridgeinventory.com/scour_critical_bridges.htm>
- Hudson International - includes an animation of the collapse of the second span
<http://members.aol.com/higrp/bridge.htm>
- MRCE web site - Schoharie Creek Thruway Bridge (2002)
<http://www.mrce.com/pages/projects/1987-3.shtml>

Six days later, a large section of the Mill Point Bridge located about 5 km (3 miles) upstream of the Schoharie Creek Bridge collapsed. Fortunately, the bridge had been closed since the flood because NYSDOT feared that its foundation had also been eroded (WJE Associates, 1987).



CAUSES OF FAILURE

Two teams investigated the Schoharie Creek Bridge failure – Wiss, Janney, Elstner (WJE) Associates, Inc. with Mueser Rutledge Consulting Engineers investigated for the NYSTA, and Thornton-Tomasetti, P.C. investigated for the New York State Disaster Preparedness Commission. The teams cooperated, and the chief role of Thornton-Tomasetti, P.C. was to review WJE's work. A number of other firms assisted in the investigation (Bridge Collapse @ 2002, Schoharie Creek Thruway Bridge @ 2002). A cofferdam was constructed around the failed piers and the site was dewatered and excavated, both to aid the investigation and the construction of the replacement bridge (WJE Associates, 1987).

Each of the teams prepared a report as to the cause of the failure, and they similarly concluded that the collapse of the Schoharie Creek Bridge was due to the extensive scour under pier three. Scour is defined as “the removal of sediment from a streambed caused by erosive action of flowing water” (Palmer and Turkiyyah, 1999). The vulnerability of scouring under pier three was affected by four important factors (Thornton-Tomasetti, P. C., 1987):

- “The shallow footings used, bearing on soil, could be undermined.” Therefore the depth of which the footings was not enough to take them below the probable limit of scour.
- The foundation of pier 3 was bearing on erodable soil. “Layers of gravel, sand and silt, interbedded with folded and tilted till,” allowed high velocity floodwaters to penetrate the “bearing stratum.”
- “The as-built footing excavations and backfill could not resist scour.” The area left around the footing due to excavation was backfilled with erodable soil and topped off with dry riprap, “rather than being backfilled with riprap stone” to the entire depth of the excavation as design plans specified.
- “Riprap protection, inspection and maintenance were inadequate.”

The process of scouring under the piers began shortly after the bridge was built. In 1955, the bridge footings experienced floodwater flows unanticipated in the design of the bridge, a 100-year flood, and it is believed that the majority of the scouring energy was dissipated into



moving the original riprap layer from around the footings. Once the backfill had been exposed, the years of peak flows removed the backfill material, and the backfill material in turn was replaced by sediment settling into the scoured holes (WJE Associates, 1987).

The 1955 flood had an estimated flow of 2.17 million liters per second (76,500 cfs). The 1987 flood had an estimated flow of 1.8 million liters per second (63,000 cfs) and an estimated velocity of 4.6 meters per second (15 fps). However, after the 1955 flood, berms were constructed upstream, and the velocity at the bridge may have been the same as the 1955 flood. Furthermore, the riprap placed at construction had probably been washed away during the 1955 flood, and had not been replaced (WJE Associates, 1987).

This process continued until so much material was removed that there was a loss of support capacity (Shepherd and Frost, 1995). The upstream end of pier 3 fell into a scour hole approximately 3 meters (9 feet) deep (NTSB, 1988). It was estimated that approximately 7.5 to 9 meters (25 to 30 feet) of the pier was undermined (WJE Associates, 1987).

The damage due to scour is shown at the Hudson International web site (<http://members.aol.com/higrp/bridge.htm>). The bridge design originally called for leaving the sheet piles (which were used to keep water out of the excavation area during construction) around the piers (Levy and Salvadori 1992). The specified riprap would then fill the area left between the pier footings and sheeting.

Unfortunately, the sheet piles were not left in place. Possibly, they could have prevented the scour altogether. Levy and Salvadori note (p. 146) that “in the contract issued in 1980 for maintenance work, all reference to new stone riprap had been deleted by a nonengineer state employee who decided, after viewing the site from shore, that it was unnecessary.” The NTSB also noted this incident (NTSB, 1988).

The riprap was also too light. The specification called for riprap with 50 % of the stones heavier than 1.3 kN (300 pounds) and the remainder between 0.44 and 1.3 kN (100 to 300 pounds). However, the investigators found that riprap weights of 4.4 to 6.7 kN (1,000 to 1,500 pounds) should have been specified (WJE Associates, 1987).

Although the main cause of the bridge failure was scour, there were several other items considered during the investigation of the collapse. These items include the design of the superstructure, quality of materials and construction, inspection and maintenance of



superstructure, inspection and maintenance of piers above streambed, and inspections performed using the guidelines available at the time of inspections. These items did not contribute to the collapse of the Schoharie Creek Bridge (Thornton-Tomasetti, P. C., 1987).

Thornton-Tomasetti found six items that aggravated the tendency for scour (pp. 3-5, Thornton-Tomasetti, P. C., 1987):

- The flood was greater than that anticipated by the designers, and followed the 1955 flood and others that had disturbed the riprap.
- A curve in the river upstream of the bridge directed a higher-velocity flow toward pier 3.
- Drift material caught against the piers directed water downward at the base of pier 3.
- Berms built in 1963 directed floodwaters under the bridge.
- An embankment west of the creek channel increased flood velocities.
- The Mohawk River dam downstream was set for winter conditions and was 3 meters (10 feet) lower than in the 1955 flood, increasing the hydraulic gradient.

Furthermore, Thornton-Tomasetti found a number of other factors that contributed to the severity of the collapse (pp. 5-6, Thornton-Tomasetti, P. C., 1987):

- The bridge bearings allowed the spans to lift or slide off of the concrete piers.
- The simple spans were not redundant.
- The lightly reinforced concrete piers did not have enough ductility to permit frame action.
- The plinth reinforcement stopped the hinge action of the plinth cracks. Therefore, instead of dropping slowly into the scour hole, the plinth cracked suddenly.

The first two elements were common practice when the bridge was designed in the 1950's.

The National Transportation Safety Board conducted its own investigation and concluded that the probable cause of the accident was failure to maintain riprap. As contributing



factors, they pointed to ambiguous construction plans and specifications, an inadequate NYSTA bridge inspection program, and inadequate oversight by the NYSDOT and FHWA (NTSB, 1988).

SCOUR AND COUNTERMEASURES

Scour removes material through three mechanisms (Thornton et al., 1988, Palmer and Turkiyyah, 1999). These are:

1. Long term aggradation or degradation, the change in channel bottom elevation that occurs through normal erosion and deposition of material in the river bed. Clearly the degradation is of concern from a bridge safety standpoint.
2. Contraction scour when the stream width is narrowed by natural processes or bridge abutment and pier construction. By the continuity equation $Q = Av$ (where Q = flowrate, A = cross-sectional area, and v = velocity), if the channel cross sectional area decreases then the velocity must increase, resulting in an additional lowering of the channel bottom elevation.
3. “Local scour occurs when flow is obstructed by a pier or abutment placed in the floodplain. Vortexes that form at the pier or abutment remove stream bed material.” (p. 62, Huber, 1991).

Clearly, at a bridge pier, all three processes occur and are additive. Because the last two mechanisms occur only after the bridge has been constructed, the extent of potential scour may be difficult to estimate in advance.

Scour may be countered by riprap, by supporting piers on piles, by providing cofferdams around piers, and through other measures. The key is an adequate prediction of the hydraulic forces that occur during powerful floods. The analysis should also include the effects of potential land use changes upstream, such as increases in runoff from development and associated paving.

LESSONS LEARNED

The NTSB suggested a number of ways that the disaster could have been prevented, or that the loss of life could have been reduced. The thruway bridge, like other bridges on the Schoharie Creek, could have been supported on piles, which would have resisted scour. The AASHTO 1949 provisions were unclear on whether piles were required for this bridge. In the absence of the piles, leaving the sheet piling in place and providing enough riprap would have



helped protect the pier. However, the quantity estimates provided to the contractor by the design engineer did not have enough sheet piling or riprap for pier protection. The use of continuous spans, rather than simple spans, would have provided redundancy once pier three failed, and perhaps allowed for the redistribution of forces between the spans. Also, the plinth reinforcement added after the bridge construction was not anchored in the columns (NTSB, 1988). The reinforcement does not cross the crack in the plinth of pier 3, shown in figure 7.

However, the key lesson pointed out by the NTSB was operational, not technical. It is important for bridge owners to identify the critical features that can lead to the collapse of a bridge, and to ensure that those critical features are inspected frequently and adequately (NTSB, 1988).

Technical Aspects. The WJE Associates report notes that bridges must be designed for hydraulic, geotechnical, and structural effects. Of the three, only the geotechnical design, relying on the support strength of the glacial till, was satisfactory (WJE Associates, 1987).

Bridge inspections play a major role in evaluating the superstructure and substructure for deterioration to determine if maintenance is required. Bridge inspections in New York State were required on an annual/biannual basis. The state also required diver inspections of the underwater structures every five years (Levy and Salvadori, 1992).

Although the Schoharie Creek Bridge had been inspected annually or biennially since 1968, an underwater inspection of the piers footings had never been performed. The bridge was scheduled for an underwater inspection in 1987, but the bridge collapsed before the inspection took place (NTSB, 1988).

The Thornton-Tomasetti report notes “where riprap is used to prevent scour, inspection and restoration of protective riprap should be performed after every significant flood to avoid ... progressive damage, and the replacement stones used should be heavier than those which were observed to shift.” (p. 20, Thornton-Tomasetti, 1987).

Due to the collapse of the Schoharie Creek Bridge and other bridges failing in a similar manner, bridge inspectors were further trained to recognize scour potential by



examining and comparing any changes in the conditions from previous inspections (Huber, 1991). Scouring failures also sparked the much-needed research for detecting scour potential.

The Catalog And Expert Evaluation of Scour Risk And River Stability (CAESAR) system was developed by the University of Washington for evaluating scour through computer technology and for aiding bridge inspectors during the assessment process. The report documenting the program discusses the necessity of identifying “screamers,” those indicators of imminent collapse that require an agency to close a bridge (Palmer and Turkiyyah, 1999).

Educational Aspects. The bridge failures of the past demonstrate how important bridge inspection is for management and safety of the transportation network. The failures also emphasize how important it is to design footings deep enough to avoid loss of support capacity due to scour (Shepherd, 1995).

CHANGES TO ENGINEERING AND MANAGEMENT PRACTICES

When the bridge was built, the tools of the day were not adequate for predicting scour. While the bridge was in service, the inspection procedures used were not sufficient to detect the scour. Since the collapse of the Schoharie Creek Bridge, important advances have been made. A study conducted in 1989 revealed that 494 bridges failed during the years 1951 and 1988 as a result of hydraulic conditions, primarily due to scouring (Huber, 1991).



SUMMARY AND CONCLUSIONS

The collapse of the Schoharie Creek Bridge was an important event in the development of bridge design and inspection procedures. It is important to accurately predict the effects of scour, and to design bridges to resist those effects. Lessons learned include:

1. Proper selection of a critical storm for the design of bridges crossing water.
2. The need for regular inspections of the superstructure, substructure, and underwater features of the bridge.
3. The importance of adequate erosion protection around piers and abutments susceptible to scour.